Journal of Medicinal Chemistry

pubs.acs.org/jmc

Article

# Discovery of GPCR Antagonists with Potent *In Vitro* and *In Vivo* Macrofilaricidal Activity

*Published as part of Journal of Medicinal Chemistry special issue "Bridging Gaps in Global Health with Medicinal Chemistry".*

Bruce A. Rosa, Zhenfu Han, Ashutosh Arun, Nancy Tricoche, Ricardo Peguero, Victoria Banas, Melanie Shadrick, Michelle Fath, Phawiya Suksomboon, Suman Bharti, Mitchell Bancks, Elena G. Rehborg, Mostafa Zamanian, Fidelis Cho-Ngwa, Sara Lustigman,* James W. Janetka,* and Makedonka Mitreva*

Cite This: https://doi.org/10.1021/acs.jmedchem.6c01435

Read Online

ACCESS | Metrics & More | Article Recommendations | Supporting Information

**ABSTRACT:** Chronic filarial infections remain a global health burden, with limited adulticidal therapies highlighting the need for new drugs. We explored repurposing human GPCR antagonists, including clemizole, pimozide, proroxan, and suloctidil, along with 45 rationally designed analogs for activity against *Brugia pahangi* and two *Onchocerca* species. Of those, 27 showed *in vitro* adulticidal activity. *In vivo*, clemizole and analog **C-8** significantly reduced worm burden by 60.5% and 50.8%, respectively, while **S-17** and **PMZ-6** modestly reduced worm burden (36% and 25%, respectively); however, all three significantly reduced worm fecundity. **C-8** also downregulated GPCR expression in surviving adult females after *in vivo* treatment. Radioligand binding assays revealed selective human GPCR affinities, with clemizole and suloctidil analogs having increased parasite selectivity. *Caenorhabditis elegans* reverse genetics screen identified gar-3 and ser-7 as putative nematode targets of clemizole and its analogs. Clemizole, **C-8,** and **S-17** represent promising leads for further optimization as antifilarial drugs.

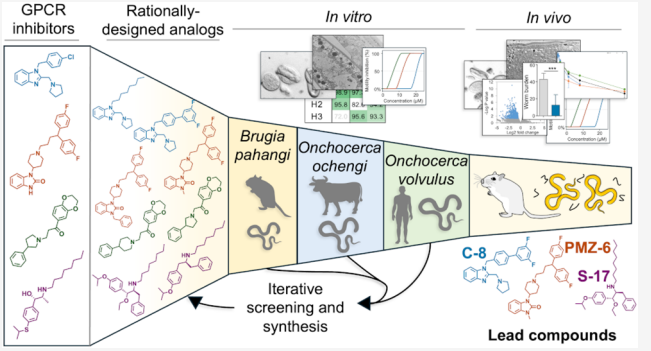


## 1. INTRODUCTION

Chronic filarial infections remain a global health burden. River Blindness, caused by the filarial nematode *Onchocerca volvulus*, is targeted for elimination in 2030. There are no vaccines against onchocerciasis, nor drugs that directly kill the adult stages (macrofilaricides or adulticides).[1−3] Control programs since the 1990s attempt to interrupt transmission with annual or biannual mass drug administration (MDA) of the donated microfilaricidal drug ivermectin (IVM), which kills microfilariae (mf) released by adult female worms that live in the human body for 10−14 years.[4−7] Although IVM also has sterilizing effects (suppressing microfilarial production) and reduces the life expectancy of the adult worms,[8] the longevity and fecundity of these worms made the WHO's 2025 elimination goal unlikely with IVM alone,[9−11] with only a 31% reduction by 2013, following 10 years of MDA.[12] Presently, ∼25 million people in sub-Saharan countries are infected,[13] with ∼300,000 individuals blind, and 800,000 visually impaired. Operational challenges to mass drug administration (MDA) and the absence of adulticidal drugs have pushed the WHO onchocerciasis elimination targets to 2030.[14,15] Predictive modeling indicates that relying solely on annual ivermectin through 2045 would require delivering as many as 2.63 billion treatments under a standard control program, or as few as 1.15 billion treatments via a more aggressive elimination strategy.[16] However, sustaining the required high coverage and therapeutic compliance over this multidecade horizon presents severe logistical, financial, and political hurdles.[11,17,18] Furthermore, relying exclusively on continued ivermectin mono- or cotherapies over this timeline is severely threatened by increasing global reports of suboptimal parasite clearance patterns and potential drug resistance.[19]

Received: May 4, 2026
Revised: July 2, 2026
Accepted: July 13, 2026

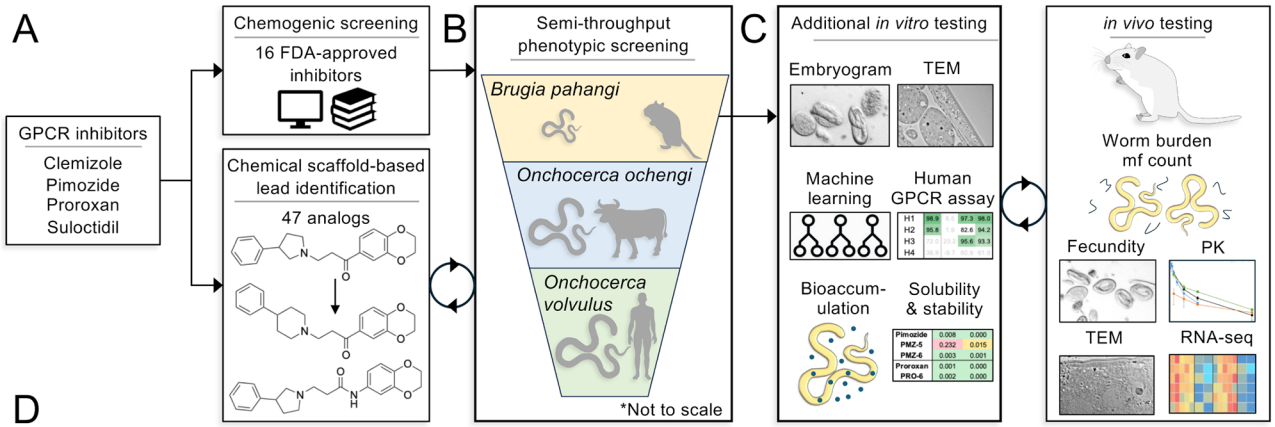


D

| Entry | Compound modifications: Clemizole | Compound modifications: Modification sites | *Brugia pahangi* Day 3 $IC_{50}$ (μM): Female F-$IC_{50}$ | Female $R^2$ | Male M-$IC_{50}$ | Male $R^2$ | *Onchocerca ochengi* Motility Inhibition @ 100 μM (%): Female Day 7 | Male Day 5 | Day 7 $IC_{50}$ (μM): Female $IC_{50}$ | Female $R^2$ | Day 5 $IC_{50}$ (μM): Male $IC_{50}$ | Male $R^2$ | *Onchocerca volvulus* L3 molting, day 6 $IC_{50}$ (μM) | $R^2$ | L4 motility inhibition (%) 10μM Day 3 / *Day 8 | L4 viability inhibition (%) 10μM Day 3 / *30μM Day 14 | HepG2 cells cytotoxicity $CC_{50}$ (μM) Day 1 | $R^2$ Day 1 | Selectivity Index (HEPG2 $CC_{50}$ / *B. pahangi* $IC_{50}$): Female F-SI | Male M-SI |
|---|---|---|---|---|---|---|---|---|---|---|---|---|---|---|---|---|---|---|---|---|
| **CLE** | | | 5.4 | 0.99 | 11.4 | 0.79 | 100 | 100 | >30 | - | ≥10 | - | 2.5 | 0.93 | *72 | Inactive | 57.2 | 0.92 | 10.7 | 5.0 |
| **C-1** | H | | Inactive | | Inactive | | 100 | 100 | ND | ND | ND | ND | ND | ND | ND | ND | 48.4 | 0.75 | ND | ND |
| **C-2** | H | | Inactive | | Inactive | | ND | ND | ND | ND | ND | ND | ND | ND | ND | ND | >50 | - | ND | ND |
| **C-3** | | | 4.1 | 0.99 | 8.9 | 0.66 | ND | ND | ND | ND | ND | ND | ND | ND | ND | ND | 81.0 | 0.99 | 19.6 | 9.1 |
| **C-4** | n-$C_8H_{17}$ | | 0.33 | 0.50 | 0.68 | 0.92 | 88 | 100 | ND | ND | ND | ND | 6.2 | 1.0 | ND | *74 | 26.6 | 0.83 | 80.3 | 39.2 |
| **C-5** | H | | Inactive | | 10.2 | 0.62 | ND | ND | ND | ND | ND | ND | ND | ND | ND | ND | 73.3 | 0.43 | ND | 7.2 |
| **C-6** | | | 6.6 | 0.94 | 7.9 | 0.65 | ND | ND | ND | ND | ND | ND | ND | ND | ND | ND | 56.0 | 0.98 | 8.5 | 7.1 |
| **C-7** | n-$C_8H_{17}$ | | 1.2 | 0.94 | 1.4 | 0.87 | 100 | 100 | ND | ND | ND | ND | 1.1 | 0.82 | 69.4 | Inactive | 42.9 | 0.97 | 36.1 | 30.7 |
| **C-8** | | | 3.9 | 0.99 | 2.8 | 0.72 | 100 | 100 | 0.35 | 0.95 | 1.7 | 1.0 | 3.2 | 0.83 | Inactive | Inactive | 17.7 | 0.89 | 4.5 | 6.4 |
| **C-9** | H | | Inactive | | Inactive | | ND | ND | ND | ND | ND | ND | ND | ND | ND | ND | >50 | - | ND | ND |
| **C-10** | | | Inactive | | Inactive | | ND | ND | ND | ND | ND | ND | ND | ND | ND | ND | >50 | - | ND | ND |
| **C-11** | | | 10.6 | 0.98 | Inactive | | ND | ND | ND | ND | ND | ND | ND | ND | ND | ND | 16.2 | 0.95 | 1.5 | ND |
| **C-12** | | H | Inactive | | Inactive | | ND | ND | ND | ND | ND | ND | ND | ND | ND | ND | >50 | - | ND | ND |
| **C-13** | | H | Inactive | | Inactive | | ND | ND | ND | ND | ND | ND | ND | ND | ND | ND | >50 | - | ND | ND |

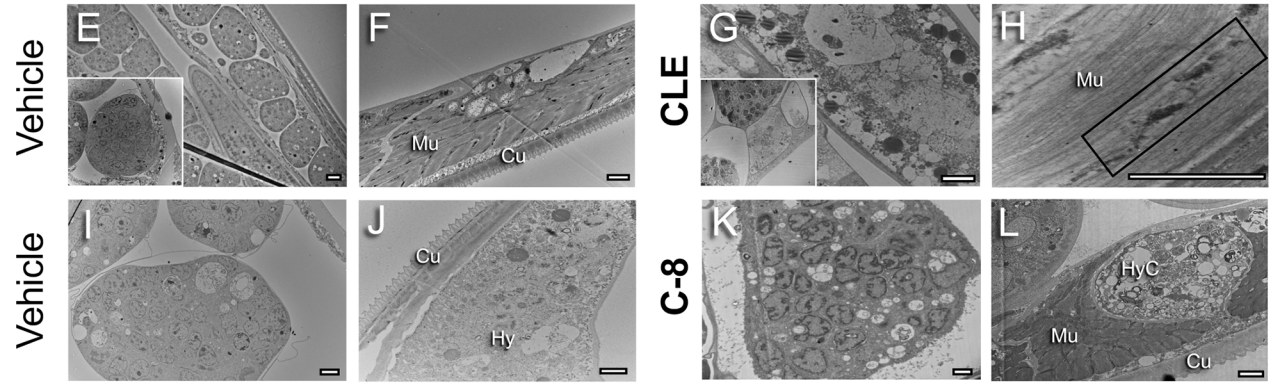


**Figure 1.** Overall experimental workflow, and semithroughput phenotypic screening and *in vitro* transmission electron microscopy (TEM) results for clemizole (**CLE**) and analogs. Experimental overview including (**A**) two orthogonal approaches to compound selection and development, (**B**) the semithroughput *in vitro* phenotypic screening using a multifaceted screening funnel spanning filarial nematode species and (**C**) additional *in vitro* testing approaches, and *in vivo* testing approaches. (**D**) Activity and selectivity of **CLE** and analogs in three different filarial nematode species. ND = Not Done. "Inactive" = not active in initial *B. pahangi* screens at 10 μM (so $IC_{50}$ values were not calculated), or <50% inhibition in *O. volvulus*. $IC_{50}$ = inhibitory concentration corresponding to 50% inhibition of worm motility; $R^2$ values indicate how well the fitted dose−response


https://doi.org/10.1021/acs.jmedchem.6c01435
J. Med. Chem. XXXX, XXX, XXX−XXX

**Figure** 1. continued

curve matches the experimental data points; Complete $IC_{50}$ statistics are provided in Table S1. $CC_{50}$ = Cytotoxicity concentration, corresponding to 50% death of HepG2 cells. "Selectivity index" represents the ratio of $CC_{50}$ to $IC_{50}$, corresponding to the fold-increase of efficacy in worms relative to mammalian cells. Panels E-L show ultrastructural alterations induced by 3 days of 30 $\mu$M *in vitro* treatment in adult female *B. pahangi*. (**E**) A vehicle-treated worm with a normal gonad with a healthy embryo shown in the inset, and (**F**) a normal hypodermis and cuticle. (**G**) A necrotic gonad full of electron dense debris from a **CLE**-treated worm, with several necrotic embryos shown in high magnification in the inset. (**H**) A muscle fiber from a **CLE**-treated worm with electron dense debris scattered throughout the muscle fiber (boxed region). (**I&J**) Normal ultrastructure of vehicle-treated worms from a second experiment for **C-8** treatment. (**K**) A deformed, highly vacuolated embryo from a **C-8** treated worm. (**L**) A destroyed, necrotic hypodermal cord of a **C-8** treated worm. Cu: cuticle; Mu: muscle; Hy: hypodermis; HyC: hypodermal chord. Scale bars represent 2 $\mu$m. Brightness and contrast adjustments were applied to the entire image.

Decades of research have yielded no current alternatives to MDA with IVM, and high cost precludes treatment in hypo-endemic areas, allowing transmission via migration and parasite reintroduction.[11] Emerging suboptimal IVM efficacy against *O. volvulus* mf further threatens MDA effectiveness[3,20−23] and undermines elimination progress. Doxycycline, the only proven adulticidal drug, kills adult worms by targeting *Wolbachia*, but takes 18 months to work and cannot be used in children under 9 years or pregnant women (transmission reservoirs[24]), and requires long (4−6 weeks) treatment regimens infeasible for MDA.[25] It is currently limited to "Test & Treat" campaigns.[26] The macrocyclic lactone moxidectin demonstrates superior and more sustained microfilarial suppression compared to IVM by halting embryogenesis[27,28] and was added to the WHO's essential medicines list in 2025.[29] Clinical data further demonstrates that a combination of moxidectin plus albendazole safely clears Wuchereria bancrofti microfilariae for up to 2 years, presenting a significantly longer-lasting effect than traditional ivermectin-based coadministrations. However, it also lacks direct macrofilaricidal efficacy against adult worms in humans.[19] These limitations underscore the urgent need for new adulticidal drugs with alternate mechanisms of action, greater efficacy, and pan-filarial activity. To address this deficit, several macrofilaricidal candidates are being clinically evaluated. Emodepside and the repurposed veterinary benzimidazole oxfendazole are currently undergoing Phase I/II clinical trials to assess safety and adulticidal efficacy.[30,31] Oxfendazole is particularly promising because it acts as a selective macrofilaricide with no prominent direct activity against microfilariae, safely avoiding microfilariae-induced inflammatory adverse events during treatment.[19] Clinical evaluation of the anti-*Wolbachia* antibiotic fusidic acid has been initiated to investigate short-course curative regimens.[32] However, given the high attrition rates typical of clinical drug development (including the discontinuation of promising candidates such as flubentylosin and AWZ1066S due to limitation in efficacy and host toxicity[19]), there remains a critical need for distinct pan-filarial scaffolds. Consequently, continuously expanding the discovery pipeline with structurally novel macrofilaricidal chemotypes is essential.

Earlier, omics-driven prioritization and phenotypic screening of an FDA-approved library of compounds against *Brugia pahangi* adult worms *in vitro* identified several antifilarial hits,[33] including several CNS-active drugs targeting G-protein Couple Receptors (GPCRs). GPCRs are among the most targeted protein families, ∼34% of FDA-approved drugs act on 108 GPCRs, with 66 more in clinical trials,[34] treating conditions including hypertension, depression, Alzheimer's disease and infectious diseases.[35] Importantly, structural data for many GPCRs has enabled rational drug design.[34,36] GPCRs are also promising anthelmintic targets in trematodes[37] and other nematodes.[38] For example, nuciferine is a potent antagonist of a schistosome serotonergic GPCR[37] and praziquantel (effective against schistosomiasis, schistosomula and adults) targets a mammalian serotonergic GPCR ($5HT_{2B}$),[39] but appears to act through targeting transient receptor potential (TRP) channels in helminths.[40−42] In nematodes, SER-4 agonists cleared *Haemonchus contortus* infections in jirds.[43] Notably, the *O. volvulus* genome contains 230 GPCRs, with unique expansion in the Srt family and duplications in Srx and Srsx families.[44]

In a previous study, we identified four GPCR antagonists, clemizole (**CLE**), pimozide (**PMZ**), proroxan (**PRO**)(FDA-approved drugs), and suloctidil (**SUL**; non-FDA-approved compound) as having potent anthelmintic activity against several parasitic filarial worms.[33] **CLE**, a benzimidazole antihistamine, is a selective H1 antagonist and TRPC5 inhibitor.[45] **PMZ**, a diphenylbutylpiperidine antipsychotic, inhibits $D_2$−$D_4$ dopamine, histamine, serotonin and alpha-adrenergic receptors.[46] **PRO** is a nonselective alpha-blocker targeting $\alpha$-adrenoreceptor.[47] **SUL** is an adrenergic receptor antagonist[48] that also inhibits other GPCRs, including the H2 receptor.[49] Here, we expanded on these findings by advancing hit-to-lead studies across these structurally diverse GPCR antagonist classes.

## 2. RESULTS AND DISCUSSION

To identify additional GPCR antagonists with adulticidal anthelmintic activity,[33] we pursued two approaches (Figure 1A): 1) chemogenomic screening of human GPCR ligands based on the antagonists **CLE**, **PMZ**, **PRO** and **SUL**, and 2) scaffold-based lead identification to reduce toxicity, improved selectivity and pharmacokinetic (PK) properties. Since *O. volvulus*, our target species, lacks an animal model for adult worm harvesting, we implemented a cost-effective, stepwise *in vitro* screening funnel (Figure 1B); primary screens with adult *B. pahangi*, secondary screens with *O. ochengi* (worms harvested from infected cattle;[50] close relative to *O. volvulus*[51,52]), and tertiary screens with *O. volvulus* L3 and L4 larvae.[53] Like other nematodes, filarial parasites possess a collagen-rich cuticle that functions as a primary semipermeable barrier, regulating the passive diffusion and subsequent efficacy of anthelmintic compounds.[54,55] Findings from drug bioaccumulation screening suggest that some inactive analogs are incapable of penetrating the filarial nematode cuticle due to differential hydrophobicity.[33] This knowledge can be directed at improving uptake of inhibitors through the nematode cuticle and used to optimize the compounds for potency.[56] The target species, *O. volvulus*, reaches substantial lengths, with adult females measuring approximately 30−50 cm (diameter ∼ 300 $\mu$m), while *O. ochengi* (the closely related sister species that we


https://doi.org/10.1021/acs.jmedchem.6c01435
J. Med. Chem. XXXX, XXX, XXX−XXX

**Scheme 1. The Preparation of Clemizole (CLE) Analogs**[a]

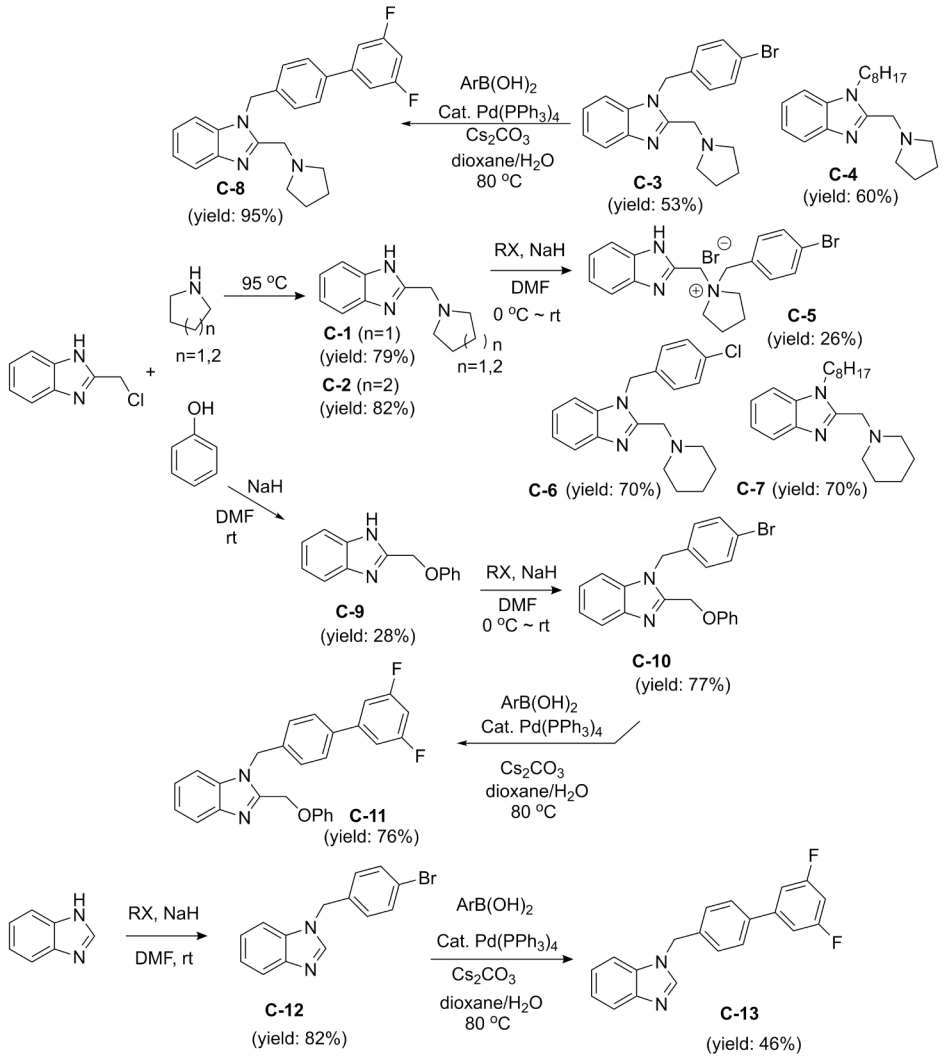


[a]The condensation of 2-chloromethylbenzimidazole with pyrrolidine or piperidine provided intermediate **C-1** and **C-2**, which upon deprotonation by sodium hydride were subjected to the nucleophilic substitution with appropriate alkyl halides to furnish **C-3**, **C-4**, **C-5**, **C-6**, **C-7**. **C-3** underwent subsequently Suzuki coupling reaction with 3,5-difluorophenylboronic acid to give **C-8**. **C-9** was synthesized through the coupling of 2-chloromethylbenzimidazole with sodium phenoxide, which was generated in situ from phenol with sodium hydride. Deprotonation of **C-9** by sodium hydride, followed by alkylation with 4-bromobenzyl bromide gave **C-10**, which reacted with 3,5-difluorophenylboronic acid under Suzuki coupling condition to yield **C-11**. In a similar fashion, **C-12** and **C-13** were produced, starting with benzimidazole.

screen) reaches ~ 25 cm; in comparison, *B. pahangi*, used in our primary screening, is ~5 cm in length.

Adult *B. pahangi* responses were evaluated (Figure 1C) using (i) motility inhibition (MI) over 3 days of treatment. For active compounds (≥50% MI), motility $IC_{50}$ statistics including $R^2$ values, *P* values, standard error values and 95% confidence intervals are provided in Table S1 (F-$IC_{50}$ for female, M-$IC_{50}$ for male), and $IC_{50}$ curves are provided in Supporting Information. Since adult *B. pahangi* worms must be obtained from individual infected gerbil hosts rather than from a fully standardized *in vitro* source, batch-to-batch variability in baseline worm activity and motility is expected, despite efforts to tightly control infection, recovery, and culture conditions. For this reason, motility inhibition values at single concentrations with one batch of worms may not correlate precisely with $IC_{50}$ values calculated using a subsequent batch. The "selectivity index" (F−SI for female, M-SI for male) was calculated as the ratio of HepG2 cell cytotoxicity ($CC_{50}$; calculated for all compounds, with detailed statistics in Table S1 and plots in Supporting Information) to the *B. pahangi* $IC_{50}$. (ii) Female fecundity was measured as the reduction of active vs dead microfilariae (mf) relative to DMSO controls (%; $P \leq 0.05$, two-tailed pooled student's *t* tests; complete statistics provided in Table S1). (iii) Embryograms assessed differential embryonic development within the uterine of female worms ("embryogenesis"; FDR-adjusted $P \leq 0.05$, two-tailed student's *t* tests; Table S1); (iv) Transmission electron microscopy (TEM) of uterine content ultrastructure; (v) for representative compounds transcriptional profiling of treated worms (harvested from infected and treated gerbils); and vi) GPCR binding across a panel of 43 human GPCRs receptor (radioligand binding assay; Table S2). Based on efficacy, selectivity and pharmacokinetic properties, we identified four lead compounds that underwent *in vivo* evaluation.


https://doi.org/10.1021/acs.jmedchem.6c01435
J. Med. Chem. XXXX, XXX, XXX−XXX

### 2.1. Expanding the Chemical Space by Evaluating Known Human GPCR Inhibitors

We conducted chemoinformatic searches based on GPCR targets of **CLE**, **PMZ**, **PRO** and **SUL**, to select 16 additional antagonists (5 histamine, 6 dopaminergic, 2 $\alpha$-adrenergic, 3 $\beta$-adrenergic) for evaluation. Eleven of the 20 total compounds caused ≥50% motility inhibition (MI) at 10 $\mu$M (4 replicates, repeated twice), including 5 in both sexes (Figure S1). Of these 5, two were histamine antagonists: **CLE** and azelastine, a second generation antihistamine used to treat hay fever and conjunctivitis among other conditions[57] (**CLE** F-$IC_{50}$ = 5.4, F−SI = 10.7, M-$IC_{50}$ = 11.4 $\mu$M, M-SI = 5.0; Azelastine F-$IC_{50}$ = 1.1 $\mu$M, F−SI = 27.6, M-$IC_{50}$ = 23.4 $\mu$M, M-SI = 1.3). Dopamine antagonists **PMZ** and melperone were active in *B. pahangi* females (**PMZ** F-$IC_{50}$ = 2.3 $\mu$M, F−SI = 6.9, M-$IC_{50}$ = 0.59 $\mu$M, M-SI = 26.9; melperone F-$IC_{50}$ = 14.3 $\mu$M and F−SI > 3.5). Among adrenergic blockers, **PRO** and **SUL** were active in both sexes (**PRO** F-$IC_{50}$ = 4.2 $\mu$M, F−SI = 23.6, M-$IC_{50}$ = 2.5 $\mu$M, M-SI = 36.9; **SUL** F-$IC_{50}$ = 7.9, F−SI = 0.67, M-$IC_{50}$ = 1.8 $\mu$M, M-SI = 2.9). All four primary hits increased mf killing by at least 75.7% ($P \leq 2.5 \times 10^{-3}$; Table S1). **CLE** and **PRO** also increased the proportion of embryos (by at least 10.7%, $P \leq 0.048$) while reducing mf counts (−10.3% and −9.8%, $P = 0.048$ for both), with **PRO** decreasing egg counts (−13.3%, $P = 0.048$).

All 20 compounds were also screened for *O. ochengi* adult female viability and adult male MI. Fourteen showed >70% MI, six in both sexes (Figure S1) including **CLE**, **PMZ** and **SUL**, as well as dopamine antagonists aripiprazole and chlorpromazine, and the alpha-adrenergic blocker prazosin. Aripiprazole was *O. ochengi*-specific and active in both sexes. Both **CLE** and **PMZ** inhibited *O. ochengi* motility in females ≥ 30 $\mu$M $IC_{50}$, but **PMZ** was more potent against males (≥3 $\mu$M vs ≥10 $\mu$M for **CLE**; Table S1). Five compounds had >50% MI in *O. volvulus* L4 larval stage (10 $\mu$M, 8 days). **CLE** and **PMZ** inhibited L3 molting with $IC_{50}$ = 2.5 $\mu$M and 2.9 $\mu$M, respectively (Table S1).

Fifteen compounds were active in at least one filarial species, sex or stage. Chlorpromazine and prazosin were excluded from further studies due to inactivity in *B. pahangi*, despite activity in *Onchocerca* species. These differences may be due to species- or sex-specific GPCR expression, as observed for emodepside with adult *B. malayi*, attributed to SLO-1K splice variation.[58] Azelastine and melperone were excluded due to inactivity in female *Onchocerca*.

For further optimization, one representative from each active class was selected (**CLE**, **PMZ**, **PRO** and **SUL**) due to their synthetic tractability and potential for analog development, activity against at least one *Onchocerca* species and strong potency in *B. pahangi* (F-$IC_{50}$ = 2.3−7.9 $\mu$M, M-$IC_{50}$ = 0.59−11.4 $\mu$M). Anthelmintics must cause irreversible damage to the worm due to transient host exposure, so we tested the durability of the effects of these four representatives. Adult *B. pahangi* were treated with 5−60 $\mu$M (~3× $IC_{50}$ at day 1) for 24 h, washed and monitored for 5 days. All representative compounds were 100% effective by 48 h, and none recovered motility, indicating irreversible damage (Figure S2). To explore structure−activity relationships (SAR) and enhance potency and worm selectivity, we synthesized focused libraries of derivatives.

### 2.2. Structure Activity Relationships

**2.2.1. Clemizole Analogs.** We synthesized new compounds based the CLE chemical scaffold (Scheme 1). First, we varied the N-substituents 4-chlorobenzyl (benzimidazole ring nitrogen; $R^1$) and then explored replacements of the pyrrolidine ring ($R^2$). Without substitution, *B. pahangi* MI was diminished (**C-1** and **C-2**). When $R^1$ is changed to 4-bromobenzyl (**C-3**), potency against *B. pahangi* slightly improved (F-$IC_{50}$ = 4.1 $\mu$M, M-$IC_{50}$ = 8.9 $\mu$M), and when replaced by a biphenyl (**C-8**; inspired by the diphenyl portion of pimozide), potency further improved (F-$IC_{50}$ = 3.9 $\mu$M, M-$IC_{50}$ = 2.8 $\mu$M; **CLE** F-$IC_{50}$ = 5.4 $\mu$M, M-$IC_{50}$ = 11.4 $\mu$M). When $R^1$ was substituted with a long alkyl group such as n-octyl, potency as well as selectivity greatly improved (e.g., **C-4**, F-$IC_{50}$ = 0.33 $\mu$M, F−SI = 80.3, M-$IC_{50}$ = 0.7 $\mu$M, M-SI = 39 and **C-7**, F-$IC_{50}$ = 1.2 $\mu$M, F−SI = 36.1, M-$IC_{50}$ = 1.4 $\mu$M, M-SI = 30.7). We performed an LC-MS bioaccumulation assay for **CLE**, **C-3** and **C-4** on female *B. pahangi* lysate following 20 min of 30 $\mu$M incubation (N = 2; Table S1). We detected 4.2-fold and 2.4-fold more **C-4** bioaccumulation than **CLE** and **C-3** (4.4 $\mu$M vs 1.1 $\mu$M and 1.8 $\mu$M, respectively), indicating that the **CLE** $R^1$ substitution with a long alkyl group such as n-octyl improves uptake through the cuticle. While potency was retained when $R^2$ was replaced with a 6-membered piperidine ring (**C-6**, F-$IC_{50}$ = 6.6 $\mu$M, M-$IC_{50}$ = 7.9 $\mu$M), replacing it with a phenoxy group (**C-10**) or removing it (**C-12**, **C-13**) eliminated MI. The hybrid analog **C-11**, with a di-F-biphenyl group based on the pimozide structure, retained activity only in female *B. pahangi* (F-$IC_{50}$ = 10.6 $\mu$M). Overall, 7 newly synthesized compounds were active in *B. pahangi*. Of those, 2 were sex-specific (**C-5**, male; **C-11**, female). Four female-active analogs had a better F-$IC_{50}$ than **CLE** (F-$IC_{50}$ range 0.33−4.14 $\mu$M vs 5.4 $\mu$M), and all 6 male-active analogs had better activity than **CLE** (M-$IC_{50}$ 0.68−10.2 $\mu$M vs 11.4 $\mu$M).

Female fecundity was significantly affected by all active analogs including **C-3**, **C-7** and **C-11** (100% dead/inactive mf; $P \leq 8.4 \times 10^{-7}$), and **C-12** and **C-13**, which did not reduce motility (96% and 98% dead/inactive mf, $P \leq 4.6 \times 10^{-8}$). **C-3** increased uterine premf while decreasing mf (13.2% and 10.6%, respectively; $P = 0.023$). Notably, **CLE** and 8 analogs were also larvicidal, inhibiting motility of 42-day *B. pahangi* L4 female by >50%, reinforcing that these adulticidal drugs have also larvicidal potential. **C-9**, **C-10**, **C-12** and **C-13** were not larvicidal, while **C-1** and **C-2** had a stage and/or sex specific activity (active in L4 female but not in L4 male), and **C3-C8** had larvicidal activity in both sexes (Table S1).

**CLE** and its analogs **C-1**, **C-4**, **C-7** and **C-8** were adulticidal against both sexes in *O. ochengi*, with improved potency for **C-8** compared to **CLE** (**C-8** F-$IC_{50}$ = 0.35 $\mu$M, M-$IC_{50}$ = 1.7 $\mu$M; **CLE** F-$IC_{50}$ ≥ 30 $\mu$M, M-$IC_{50}$ ≥ 10 $\mu$M). Due to efficacy in both *B. pahangi* and *O. ochengi*, **CLE**, **C-4**, **C-7** and **C-8** were also tested in *O. volvulus*. L3 molting inhibition $IC_{50}$ values were 2.5, 6.2, 1.1, and 3.2 $\mu$M (respectively), while only **C-4** reduced *O. volvulus* L4 viability following a 14-day 30 $\mu$M exposure (by >70%; Figure 1D; Table S1).

Based on consistent efficacy across species and sexes, **C-4**, **C-7** and **C-8** were the best **CLE** analogs. TEM structural analyses confirmed **CLE** and **C-8** affect the wellness and fecundity of adult female *B. pahangi in vitro* (compared to vehicle Figure 1E, 1F). Specifically, we observed severe deformities in the gonads of **CLE**-treated worms (lost integrity and filled with unrecognizable necrotic material; Figure 1G), and the few recognizable embryonic developmental stages were


https://doi.org/10.1021/acs.jmedchem.6c01435
J. Med. Chem. XXXX, XXX, XXX−XXX

**Scheme 2. Synthesis of Pimozide (PMZ) Analogs**[a]

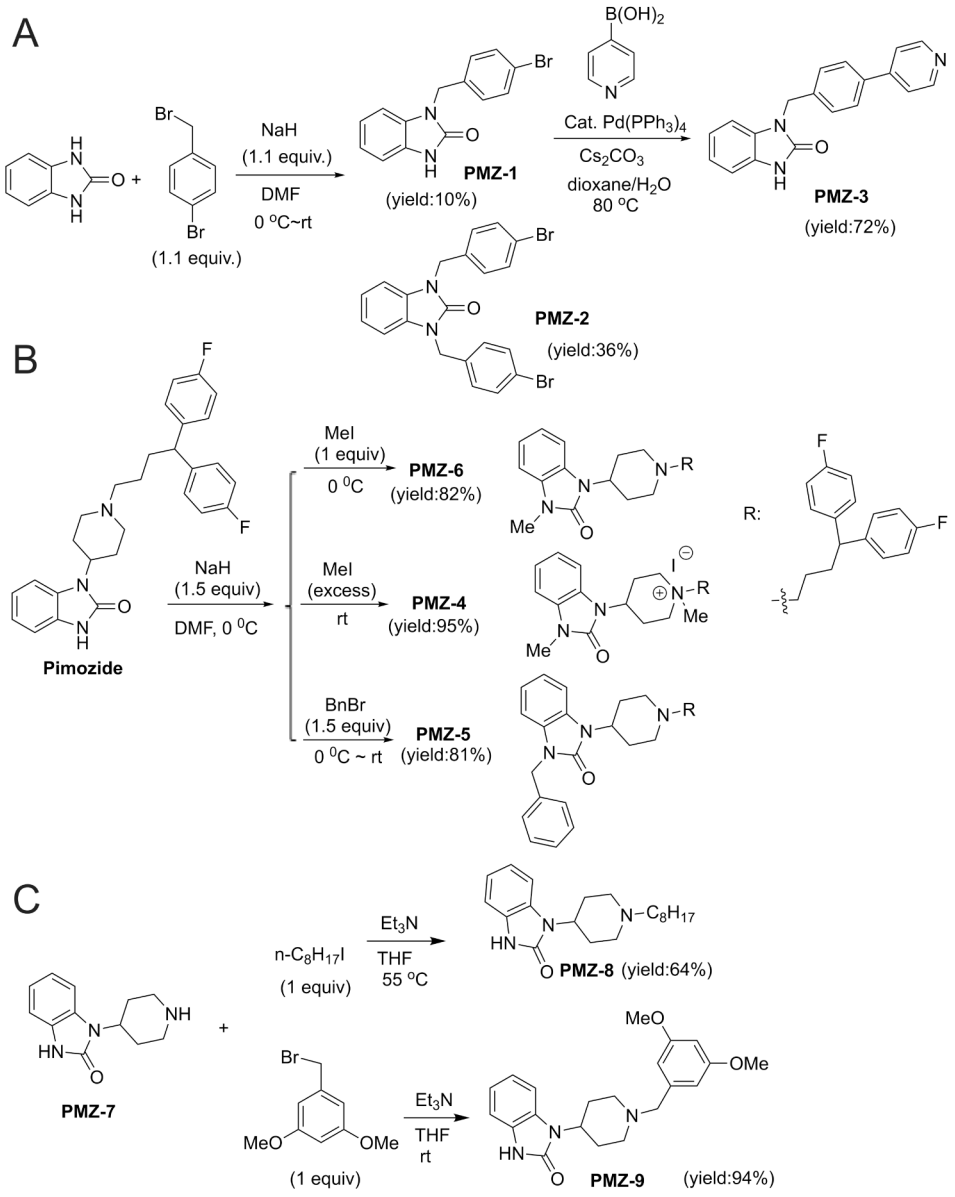


[a](**A**) Deprotonation of benzimidazolone with sodium hydride, followed by the nucleophilic substitution with 4-bromobenzyl bromide afforded **PMZ-1** and **PMZ-2**. **PMZ-1** underwent Suzuki coupling reaction with 4-pyridineboronic acid to give **PMZ-3**. (**B**) In a similar fashion, **PMZ-4**, **PMZ-5** and **PMZ-6** were prepared with the pimozide as the starting material. (**C**) The reaction of 4-(2-keto-1-benzimidazolinyl)piperidine (**PMZ-7**), which is commercially available, with appropriate alkyl halides in the presence of base yielded **PMZ-8** and **PMZ-9**.

severely deformed (inset, Figure 1G). While the hypodermis of **CLE**-treated worms was mostly normal, electron-dense debris was frequently observed near disrupted muscle fibers (Figure 1H). Compared to vehicle-treated worms, **C-8**-treated worms displayed vacuolated embryos and marked damage to regions of the hypodermis; most notably the hypodermal chords appeared destroyed (Figure 1I, 1J, 1K and 1L).

**2.2.2. Pimozide Analogs.** For **PMZ**, we modified the nitrogen substituent $R^2$ of the phthalimide to various benzylic groups and investigated different substituents on the piperidine ring (Scheme 2). Inspired by the increased potency of the **CLE** analogs, we synthesized N-4-bromobenzyl analog **PMZ-1** and disubstituted analogs **PMZ-2** and **PMZ-3** having an N-4-pyridinylbenzyl group, but all 3 were inactive (Figure 2A). The activity was also lost when the difluorophenyl butane group attached to piperidine ring was removed or replaced by n-octyl or 3,5-dimethoxybenzyl (**PMZ-7**, **PMZ-8** and **PMZ-9**). *N*-methyl and N-benzyl substitution on the pimozide-free amine NH $R^1$ retained activity for **PMZ-5** and **PMZ-6** but the alkylated piperidine analog **PMZ-4** was inactive, indicating that the basicity (high $pK_a$) of the piperidine might be important for targeting *B. pahangi* (**PMZ-5** F-$IC_{50}$ = 0.76 $\mu$M, F−SI = 8.3, M-$IC_{50}$ = 0.88 $\mu$M, M-SI = 7.2; **PMZ-6** F-$IC_{50}$ = 1.8 $\mu$M, F−SI = 10.5, M-$IC_{50}$ = 0.24 $\mu$M, M-SI = 77.7). In addition, the constant positive charge in **PMZ-4** might hinder its ability to penetrate the worm cuticle and reach the putative receptor, potentially leading to its inactivity against *B. pahangi*. Female *B. pahangi* lysate bioaccumulation assays with the best analog (**PMZ-5**; detected) vs the inactive (**PMZ-9**; undetectable) corresponded with their differential activity (Table S1). While


https://doi.org/10.1021/acs.jmedchem.6c01435
J. Med. Chem. XXXX, XXX, XXX−XXX

| A Entry | Compound modifications: Pimozide / Modification sites | *Brugia pahangi* Day 3 $IC_{50}$ (μM) Female F-$IC_{50}$ | Female $R^2$ | Male M-$IC_{50}$ | Male $R^2$ | *Onchocerca ochengi* Motility Inhibition @ 100 μM (%) Female Day 7 | Male Day 5 | *Onchocerca volvulus* L3 molting, day 6 $IC_{50}$ (μM) | $R^2$ | L4 motility inhibition @ 10 μM (%) / *viability inhibition @ 30 μM (%) | HepG2 cells cytotoxicity $CC_{50}$ (μM) Day 1 | $R^2$ Day 1 | Selectivity Index ($HEPG2\ CC_{50}$ / *B. pahangi* $IC_{50}$) Female F-SI | Male M-SI |
|---|---|---|---|---|---|---|---|---|---|---|---|---|---|---|
| **PMZ** | H | 2.3 | 0.99 | 0.59 | 1.0 | 80 | 100 | 2.9 | 0.70 | 100 (Day 8) | 15.8 | 0.87 | 6.9 | 26.9 |
| **PMZ-1** | H | Inactive | | Inactive | | ND | ND | ND | ND | ND | >50 | - | ND | ND |
| **PMZ-2** | | Inactive | | Inactive | | ND | ND | ND | ND | ND | >50 | - | ND | ND |
| **PMZ-3** | H | Inactive | | Inactive | | ND | ND | ND | ND | ND | >50 | - | ND | ND |
| **PMZ-4** | Me | Inactive | | Inactive | | ND | ND | ND | ND | ND | >50 | - | ND | ND |
| **PMZ-5** | | 0.76 | 0.89 | 0.88 | 0.82 | 0 | 100 | 0.80 | 0.96 | 100 (Day 3) | 6.3 | 0.88 | 8.3 | 7.2 |
| **PMZ-6** | Me | 1.8 | 0.99 | 0.24 | 0.96 | 100 | 100 | 3.6 | 0.94 | *91 (Day 14) | 18.5 | 0.72 | 10.5 | 77.7 |
| **PMZ-7** | H | Inactive | | Inactive | | ND | ND | ND | ND | ND | >50 | - | ND | ND |
| **PMZ-8** | H | Inactive | | Inactive | | ND | ND | ND | ND | ND | 73.2 | 0.91 | ND | ND |
| **PMZ-9** | H | Inactive | | Inactive | | ND | ND | ND | ND | ND | >50 | - | ND | ND |

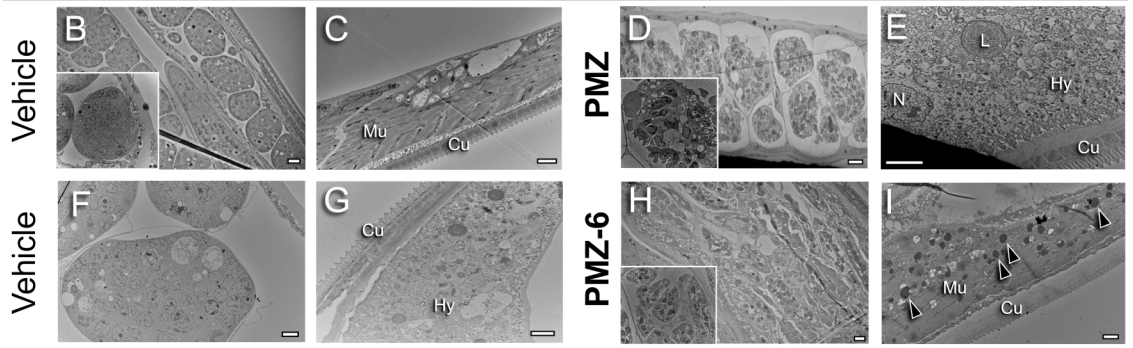


**Figure 2.** Semithroughput phenotypic screening and *in vitro* transmission electron microscopy (TEM) results for pimozide (**PMZ**) and analogs. (**A**) Activity and selectivity of **PMZ** and analogs in three different filarial nematode species. ND = Not Done. "Inactive" = not active in initial *B. pahangi* screens at 10 μM, so $IC_{50}$ values were not calculated. $IC_{50}$ = inhibitory concentration corresponding to 50% inhibition of worm motility; $R^2$ values indicate how well the fitted dose−response curve matches the experimental data points; Complete $IC_{50}$ statistics are provided in Table S1. $CC_{50}$ = Cytotoxicity concentration, corresponding to 50% death of HepG2 cells. "Selectivity index" represents the ratio of $CC_{50}$ to $IC_{50}$, corresponding to the fold-increase of efficacy in worms relative to mammalian cells. Panels B−I show ultrastructural alterations induced by 3 days of 30 μM *in vitro* treatment in adult female *B. pahangi*. (**B**) A vehicle-treated worm with a normal gonad with a healthy embryo shown in the inset, and (**C**) a normal hypodermis and cuticle. (**D**) A **PMZ**-treated worm with a gonad full of necrotic embryos; a single necrotic embryo, loaded with electron dense material, is shown in high magnification in the inset. (**E**) An abnormal hypodermis of a **PMZ**-treated worm displaying numerous vacuoles, as well as a large lysosome (L) and a ruffled nucleus (N). (**F&G**) Normal ultrastructure of vehicle-treated worms from **PMZ-6** treatment. (**H**) A deformed gonad loaded with various necrotic, unrecognizable developmental stages from a **PMZ-6** treated worm; a cluster of necrotic material is shown in the inset where electron dense debris is apparent. (**I**) The hypodermis of a **PMZ-6** treated worm displaying numerous, small and immature lysosomes scattered throughout muscle fibers (black arrowheads). Cu: cuticle; Mu: muscle; Hy: hypodermis. Scale bars represent 2 μm. Brightness and contrast adjustments were applied to the entire image.

**PMZ** concentration was 5-fold higher than **PMZ-5**, **PMZ-5** F-$IC_{50}$ was 3-fold better compared to **PMZ** (0.76 vs 2.3 μM), supporting that while less **PMZ-5** penetrates the worm, its potency is much higher. **PMZ** and the two adulticidal analogs **PMZ-5** and **PMZ-6** showed larvicidal activity against L4 males and female *B. pahangi*. In *Onchocerca* species, **PMZ-5** was active only in male *O. ochengi*, and **PMZ-6** was active against both female and male. Both compounds inhibited *O. volvulus* L4 viability or motility by >90% and reduced *O. volvulus* L3 molting ($IC_{50}$ = 0.80 μM and $IC_{50}$ = 3.6 μM, respectively). **PMZ-5** was the most effective, and is equipotent to the anthelmintic emodepside,[59] which has macrofilaricidal activity


https://doi.org/10.1021/acs.jmedchem.6c01435
J. Med. Chem. XXXX, XXX, XXX−XXX

A

| Entry | Proroxan compound modifications: Proroxan R1 | R2 | *Brugia pahangi* Day 3 $IC_{50}$ (μM) Female F-$IC_{50}$ | $R^2$ | Male M-$IC_{50}$ | $R^2$ | *Onchocerca ochengi* Motility Inhibition @ 100 μM (%) Female Day 7 | Male Day 5 | *Onchocerca volvulus* L3 molting, day 6 $IC_{50}$ (μM) | $R^2$ | L4 viability inhibition (%) 30μM Day 14 | HepG2 cells cytotoxicity $CC_{50}$ (μM) Day 1 | $R^2$ Day 1 | Selectivity Index (HEPG2 $CC_{50}$ / *B. pahangi* $IC_{50}$) Female F-SI | Male M-SI |
|---|---|---|---|---|---|---|---|---|---|---|---|---|---|---|---|
| **PRO** | | | 4.2 | 0.99 | 2.5 | 0.93 | 0 | 100 | Inactive | | Inactive | 99.8 | 0.88 | 23.6 | 39.4 |
| **PRO-1** | | | 10.9 | 0.92 | 0.65 | 0.92 | 0 | 100 | 4.3 | 0.75 | 48% | 85.4 | 0.85 | 7.8 | 132.2 |
| **PRO-2** | | | Inactive | | Inactive | | ND | ND | ND | ND | ND | >50 | - | ND | ND |
| **PRO-3** | | | 1.2 | 0.96 | Inactive | | 0 | 100 | Inactive | | ND | 93.61 | 0.95 | 75.1 | ND |
| **PRO-4** | | | Inactive | | Inactive | | ND | ND | ND | ND | ND | >50 | - | ND | ND |
| **PRO-5** | | | Inactive | | Inactive | | ND | ND | ND | ND | ND | >50 | - | ND | ND |
| **PRO-6** | | | Inactive | | Inactive | | ND | ND | ND | ND | ND | >50 | - | ND | ND |
| **PRO-R** | | | 4.4 | 0.97 | 1.5 | 0.99 | ND | ND | ND | ND | ND | 46.8 | 0.97 | 10.5 | 30.9 |
| **PRO-S** | | | 5.5 | 0.96 | 0.90 | 0.83 | ND | ND | ND | ND | ND | 48.6 | 0.98 | 8.9 | 54.2 |

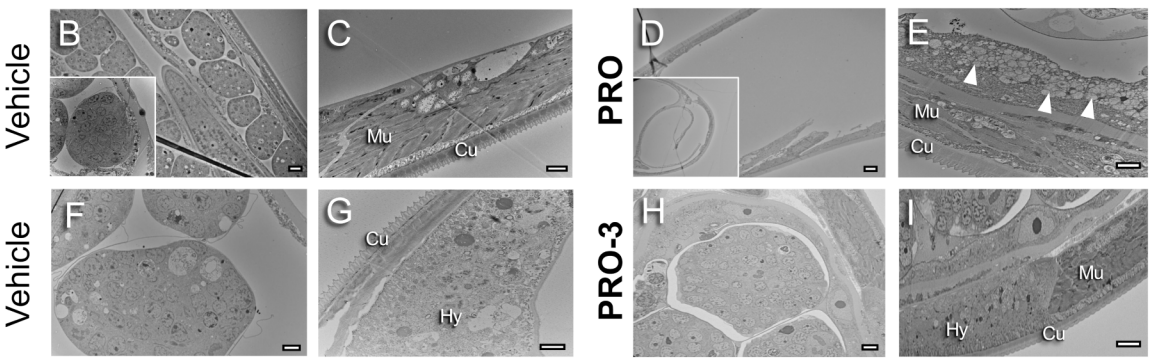


**Figure 3.** Semithroughput phenotypic screening and *in vitro* transmission electron microscopy (TEM) results for proroxan (**PRO**) and analogs. (**A**) SAR study of proroxan analogs and analogs, and their activity and selectivity against 3 filarial species. MI = motility inhibition; VI = viability inhibition; Molt-I = molting inhibition; ND = Not Done; "Inactive" = not active in initial *B. pahangi* screens at 10 μM (so $IC_{50}$ values were not calculated), or <50% inhibition in *O. volvulus*. Panels B–I show ultrastructural alterations induced by 3 days of 30 μM *in vitro* treatment in adult female *B. pahangi*. (**B**) A vehicle-treated worm with a normal gonad with a healthy embryo shown in the inset, and (**C**) a normal hypodermis and cuticle. (**D**) An empty gonad from a **PRO**-treated worm shown in a longitudinal section; another empty gonad is shown in cross section in the inset. (**E**) The hypodermis of a **PRO**-treated worm displaying numerous membrane-bound vesicle-like structures (white arrowheads). (**F&G**) Normal ultrastructure of vehicle-treated worms from a second experiment for **PRO-3** treatment. (**H**) A normal, healthy embryo and (**I**) a normal hypodermis from a **PRO-3** treated worm. Cu: cuticle; Mu: muscle; Hy: hypodermis. Scale bars represent 2 μm. Brightness and contrast adjustments were applied to the entire image.

in filarial nematodes,[60] and is used clinically to treat a range of gastrointestinal nematodes in dogs and cats; at present it is in clinical trials as a macrofilaricidal drug against *O. volvulus* infection[61] and against soil transmitted helminths[62] in humans. Female fecundity and reproductive output were consistent with motility inhibition results, with significant mf activity reduction was only observed for the 2 active analogs (100% dead/inactive active mf; $P = 1.8 \times 10^{-11}$ for **PMZ-5** and $P = 1.4 \times 10^{-3}$ for **PMZ-6**).

Structural analyses by TEM of *B. pahangi* adult female worms treated with **PMZ** and **PMZ-6** *in vitro* (compared to vehicle, Figure 2B, C and F, G) indicated that while the **PMZ**-treated worms appeared to maintain the integrity of the gonads and the uterine walls, the various developmental stages within the gonad were clearly destroyed (Figure 2D and inset). The hypodermis of **PMZ**-treated worms was also markedly vacuolated, and nuclei detected within the hypodermis appeared ruffled (Figure 2E). The **PMZ-6** treated worms displayed ultrastructural abnormalities like those observed after treatment with **PMZ**; largely necrotic gonad contents, although the walls of the gonad still appeared intact (Figure 2H), and electron dense lysosomes were scattered throughout the muscle fibers (Figure 2I).

**2.2.3. Proroxan Analogs.** **PRO** had excellent potency against adult *B. pahangi*, low cytotoxicity, and killed 97% of secreted mf ($P = 2.3 \times 10^{-5}$; F-$IC_{50}$ = 4.2 μM, M-$IC_{50}$ = 2.5


https://doi.org/10.1021/acs.jmedchem.6c01435
J. Med. Chem. XXXX, XXX, XXX−XXX

**Scheme 3. Synthesis of Proroxan (PRO) Analogs**[a]

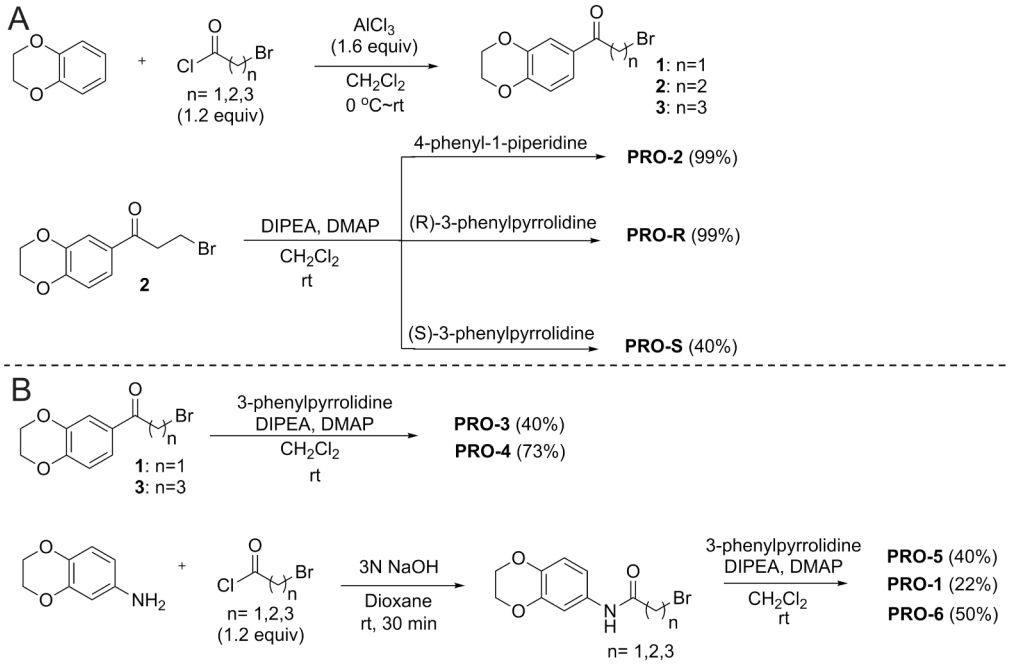


[a](**A**) Benzo(1,4)-dioxane undergoes Friedel-crafts acylation with various bromoacyl chlorides elongating the carbon chain from 1 to 3 carbons synthesizing crude products **1**−**3**. Product **2** underwent nucleophilic substitution under basic conditions with phenyl substituted piperidine and pyrrolidine reagents to give **PRO-2**, **PRO-R** and **PRO-S**. Similar reaction conditions were applied to **1** and **3** with 3-phenylpyrrolidine and afforded **PRO-3** and **PRO-4**. (**B**) Amide-linked analogs were synthesized using 3,4-ethylenedioxyaniline starting material with the same group of bromoacyl chlorides. Nucleophilic substitution with the free primary amine under basic conditions gives crude amide substituted products which all were coupled to 3-phenylpyrrolidine to give the amide-linked analogs **PRO-5**, **PRO-1** and **PRO-6**.

$\mu$M; $CC_{50}$ = 99.8 $\mu$M; F−SI = 23.6 and M-SI = 39.4; Figure 3A). Replacing the phenyl pyrrolidine moiety with a phenylpiperidine moiety (**PRO-1**) decreased female but increased male *B. pahangi* potency (F-$IC_{50}$ = 10.9 $\mu$M, M-$IC_{50}$ = 0.65 $\mu$M; Scheme 3). Although **PRO-1** cytotoxicity was slightly increased, it improved mf reduction to 100% ($P = 4.3 \times 10^{-9}$; $CC_{50}$= 85.4 $\mu$M, F−SI = 7.8 and M-SI = 132.2). Activity was lost when with the addition of an amide linker (**PRO-2**). Interestingly, shortening the carbon chain by one atom (**PRO-3**) lead to increased potency against female *B. pahangi* (F-$IC_{50}$ = 1.2 $\mu$M) but lost activity against males. **PRO-3** cytotoxicity was comparable to **PRO**, but showed much higher selectivity ($CC_{50}$ = 93.6 $\mu$M; SI = 75.1), and less activity against mf (81.0%, $P$ = 0.031). Elongation to a 3-carbon chain (**PRO-4**) and amide-linking (**PRO-5** and **PRO-6**) were inactive. Modifying the benzo(1,4)-dioxane fused ring to a 1,2-dimethoxy substituted benzene (**PRO-8**) showed the best potency against males, with a slight reduction in potency against females (M-$IC_{50}$ = 0.30 $\mu$M, F-$IC_{50}$ = 6.6 $\mu$M). **PRO** contains one stereocenter at the third carbon of the pyrrolidine ring that was tested initially as a racemic mixture. Commercially available (R) or (S)-3-phenylpyrrolidine was used to synthesize **PRO-R** and **PRO-S,** which were comparable to **PRO**, so controlling the stereochemistry is not necessary to improve biological activity (F-$IC_{50}$ = 4.4 $\mu$M and 5.5 $\mu$M, respectively). However, stereochemistry remains a critical consideration for optimizing downstream ADME properties and minimizing potential off-target toxicities.[63]

**PRO**, **PRO-1** and **PRO-3** resulted in 100% mobility inhibition in male *O. ochengi*, but were not active in females. Against *O. volvulus*, all three showed low L3 molting and L4 viability inhibition, with **PRO-1** producing the most L4 viability inhibition (48%). As none of these compounds gave high levels (>50%) of MI in female *O. ochengi* or the larval *O. volvulus*, **PRO** was down-selected for further development.

Structural analyses of *B. pahangi* adult female worms (Figure 3B and 3C) showed that **PRO**-treated worms were profoundly affected, exhibiting a total loss of gonad integrity and contents (Figure 3D and inset), and the hypodermis appeared loaded with numerous membrane-bound vesicular structures (Figure 3E, white arrowheads). Surprisingly, treatment with **PRO-3** did not appear to cause any apparent ultrastructural deformities (Figure 3H and 3I).

**2.2.4. Suloctidil Analogs.** **SUL** displayed excellent potency against *B. pahangi*, but has known liver toxicity in humans[64] (F-$IC_{50}$ = 7.9 $\mu$M, M-$IC_{50}$ = 1.8 $\mu$M; Figure 4A). Accordingly, we observed high cytotoxicity, and evaluated diverse SAR while monitoring changes in cytotoxicity ($CC_{50}$ = 5.3 $\mu$M; F−SI = 0.67, M-SI = 2.9). We first replaced the *S*-isopropyl ether with *O*-isopropyl ether for *O*-ether analogs (**S-2**, **S-4** and **S-7**) followed by replacing the *N*-octyl alkyl chain with different groups (*N*-capped analogs **S-1**, **S-2**, **S-10**, **S-11**, **S-13** and **S14**; Scheme 4). The potency of the *O*-ether analogs **S-2**, **S-4** and **S-7** was slightly better against both females and males (F-$IC_{50}$ = 3.6 $\mu$M, 7.3 $\mu$M and 6.0 $\mu$M, respectively; M-$IC_{50}$ = 0.67 $\mu$M, 0.28 $\mu$M and 5.3 $\mu$M). Due to decreased cytotoxicity, parasite selectivity was increased by 4.8-fold and 6.0-fold for female and male with **S-2**, 3.3-fold and 20.2-fold for **S-4**, and 5.9-fold and 1.6-fold for **S-7**. *O*-ether analogs with a benzyl group (instead of methyl for **S-2** and **S-4**) have similar activity to *S*-ether analogs (e.g., **S-9**, F-$IC_{50}$ = 24.7 $\mu$M, M-$IC_{50}$ = 0.80 $\mu$M).

Due to its two chiral centers, we synthesized the three **SUL** diastereomers (**S-9, S-12, S-15**) to understand how the


https://doi.org/10.1021/acs.jmedchem.6c01435
J. Med. Chem. XXXX, XXX, XXX−XXX

**A**

| Entry | Compound: Suloctidil / Modifications | | | | | | *Brugia pahangi*: Day 3 $IC_{50}$ (μM) | | | | *Onchocerca ochengi*: Motility Inhibition @ 100 μM (%) | | *Onchocerca ochengi*: Day 7 $IC_{50}$ (μM) | | *Onchocerca ochengi*: Day 5 $IC_{50}$ (μM) | | *Onchocerca volvulus* | HepG2 cells cytotoxicity | | Selectivity Index | |
|---|---|---|---|---|---|---|---|---|---|---|---|---|---|---|---|---|---|---|---|---|---|
| | | | | | | | Female | | Male | | Female | Male | Female | | Male | | L3 molting inhibition (%) Day 6 @ 3 μM / *10 μM | $CC_{50}$ (μM) | $R^2$ | (HEPG2 $CC_{50}$ / *B. pahangi* $IC_{50}$) | |
| | | | | | | | | | | | | | | | | | | | | Female | Male |
| | X | $R^1$ | $R^2$ | $R^3$ | $R^4$ | $R^5$ | F-$IC_{50}$ | $R^2$ | M-$IC_{50}$ | $R^2$ | Day 7 | Day 5 | $IC_{50}$ | $R^2$ | $IC_{50}$ | $R^2$ | | Day 1 | Day 1 | F-SI | M-SI |
| **SUL** | S | H | OH | H | Me | n-$C_8H_{17}$ | 7.9 | 0.98 | 1.8 | 0.95 | 100 | 100 | 1.8 | 1.0 | 2.6 | 1.0 | 18.6 / 100* | 5.3 | 0.94 | 0.67 | 2.9 |
| **S-1** | O | OH | H | $CH_2Ph$ | H |  | Inactive | | 25.5 | 0.90 | ND | ND | ND | ND | ND | ND | ND | 43.0 | 0.61 | ND | 1.7 |
| **S-2** | O | H | OH | $CH_2Ph$ | H | n-$C_8H_{17}$ | 3.6 | 1.0 | 0.67 | 0.84 | 100 | 100 | 3.3 | 0.94 | 5.4 | 1.0 | Inactive | 11.5 | 0.63 | 3.2 | 17.2 |
| **S-3** | O | OH | H | $CH_2Ph$ | H | H | Inactive | | 11 | 0.59 | ND | ND | ND | ND | ND | ND | ND | >50 | - | ND | >4.5 |
| **S-4** | O | OH | H | $CH_2Ph$ | H | n-$C_8H_{17}$ | 7.3 | 1.0 | 0.28 | 0.86 | 100 | 100 | ND | ND | ND | ND | Inactive | 16.2 | 1.0 | 2.2 | 58.2 |
| **S-5** | O | OH | H | $CH_2Ph$ | H | 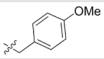 | 6.5 | 0.86 | 1.1 | 0.86 | 100 | 100 | ND | ND | ND | ND | Inactive | 24.7 | 0.98 | 3.8 | 22.2 |
| **S-6** | O | H | OH | H | Me | H | Inactive | | Inactive | | ND | ND | ND | ND | ND | ND | ND | >50 | - | ND | ND |
| **S-7** | O | H | OH | H | Me | n-$C_8H_{17}$ | 6.0 | 0.98 | 5.3 | 0.54 | ND | ND | ND | ND | ND | ND | ND | 23.8 | 0.71 | 4.0 | 4.5 |
| **S-8** | S | OH | H | H | Me | Boc | Inactive | | Inactive | | ND | ND | ND | ND | ND | ND | ND | >50 | - | ND | ND |
| **S-9** | S | OH | H | H | Me | n-$C_8H_{17}$ | 24.7 | 0.94 | 0.80 | 0.76 | 100 | 100 | ND | ND | ND | ND | 52.5 | 4.0 | 0.52 | 0.16 | 4.9 |
| **S-10** | S | OH | H | H | Me | n-$C_6H_{13}$ | 12.0 | 1.0 | 2.7 | 0.90 | 100 | 100 | 3.3 | 0.80 | 2.6 | 0.94 | 56.4 | 9.5 | 0.98 | 0.79 | 3.5 |
| **S-11** | S | OH | H | H | Me | n-$C_{10}H_{21}$ | 6.3 | 0.92 | 0.50 | 0.75 | ND | ND | ND | ND | ND | ND | ND | 6.6 | 0.85 | 1.0 | 13.1 |
| **S-12** | S | H | OH | Me | H | n-$C_8H_{17}$ | 7.8 | 0.99 | 0.82 | 0.94 | 100 | 100 | ND | ND | ND | ND | ND | 6.6 | 0.88 | 0.86 | 8.1 |
| **S-13** | S | H | OH | Me | H |  | Inactive | | 1.4 | 0.81 | ND | ND | ND | ND | ND | ND | ND | 20.2 | 0.89 | ND | 14.6 |
| **S-14** | S | H | OH | Me | H |  | Inactive | | Inactive | | ND | ND | ND | ND | ND | ND | ND | >50 | - | ND | ND |
| **S-15** | S | OH | H | Me | H | n-$C_8H_{17}$ | 1.1 | 0.67 | 1.3 | 0.54 | 100 | 100 | ND | ND | ND | ND | ND | 6.6 | 1.0 | 6.3 | 5.1 |
| **S-16** | O | H | H | $CH_2Ph$ | H | n-$C_8H_{18}$ | 8.3 | 0.66 | 1.0 | 0.64 | 100 | 100 | 0.14 | 1.0 | 0.87 | 1.0 | Inactive | 14.0 | 1.0 | 1.7 | 13.4 |
| **S-17** | O | OEt | H | $CH_2Ph$ | H | n-$C_8H_{19}$ | 6.5 | 0.61 | 2.6 | 0.77 | 100 | 100 | 0.29 | 1.0 | 3.6 | 0.93 | 58.2 | 20.7 | 0.99 | 3.2 | 8.0 |

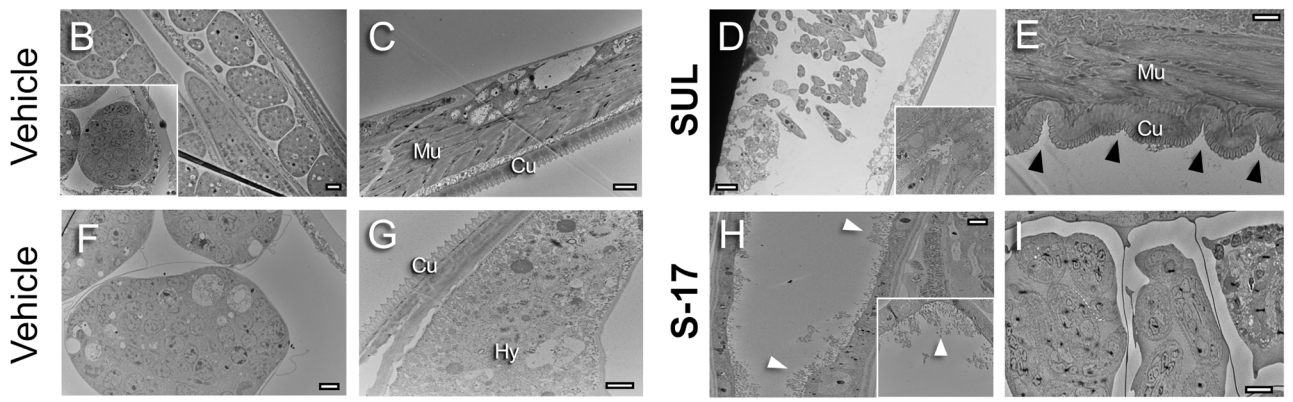


**Figure 4.** Semithroughput phenotypic screening and *in vitro* transmission electron microscopy (TEM) results for suloctidil (**SUL**) and analogs. (**A**) Activity and selectivity of **SUL** analogs in three different filarial nematode species. **S-9**, **S-12**, and **S-15** are diastereomers of each other. ND = Not Done. "Inactive" = not active in initial *B. pahangi* screens at 10 μM (so $IC_{50}$ values were not calculated), or <50% inhibition in *O. volvulus*. $IC_{50}$ = inhibitory concentration corresponding to 50% inhibition of worm motility; $R^2$ values indicate how well the fitted dose−response curve matches the experimental data points; Complete $IC_{50}$ statistics are provided in Table S1. $CC_{50}$ = Cytotoxicity concentration, corresponding to 50% death of HepG2 cells. "Selectivity index" represents the ratio of $CC_{50}$ to $IC_{50}$, corresponding to the fold-increase of efficacy in worms relative to mammalian


https://doi.org/10.1021/acs.jmedchem.6c01435
J. Med. Chem. XXXX, XXX, XXX−XXX

**Figure** 4. continued

cells. Panels B–I show ultrastructural alterations induced by 3 days of 30 $\mu$M *in vitro* treatment in adult female *B. pahangi*. (**B**) A vehicle-treated worm with a normal gonad with a healthy embryo shown in the inset, and (**C**) a normal hypodermis and cuticle. (**D**) A gonad of a **SUL**-treated worm containing several inclusions that resemble sperm, but no recognizable developmental stages; a deformed gut containing no microvilli is shown in the inset. (**E**) An abnormal hypodermis of a **SUL**-treated worm, where the cuticle is markedly undulant (black arrowheads) and the underlying muscle fibers appear deformed. (**F**&**G**) Normal ultrastructure of vehicle-treated worms from a second experiment for **C-8** treatment. (**H**) A deformed gut from an **S-17** treated worm, where microvilli appear destroyed (white arrowheads). Another deformed gut is shown in high magnification in the inset. (**I**) A gonad of an **S-17** treated worm displaying mostly normal, healthy microfilariae with few deformed microfilariae. Cu: cuticle; Mu: muscle; Hy: hypodermis; Scale bars represent 2 $\mu$m. Brightness and contrast adjustments were applied to the entire image.

**Scheme 4. Synthesis of SUL Derivatives and Analogs**[a]

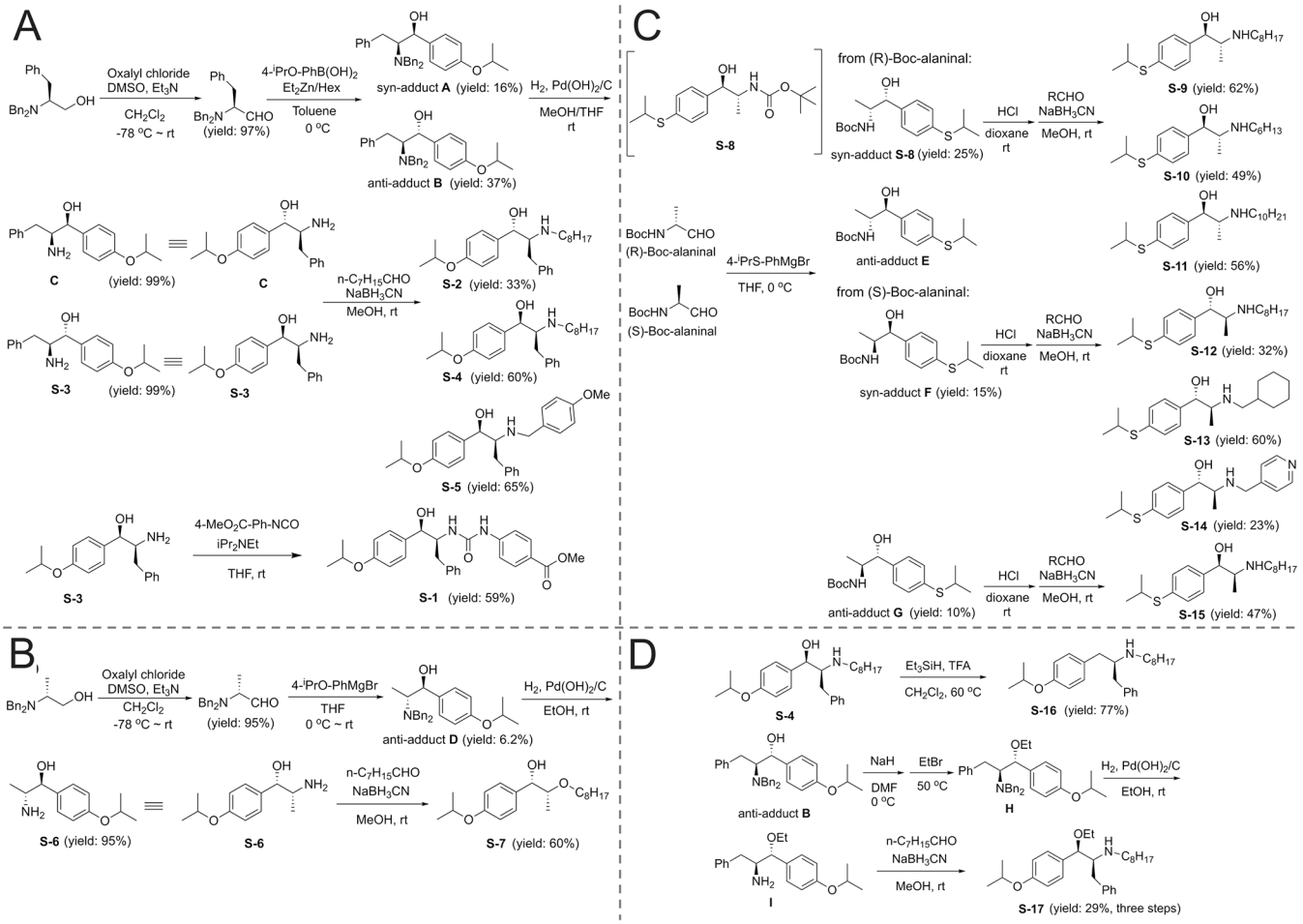


[a](**A**) Suloctidil analogs have two stereo centers which are created through nucleophilic reaction between aldehydes and organometallic species. The synthesis of "phenylalaninol type" suloctidil analogs is shown. Swern oxidation of N,N-dibenzyl-L-phenylalaninol gave N,N-dibenzyl-L-phenylalaninal. Subsequent nucleophilic addition by organozinc species generated in situ from diethyl zinc with 4-isopropoxyphenylboronic acid afforded syn-adduct A and antiadduct B, which upon debenzylation via Pd/C catalyzed hydrogenation yielded **C** and **S-3.** They then underwent reductive amination with appropriate aldehydes to afford **S-2**, **S-4**, **S-5**. Coupling of **S-3** with 4-methoxycarbonylphenyl isocyanate gave **S-1**. (**B**) The preparation of "alaninol type" suloctidil analogs is depicted in Scheme 4B and was followed in a similar strategy as "phenylalaninol type" described before. Swern oxidation of N,N-dibenzyl-D-alaninol afforded N,N-dibenzyl-D-alaninal, which then reacted with 4-isopropoxyphenylmagnesium bromide to give antiadduct **D** preferentially. Subsequent debenzylation through Pearlman's catalyst catalyzed hydrogenation furnished **S-6,** which underwent reductive amination to yield **S-7**. (**C**) The suloctidil diastereomers and other thioether type analogs were synthesized starting with (R) or (S)-Boc-alaninal. Nucleophilic addition of 4-(isopropylthio)phenylmagnesium bromide to Boc-alaninal afforded syn-adduct **S-8**, antiadduct **E** from (R)-Boc-alaninal and syn-adduct **F**, antiadduct **G** from (S)-Boc-alaninal. Subsequent Boc deprotection, followed by reductive amination with appropriate aldehyde yielded **S-9**, **S-10**, **S-11**, **S-12**, **S-13**, **S-14**, **S-15** respectively. (**D**) The preparation of dehydroxy suloctidil analog **S-16** and ethyl-capped suloctidil analog **S-17**. Deoxygenation of **S-4**, mediated with $Et_3SiH$ and TFA, afforded **S-16**. Starting with antiadduct **B**, deprotonation with sodium hydride followed by ethyl alkylation gave intermediate **H**, which was subsequently debenzylated via Pearlman's catalyst catalyzed hydrogenation to furnish intermediate **I**. Finally, reductive amination from **I** yielded **S-17**.

orientation of methyl and hydroxyl groups affects potency. **S-15** was improved (F-$IC_{50}$ = 1.1 $\mu$M, M-$IC_{50}$ = 1.3 $\mu$M), **S-12** was within **SUL** range (F-$IC_{50}$ = 7.8 $\mu$M, M-$IC_{50}$ = 0.82 $\mu$M) and **S-9** was much worse against females but better against males (F-$IC_{50}$ = 25 $\mu$M, M-$IC_{50}$ = 0.80 $\mu$M). **S-9** did not increase selectivity for females, but improved M-SI by 5.9-fold,


https://doi.org/10.1021/acs.jmedchem.6c01435
J. Med. Chem. XXXX, XXX, XXX−XXX

A *In vivo* treatment

| Compound | Animal model | Administration | Dose (mg/kg) | Exposure ($AUC_{inf}$) ng·h/mL Avg | ng·h/mL Std. err. | μM·h Avg | μM·h Std. err. | Peak concentration ($C_{max}$) ng/mL Avg | ng/mL Std. err. | μM Avg | μM Std. err. | Half-life ($t_{1/2}$) hours Avg | hours Std. err. | Apparent clearance $CL_{app}$ (L/h/kg) Avg | Std. err. |
|---|---|---|---|---|---|---|---|---|---|---|---|---|---|---|---|
| **CLE** | Gerbil | PO | 50 | 812.3 | 104.4 | 2.49 | 0.32 | 252.0 | 50.0 | 0.8 | 0.2 | 4.9 | 0.7 | 62.6 | 8.0 |
| **C-7** | Gerbil | PO | 50 | 221.1 | 24.6 | 0.68 | 0.08 | 28.7 | 14.2 | 0.1 | 0.0 | 9.7 | 0.6 | 232.6 | 29.1 |
| **C-8** | Gerbil | PO | 50 | 934.4 | 96.6 | 2.32 | 0.24 | 206.3 | 35.1 | 0.5 | 0.1 | 5.6 | 0.4 | 54.7 | 6.0 |
| **C-4** | Mice | IP+PO | 3+10 | 838.7 | 32.3 | 2.68 | 0.10 | 662.5 | 184.5 | 2.1 | 0.6 | 1.1 | 0.4 | 11.9 | 0.5 |
| **PMZ** | Gerbil | PO | 50 | 2853 | - | 6.18 | - | 134.0 | - | 0.3 | - | 9.3 | - | 17.5 | - |
| **PMZ-5** | Gerbil | PO | 50 | 3269 | 525.8 | 5.93 | 0.95 | 255.3 | 23.7 | 0.5 | 0.0 | 13.8 | 0.9 | 16.0 | 2.3 |
| **PMZ-6** | Mice | IP+PO | 3+10 | 1934 | 246.2 | 4.07 | 0.52 | 695.0 | 121.0 | 1.5 | 0.3 | 2.2 | 0.7 | 5.3 | 0.7 |
| **PRO-1** | Mice | IP+PO | 3+10 | 591.4 | 22.7 | 1.68 | 0.06 | 810.0 | 159.0 | 2.3 | 0.5 | 0.6 | 0.2 | 16.9 | 0.6 |
| **SUL** | Gerbil | PO | 50 | 93.1 | 11.7 | 0.28 | 0.03 | 4.2 | 0.37 | 0.0 | 0.00 | 17.4 | 0.08 | 545.6 | 68.3 |
| **S-17** | Gerbil | PO | 50 | 6327 | 1193 | 14.86 | 2.80 | 599.7 | 256.3 | 1.4 | 0.6 | 23.0 | 13.8 | 8.5 | 1.6 |

B

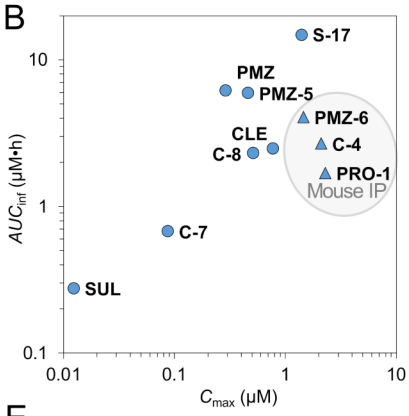


C Liver microsomes

| Compound | $t_{1/2}$ (min) | $CL_{int}$ (μL/min/mg) | Predicted *in vivo* $CL_{app}$ (L/h/kg) |
|---|---|---|---|
| **CLE** | 2.4 | 551.2 | 63.5 |
| **C-4** | 0.4 | 3302.9 | 380.8 |
| **C-6** | 1.5 | 847.3 | 97.7 |
| **C-7** | 0.7 | 1822.5 | 210.1 |
| **C-8** | 6.9 | 188.6 | 21.7 |
| **PMZ** | 13.0 | 100.8 | 11.6 |
| **PMZ-6** | 2.6 | 496.4 | 57.2 |
| **PRO** | 2.3 | 558.5 | 64.4 |
| **PRO-1** | 0.7 | 1843.9 | 212.6 |
| **SUL** | 0.5 | 2877.5 | 331.8 |
| **S-5** | 5.4 | 241.5 | 27.8 |
| **S-16** | 1.1 | 1190.6 | 137.3 |
| **S-17** | 8.5 | 153.9 | 17.7 |

D

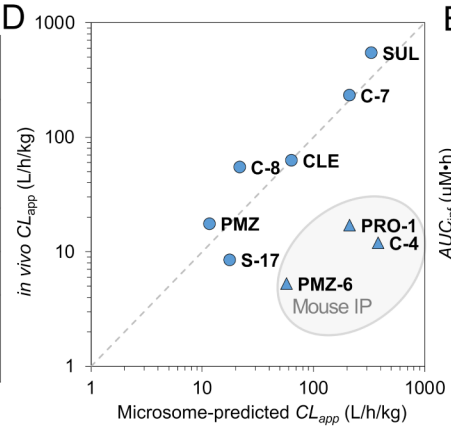


E

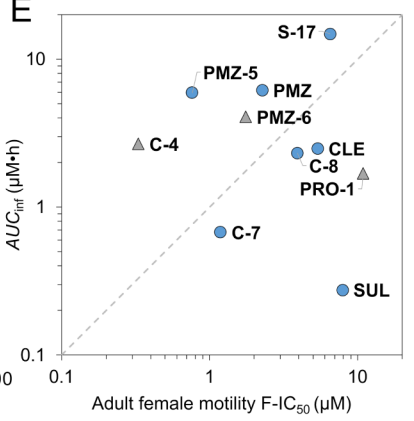


**Figure 5.** Pharmacokinetic profiling of **CLE**, **PMZ**, **SUL**, and selected analogs. (**A**) Summary of *in vivo* pharmacokinetic parameters, with darker colored shading indicating better exposure properties for pharmacokinetic performance. Compounds were administered via oral gavage (PO, 50 mg/kg) in gerbils or intraperitoneal injection (IP, 10 mg/kg) in mice (rows shaded in gray). Metrics include total exposure ($AUC_{inf}$), peak concentration ($C_{max}$), terminal half-life ($t_{1/2}$), and apparent clearance ($CL_{app}$). Standard error of the mean values are calculated, $n$ = 2 or 3 per compound, except **PMZ** ($n$ = 1). Four time points were used for gerbil testing, and eight time points were used for mouse testing. (**B**) The relationship between total systemic exposure ($AUC_{inf}$) and peak plasma concentration ($C_{max}$). (**C**) Statistics for hepatic metabolic stability in liver microsomes, including *in vitro* half-life ($t_{1/2}$) and intrinsic clearance ($CL_{int}$). Predicted *in vivo* clearance ($CL_{app}$) was calculated based on $CL_{int}$, and estimates of microsomal content in the liver and relative liver mass. (**D**) Microsome-predicted clearance (*in vitro-in vivo* extrapolation; IVIVE) values compared to observed *in vivo* apparent clearance values, for all compounds tested in both assays. The dashed line indicates equal values, and the shaded region highlights the mouse IP cohort (triangle symbols), which displays significant under-prediction of clearance compared to the gerbil PO cohort. (**E**) The pharmacokinetic-pharmacodynamic (PK−PD) relationship, between adult female *B. pahangi* motility F-$IC_{50}$ values and observed *in vivo* systemic exposure ($AUC_{inf}$). The dashed line represents a 1:1 potency-to-exposure ratio.

while **S-15** displayed 5.3-fold and 5.1-fold increased selectivity for female and male parasites, respectively.

Next, the **SUL** *OH* (hydroxyl) was either capped with an ethyl group (**S-17**) or completely removed (**S-16**); surprisingly, this *OH* group contributed little to the potency of **SUL** analogs, since both had similar activity, despite lower bioaccumulation (**S-16** F-$IC_{50}$ = 8.3 μM, M-$IC_{50}$ = 1.0 μM; **S-17** F-$IC_{50}$ = 6.5 μM, M-$IC_{50}$ = 2.6 μM). By altering or removing this hydroxyl group, we disrupt the alkanolamine core that causes suloctidil's known liver toxicity. This shows we can successfully reduce damage to mammalian cells without losing active potency against the worms.

We also investigated different *N*-substitutions ($R^5$). No substantial activity difference was observed from substituting the amino with a longer n-decyl group (**S-11**: F-$IC_{50}$ = 6.3 μM, M-$IC_{50}$ = 0.5 μM) or a shorter *n*-hexyl or cyclohexylmethyl group (**S-10**: F-$IC_{50}$ = 12.1 μM, M-$IC_{50}$ = 2.7 μM). **S-13** retained activity only in male (M-$IC_{50}$ = 1.4 μM; M-SI = 14.6). When uncapped (**S-3, S-6**), or capped with Boc (**S-8**), 4-pyridylmethyl (**S-14**) or a phenyl urea (**S-1**), the activity of the compounds to the female worms was eliminated.

*B. pahangi* fecundity is substantially reduced by **SUL**, and all active first-generation analogs killed 100% of mf ($P \leq 2.4 \times 10^{-4}$), except for **S-9** (81.3%; $P$ = 0.016). Reduction of secretions by the inactive **S-6** and **S-8**, and female-specific **S-3** was nonsignificant. Other male-specific analogs reduced mf, including by 100% for **S-1** ($P = 1.1 \times 10^{-5}$) and **S-13** ($P = 1.8 \times 10^{-11}$) and by 67.5% for **S-14** ($P = 6.6 \times 10^{-4}$). Deformed embryos significantly increased in relative abundance with **S-9** (53.5%, $P$ = 0.0028) and **S-10** (26.3%, $P$ = 0.0090), and **S-9** concurrently significantly decreased eggs (−9.6%, $P$ = 0.032), embryos (−39.5%, $P$ = 0.0020) and premf (−14.3%, $P$ = 0.049). **SUL** and its 4 adulticidal analogs **S-12**, **S-15**, **S-16** and **S17** were also larvicidal against L4 *B. pahangi*.

**SUL** induced a wide range of ultrastructural abnormalities by TEM compared to vehicle (Figure 4B and 4C), including gonads of devoid of recognizable developmental stages and filled with small inclusions that resemble nematode sperm (Figure 4D). The gut appeared deformed and lacked microvilli (inset, Figure 4E), and the cuticles and underlying muscle fibers were severely distorted with marked undulation throughout the length of the cuticle (Figure 4E, black arrowheads). **S-17** induced a similar phenotype compared to


https://doi.org/10.1021/acs.jmedchem.6c01435
J. Med. Chem. XXXX, XXX, XXX−XXX

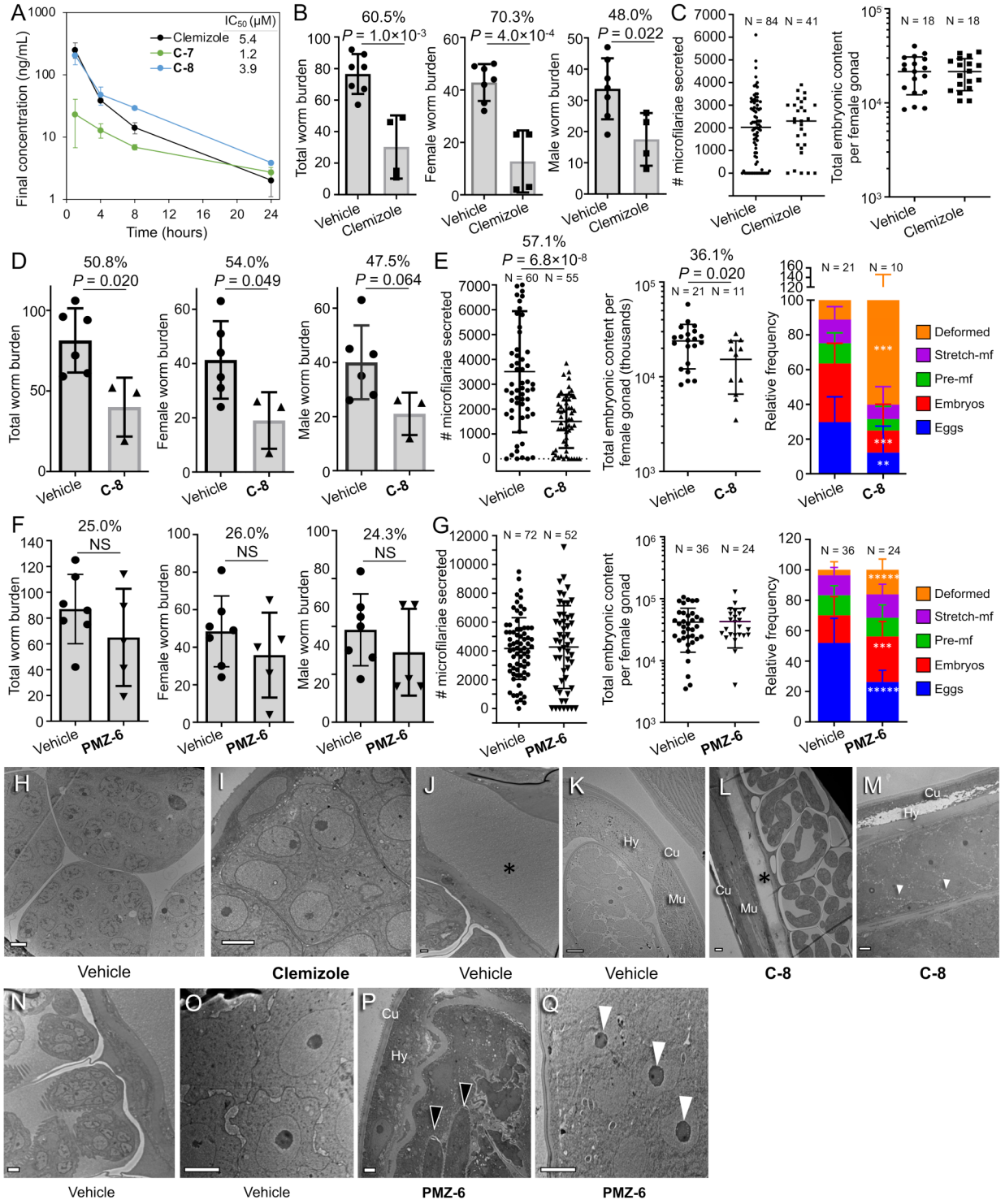


**Figure 6.** *In vivo* testing (PO, BID 6 h apart, 10 days) for clemizole (**CLE**, 25 mg/kg), **C-8** (50 mg/kg), and **PMZ-6** (25 mg/kg) in gerbils infected with *B. pahangi*. (**A**) *In vivo* PK data for **CLE** and analogs, with adult female day 3 motility $IC_{50}$ values shown. (**B**) Worm burden reduction with **CLE** treatment. (**C**) mf secretion and embryonic contents from adult female worms with **CLE** treatment (25 mg/kg). (**D**) Worm burden reduction with **C-8** treatment (50 mg/kg). (**E**) mf secretion, embryonic contents and embryogram results from adult female worms with **C-8** treatment. (**F**) Worm burden reduction with **PMZ-6** treatment. (**G**) mf secretion, embryonic contents and embryogram results from adult. Significant reduction of worm burden, mf secretion and embryonic content were tested using one-tailed pooled student's *t* tests compared to vehicle controls. For embryogram plots $^{***}P \leq 1 \times 10^{-3}$, $^{****}P \leq 1 \times 10^{-4}$, $^{*****}P \leq 10^{-5}$ vs vehicle controls, using two-tailed pooled student's *t* tests compared to vehicle controls, with FDR correction for multiple testing. A significant increase in deformed embryos, and a decrease of normal embryos and eggs was observed for both **C-8** and **PMZ-6**. Detailed statistical results for all comparisons are provided in Table S1. (**H-M**) Ultrastructural alterations induced by *in vivo* treatment with **CLE** and **C-8** compared to vehicle treatment. (**N-Q**) Ultrastructural alterations induced by *in vivo* treatment with **PMZ-6** compared to vehicle treatment. Brightness and contrast adjustments were applied to the entire image. Detailed embryogram results are provided in Figure S4. For bar graphs, error bars represent standard deviations of the mean values, and *P* values represent pooled student's *t* test comparisons to vehicle-only controls, with sample numbers as shown.


https://doi.org/10.1021/acs.jmedchem.6c01435
J. Med. Chem. XXXX, XXX, XXX−XXX

the vehicle (Figure 4F and 4G), with complete destruction of microvilli and their projections, and apparent loss of rootlets attached to the gut wall (Figure 4H). However, **S-17** did not profoundly affect embryogenesis, as mostly normal gonad contents were observed (Figure 4I).

Overall, the best potency was observed for **S-15** (stereoisomer of **SUL**): *B. pahangi* F-$IC_{50}$ = 1.0 $\mu$M, 100% *O. ochengi* MI in male and female, and decreased cytotoxicity vs **SUL** (9-fold F−SI improvement). **S-3**, which has a Me group replaced with Bn has $CC_{50}$ > 50 $\mu$M but was only active in males (M-$IC_{50}$ = 11 $\mu$M). **S-17** (OEt of **S-3**), **S-7** (S to O) and **S-16** (OEt of **S-17** to H) are also attractive leads with less cytotoxicity and good *B. pahangi* potency. All nine *B. pahangi* hits that were tested in *O. ochengi* showed 100% motility (male worms) and viability (adult female) inhibition at 100 $\mu$M, with **S-16** and **S-17** having the best potency (**S-16** F-$IC_{50}$ = 0.14 $\mu$M, M-$IC_{50}$ = 0.87 $\mu$M; **S-17** F-$IC_{50}$ = 0.29 $\mu$M, M-$IC_{50}$ = 3.6 $\mu$M). Three analogs were also larvicidal in *O. volvulus* (**S-9**, **S-10** and **S-17** > 50% L3 molting inhibition, vs 18.6% at 3 $\mu$M for **SUL**).

For all compounds, SMILES strings, IUPAC IDs, chemical formulas, and other physical properties for all compounds are provided in Table S1. All *B. pahangi* $IC_{50}$ and HepG2 $CC_{50}$ curves and statistics are provided in Supplementary Data.

### 2.3. Predictive Modeling of Anthelmintic Activity Using Machine Learning

A random forest (RF) machine learning model was used to distinguish compound properties associated with *B. pahangi* MI. For model training, compounds were categorized as "active" (≥50% MI in both sexes at day 3, 10 $\mu$M; n = 23) or "inactive" (<50%; n = 16). Based on compound properties alone (Table S3A), leave-one-out RF achieved 92.3% accuracy of classification (binomial distribution test $P = 4.4 \times 10^{-7}$; AUC = 98.64%, $P = 1.1 \times 10^{-7}$ for the ROC-derived AUC differing from 50%). The three misclassifications, **PRO** and its analogs **PRO-1** and **PRO-4**, suggest unique mechanisms of activity for this series. Excluding **PRO** and analogs improved classification accuracy to 94.1% ($P = 1.7 \times 10^{-6}$), binomial distribution test; AUC = 99.27%, $P = 2.5 \times 10^{-7}$; prediction scores and motility data in Table S3B, model performance data in Table S3C). The top predictive features (MDA > 10; Table S3D) included molecular volume, octanol/water partition coefficient, volume-normalized squared dipole, solvent-accessible surface area, count of amine groups, and hydrophobic surface area, all of which are properties presumably linked to worm cuticle penetration.[65] Prior cuticle permeability assays confirmed that hydrophobicity enhances *B. pahangi* cuticle permeability,[56] reinforcing the role of these features in guiding SAR-based drug design.

Among the **CLE** analogs, **C-8** had the highest scoring properties associated with activity (RF prediction score = 0.916, compared to 0.775 for **CLE**), and among the **PMZ** analogs, **PMZ-6** scored the highest (0.950, compared to 0.675 for **PMZ**). **SUL** had the second-highest RF prediction score among all compounds (0.995), with six active **SUL** analogs having scores >0.95, including **S-15** (the highest-scoring compound, 0.996) and **S-17** (0.951). These RF scores highlight that these particular compounds have combinations of physical properties predicted to be associated with activity in our *B. pahangi in vitro* model.

### 2.4. *In Vivo* Activity of CLE, C-8, PMZ-6, SUL, and S-17 in *B. Pahangi*-Infected Gerbils

Compounds with the best *in vitro* activity were further prioritized based on their physicochemical properties. Filarial worms reside in the lymphatic system (*Brugia* spp.) or subcutaneous tissue (*Onchocerca* spp.). To assess compound bioavailability, we tested solubility at 200 $\mu$M in fasted/fed simulated intestinal (FaSSIF, FeSSIF) and gastric fluids (FaSSGF). **CLE** analogs **C-3**, **C-4**, **C-6**, **C-7**, and **C-8** were soluble in all media; **C-11** was insoluble in FaSSIF. Among **SUL** analogs, **S-9** was insoluble in FaSSIF (with 4× lower F−SI than **SUL**), **S-2** and **S-4** were partially soluble, and **S-5**, **S-10**, **S-16**, and **S-17** were fully soluble. In FaSSGF, both **S-4** and **S-17** showed partial solubility (Figure S3A).

Statistical analysis of rodent *in vivo* pharmacokinetics (PK) was performed for **CLE**, **PMZ**, **SUL** and seven analogs of interest (Figure 5A; all raw and processed data provided in Table S4; PK curves presented in Figure S3B). In the PO gerbil model (50 mg/kg, by oral gavage), **C-8** had similar PK values to its parent **CLE**, while **C-7** had significantly lower exposure (3.7-fold lower $AUC_{inf}$; $P$ = 0.0059 two-tailed student's $t$-test), peak concentration (8.8-fold lower $C_{max}$; $P$ = 0.013) and apparent clearance (3.7-fold faster; $P$ = 0.021). **PMZ-5** had similar PK values with **PMZ**. **S-17** showed substantially improved PK properties compared to **SUL** including higher exposure (53.9-fold higher $AUC_{inf}$; $P$ = 0.027), peak concentration (143.1-fold higher $C_{max}$; N/S due to high variability from 303 to 1110 ng/mL for **S-17**) and apparent clearance (64.3-fold slower; $P$ = 0.0018). In terms of the combination of overall total exposure and peak concentration, **S-17** performed better than all analogs tested while **SUL** had the poorest PK (Figure 5B).

Metabolic stability was assessed using mice liver microsomes (MLM) to calculate half-life and intrinsic clearance rates (Figure 5C). Substantial improvements compared to parent compounds were observed for **C-8** relative to **CLE** (2.9-fold slower clearance rate) and for **S-17** compared to **SUL** (18.7-fold slower clearance rate), consistent with its improved *in vivo* PK. *In vitro-in vivo* extrapolation (IVIVE) was performed to compare liver microsome clearance to *in vivo* results (Figure 5D). Very good correlation was observed for the observed and predicted $CL_{app}$ values for gerbil PO compounds, suggesting that hepatic metabolism is the dominant clearance mechanism for these compounds (Pearson $r$ = 0.976, $P = 4.2 \times 10^{-4}$). For the *in vivo* mouse IP group (shaded gray), the liver microsome model consistently overpredicts clearance, likely the result of plasma protein binding or route-specific factors that the microsome system does not replicate.[66]

A PK/PD comparison ($AUC_{inf}/IC_{50}$; Figure 5E) was performed to compare the average *in vivo* systemic exposure ($\mu$M·h) to the *B. pahangi* adult female $IC_{50}$ values ($\mu$M) for each compound. Compounds positioned above the diagonal dashed line achieved systemic exposures exceeding their *in vitro* inhibitory concentrations, including **PMZ-6** and **S-17**.

Based on solubility, metabolic stability and PK, **CLE**, **C-8** and **PMZ-6** were selected for *in vivo* studies. **CLE** significantly reduced *B. pahangi* worm burden but had no significant effect on mf production or embryogenesis (Figure 6B, Figure 6C; 25 mg/kg PO, BID 6 h apart, 10 days; worm reduction total: 60.5%, $P = 1.0 \times 10^{-3}$; female: 70.3%, $P = 4.0 \times 10^{-4}$; male: 48.0%, $P$ = 0.022). Based on filarial modeling analysis,[67] a macrofilaricidal efficacy of 60% may be at least as beneficial to patients as the transient mf clearance elicited by many


https://doi.org/10.1021/acs.jmedchem.6c01435
J. Med. Chem. XXXX, XXX, XXX−XXX

commonly used microfilaricides (e.g., ivermectin and DEC), and is sufficient efficacy for an effective trial design. At 25 mg/kg, **C-8** did not reduce worm burden but significantly affected female fecundity (increased deformed embryos by 13.7%; $P = 5.5 \times 10^{-5}$, Figure S4A). Thus, although **C-8** showed slightly better PK than **CLE**, it required a higher 50 mg/kg dose to be adulticidal, reducing total (50.8%, $P = 0.020$), female (54.0%, $P = 0.049$) and nonsignificantly male (47.5%) worm burden (Figure 6D). At this dose, **C-8** also significantly reduced mf secretion (57.1%, $P = 6.8 \times 10^{-8}$), gonad content (36.1%, $P = 0.020$), and increased percentage of deformed embryos (49.0%, $P = 1.8 \times 10^{-4}$; Figure 6E). This 10-day treatment exposure time is less than the maximum 14-day treatment time regimen recommended in the Drugs for Neglected Diseases initiative (DNDi) target product profile (TPP) for river blindness treatments.[68]

At 25 mg/kg PO (BID 6 h apart, 10 days), **PMZ-6** modestly reduced adult worm burden (~25%; Figure 6F), but strongly affected fecundity, increasing deformed embryos ($P = 6.1 \times 10^{-10}$) while decreasing healthy embryos ($P = 3.6 \times 10^{-4}$) and eggs ($P = 2.7 \times 10^{-9}$; Figure 6G). These differences may be due to variations in $C_{max}$ or bioavailability. Ultrastructural analyses with **CLE** (Figure 6H–I), **C-8** (Figure 6J–M) and **PMZ-6** (Figure 6N–Q), revealed consistent effects on embryogenesis wellness across *in vitro* and *in vivo* studies. Detailed embryograms for all results are described in Figure S5. Complete statistics including sample sizes, $P$ values, test statistics effect sizes and confidence intervals are provided for all *in vivo* experiments in Table S1.

Preliminary studies of **SUL** analog **S-17** (50 mg/kg PO, BID 6 h apart, 10 days) show a significant effect on fecundity, including a 49.5% reduction in mf secretion ($P = 2.5 \times 10^{-5}$) and a 2.2-fold increase proportion of deformed embryos (from 11.2% to 24.1%; $P = 0.018$; Figures S4B and S5D). Higher doses or extended treatment may clarify **S-17** potential.

### 2.5. C-8 *In Vivo* -Treated Worms Had Lasting Downregulation of GPCR Expression

We analyzed RNA-seq transcriptional responses in surviving (24–27 days postlast treatment) adult *B. pahangi* female and male worms from gerbils treated with **C-8** or vehicle (25 mg/kg BID 6 h apart, 10 days; Table S5A). **C-8** significantly altered expression of 3,590 genes in females and 1,184 genes in males ($P \leq 0.05$, $|\text{Log}_2 \text{ Fold Change}| \geq 0.5$). Twelve genes were upregulated and 371 genes were downregulated by **C-8** treatment in both sexes (Figure 7A); the overlap of downregulated genes was highly significant ($P < 10^{-15}$, binomial test), indicating strong shared responses. Expression data and statistics are in Table S5B, and $P$ value distributions are shown in Figure 7B. Of the 165 *B. pahangi* GPCRs,[69,70] 9 were downregulated in both sexes ($P = 9.8 \times 10^{-3}$ for enrichment among genes downregulated in both sexes, binomial distribution test), and 44 in females ($P = 1.4 \times 10^{-4}$ for enrichment among female-downregulated genes). The most significantly enriched InterPro domain among female downregulated genes was "GPCR, rhodopsin-like, 7TM" ($P = 4.4 \times 10^{-5}$; FDR-corrected over-representation analysis[71]) and the top Gene Ontology (GO) term was "G protein-coupled receptor activity" ($P = 1.3 \times 10^{-4}$). These results suggest widespread GPCR suppression. While upregulation may be expected in the case of antagonism, in mammalian systems, chronic antagonism of GPCR receptors has been shown to result in atypical/paradoxical downregulation, possibly due to

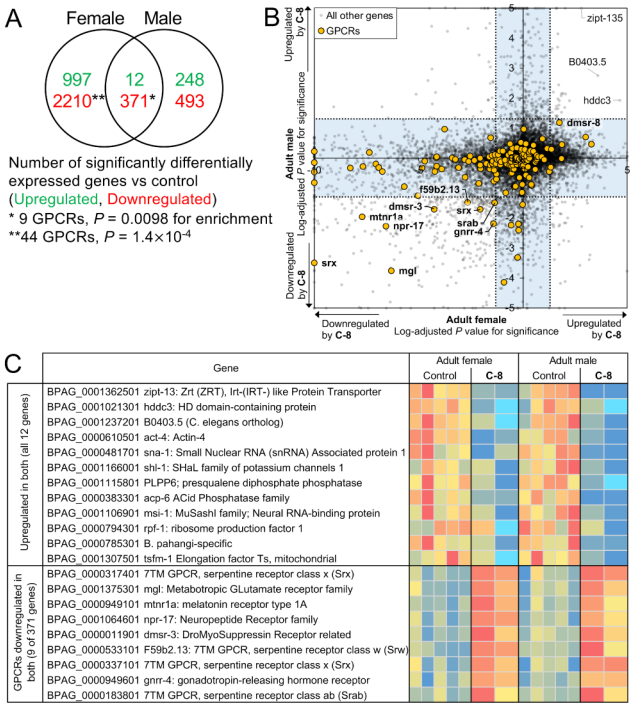


**Figure 7.** RNA-seq differential expression analysis of adult female and adult male *B. pahangi* worms treated with **C-8**, compared to vehicle-only controls. (**A**) The number of significantly differentially expressed *B. pahangi* genes in the RNA-seq analysis in **C-8**-treated worms relative to vehicle-only controls (DESeq FDR-adjusted $P \leq 0.05$, $|\text{Log}_2 \text{ Fold Change}| \geq 0.5$). An average of 23 million cleaned read pairs per sample were generated and analyzed. Significant enrichment of GPCRs was determined using negative binomial distribution tests. (**B**) Log-scaled DESeq $P$ values, with positive values indicating upregulation by **C-8** and negative values indicating downregulation by **C-8** in female worms ($x$-axis) and male worms ($y$-axis). Blue-shaded values indicate regions of no significance, where $P > 0.05$. Yellow dots indicate GPCRs, with the 9 GPCRs downregulated in both sexes labeled according to functional annotations. (**C**) Gene names and relative gene expression values for the 12 genes upregulated by **C-8** in both female and male worms (upper panel) and the 9 GPCRs among the 371 genes downregulated by **C-8** in both female and male worms.

antagonist-induced receptor internalization, or degradation in lysosomes.[72] This mechanism has been described for human 5-HT2A and 5-HT2C receptors,[72] both of which showed binding affinity with **C-8** (Figure 8; described below). Additionally, "heterologous desensitization" is well-described for human GPCRs, a process in which targeting a single GPCR affects the sensitivity and transcriptional downregulation of many other GPCRs, due to feedback regulation by the second-messenger-regulated kinases they activate.[73] While these offer some possible explanations for the widespread downregulate of GPCRs following **C-8** treatment, it is unclear exactly what mechanism underlies these findings.

*BPAG_0000956401*, an ortholog of *C. elegans* neuropeptide receptor GPCR *dmsr08* (DroMyoSuppressin Receptor; associated with hypoxia-evoked locomotory response[74]) with no ortholog in humans, was upregulated by **C-8** in female *B. pahangi* (Figure 7B). The 12 genes significantly upregulated in both sexes (Figure 7C) included muscle-related genes such as *shl-1* (important for nematode body wall muscle excitability[75]) and *act-4* (expressed primarily in nematode body wall muscle sarcomeres[76]), suggesting possible muscle or hypodermis damage, as seen in Figure 4K and 4L. Translation-associated


https://doi.org/10.1021/acs.jmedchem.6c01435
J. Med. Chem. XXXX, XXX, XXX−XXX

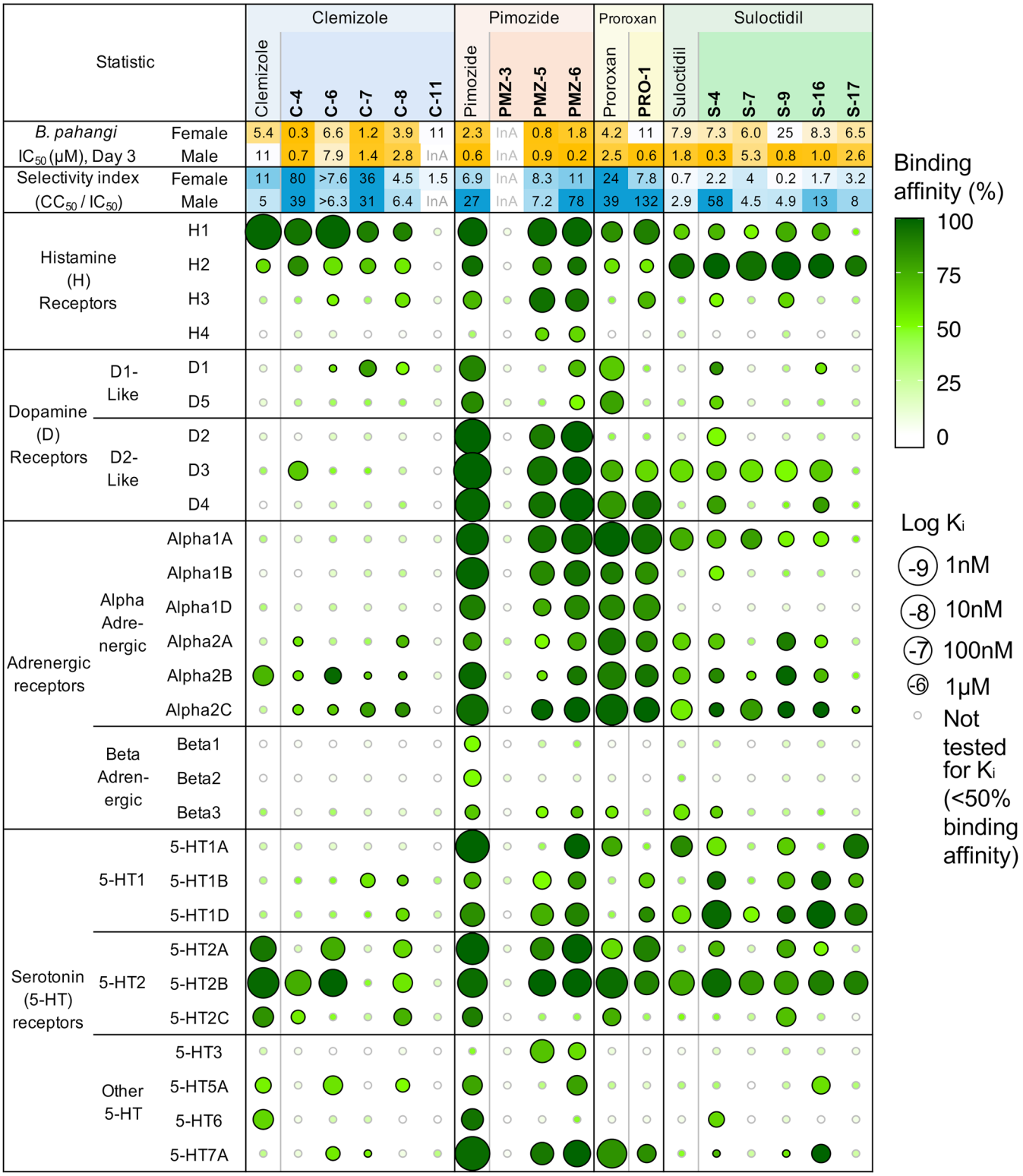


**Figure 8.** Human GPCR binding affinity (%) and Log$K_i$ (M) results against compounds of interest. Circles with gray borders indicate tests for which binding affinity was <50%, so $K_i$ was not tested. Complete results with binding affinity values and $K_i$ values, including for additional GPCRs tested, are provided in Table S2.

genes including *rpf-1* (involved in ribosome assembly and upregulated in starved worms[77]), *tfsm-1* (catalyzes the exchange of GDP for GTP during mitochondrial protein elongation[78]), and *sna-1* (responsible for spliced-leader splicing of transcripts in nematodes[79]), were also elevated, indicating increased protein synthesis demand. Additionally, stress related gene *hddc3/ZK909.3*, known for its role in ferroptosis in mammals[80] and stress responses in *C. elegans*,[81] was upregulated. These results indicate that **C-8** treatment over 10 days induced a lasting transcriptional response that also downregulates GPCR signaling, potentially contributing to its sustained negative impact on adult *B. pahangi*.


https://doi.org/10.1021/acs.jmedchem.6c01435
J. Med. Chem. XXXX, XXX, XXX−XXX

### 2.6. Binding Affinity of Representative GPCR Analogs to Human GPCRs

The 4 parent compounds and 14 top analogs were screened against 43 class A aminergic human GPCRs using radioligand binding assays (see Experimental Section). Compounds with ≥50% binding affinity underwent secondary assay to determine $K_i$ values (Figure 8; Table S2). As expected, **CLE**, **PRO**, **PMZ** and **SUL** showed strong $K_i$ for known targets, and potential new GPCR targets were also identified. **CLE** binds best to H1, followed by 5-HT2B (dissociation constants $LogK_i$ = −8.3 and −7.5, respectively). **PMZ** binds best to D2−4 ($LogK_i$ −8.0 to −8.6) and 5-HT7A (−8.1). **PMZ** was the least selective inhibitor, with 30 other GPCR $K_i$ values between −5 to −7.8. **PRO** has best $K_i$ for Alpha1A ($LogK_i$ = −8.1), followed by Alpha2C, 5-HT2B and 5-HT7A ($LogK_i$ −7.5 to −7.2), with 15 other GPCRs within −6.1 to −5.3. **SUL** binds moderately across 5-HT2B, Alpha1A, and H2 ($LogK_i$ = −6.8 to −6.3).

Four of the 5 **CLE** analogs had highest binding affinity to **CLE**'s known human H1 target, though modifications reduced affinity (−7.9 to −5.8 vs −8.3). **C-8** and **C-7** had 316.2- and 159.8-fold lower H1 affinity than **CLE**, with **C-7** showing over 30-fold higher SI for both sexes (Figure 1D). H1 antagonism in the host may enhance antifilarial activity indirectly, by enhancing eosinophil-mediated clearance.[82] **C-6** binding to Alpha2B and 5-HT2B was weaker compared to **CLE**. **C-11** showed no binding, indicating that the basic pyrrolidine group is crucial for potency. This finding guided us to retain the basic pyrrolidine or piperidine groups in subsequent modifications of clemizole analogs. **PMZ** and its analogs were broadly promiscuous, binding histamine, dopamine ($D_2$−$D_4$), alpha adrenergic and serotonin receptors, except **PMZ-3** which was inactive across GPCRs. **PMZ-5** had lower dopamine affinity compared to **PMZ** (e.g., −6.4 vs −8 for D4), indicating increased worm selectivity supported by better $IC_{50}$ (F-$IC_{50}$ 0.8 μM vs 2.3 μM). **PMZ-6** showed similar dopamine and Alpha1A affinity to **PMZ**. **PRO** and **PRO-1** were alpha adrenergic-selective, with **PRO-1** having 6.9-fold less binding to Alpha1A ($LogK_i$ = −7.2) compared to **PRO** (−8.1), and weaker affinity against all targets, while having a 3.4-fold increase in M-SI. Four of five **SUL** analogs (except **S-17**) maintained stronger H2 affinity but had reduced selectivity. **S-17** had the weakest H2 $LogK_i$ among **SUL** analogs (3.09-fold less than **SUL**), and among the best SI improvement in females, with significant *in vivo* fecundity efficacy. These findings inform SAR across the four-compound series and reinforce increased potential selectivity for worm GPCRs among the new analogs.

### 2.7. Potential Nematode Targets of CLE and Analogs Using a *C. Elegans* Reverse Genetics Screen

Based on previously published reports, **CLE** and its analogs are expected to be relatively specific for α-adrenergic, histamine and serotonin receptors,[45,83] and binding affinity to human GPCRs in this study indicated specific selectivity for human H1 and 5-HT2B (Figures 8 and 9A). We therefore tested the hypothesis that **CLE** and analogs target the nematode orthologs of the human H1 and 5-HT2B adrenergic GPCR targets, or a diversified nematode-specific form of it. The human H1 and 5-HT2B receptors belong to two orthologous protein families (OPFs: 14760 and 92761[69]), containing filarial and *C. elegans* orthologs (Figure 9B). A *C. elegans* reverse genetic screen was performed in ten established *C. elegans* amine GPCR null allele backgrounds, compared to wild type

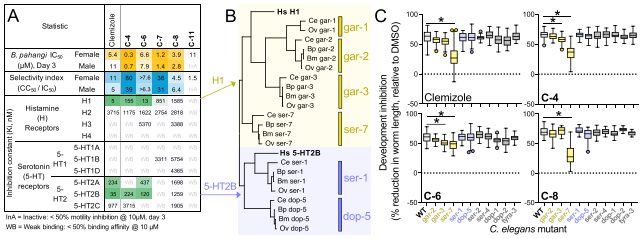


**Figure 9.** Biological assay results for **CLE** and analogs, and analysis of targets. (**A**) Assay results for: (i) Day 3 *B. pahangi* motility $IC_{50}$ (μM; orange); (ii) *B. pahangi* selectivity index, vs HepG2 cytotoxicity; (iii) Human GPCR inhibition constant ($K_i$) values (nM), based on results from radioligand binding assays. Compound:target combinations with <50% binding affinity at 10 μM were not tested. (**B**) Clustering of the most closely related *B. malayi* (Bm), *B. pahangi* (Bp), *O. volvulus* (Ov) and *C. elegans* (Ce) GPCRs with human (Hs) H1 and 5-HT2B proteins, based on GPCR domain sequences. (**C**) A *C. elegans* reverse genetic screen (48 h of 100 μM exposure). Worm lengths were compared to DMSO controls to calculate inhibition percentages, which were compared statistically to treated WT inhibition (*Cohen's *d* effect size ≥ 1 and FDR-corrected *t* test $P \leq 10^{-10}$).

(WT; N2) using a whole-organism phenotypic pipeline with development as the primary end point.[84,85] Based on amino acid sequences, nematode genes tested with this strategy clustered with (i) human H1, including gar-2 and gar-3, ser-7 (yellow), (ii) human 5-HT2B, including ser-1 and dop-5 (purple), (iii) and more distant homologues ser-2, ser-4, dop-1, dop-2 and tyra-3 (gray) (Figure 9A). Using these ten *C. elegans* GPCR null allele backgrounds, we identified that *C. elegans* lacking a functional ser-7 consistently show reduced developmental inhibition compared to WT worms when exposed to **CLE**, **C-4**, **C-6** or **C-8** treatment (student's *t*-test FDR-corrected $P \leq 4 \times 10^{-21}$, Cohen's *d* effect size ≥ 1.39), and *gar-3* mutants show statistically significant reduced developmental inhibition compared to wild type worms when exposed to **C-4** or **C-6** (FDR $\leq 3 \times 10^{-12}$, Cohen's *d* effect size ≥ 1.05; Figure 9C), supporting our hypothesis and identifying putative receptor targets in the nematodes. Compounds were treated at 100 μM for this assay, since the free-living *C. elegans* typically requires substantially higher concentrations than parasitic nematode species, due to lower cuticle permeability and its robust small molecule detoxification system.[86−88] All compounds tested were soluble at this concentration in the assay media during testing.

## 3. CONCLUSIONS

Mathematical modeling has shown that an adulticidal drug with only 60% efficacy when used in combination with IVM can significantly advance elimination of transmission.[89] Our study supports the adulticidal potential of the repurposed GPCR antagonists, and moreover *in vivo* CLE and C8 testing show 60% and 51% reduction in overall adult worm burden, respectively. Through iterative synthesis and screening, we identified 27 active analogs from the 4 parent compounds (CLE, PMZ, PRO, and SUL), with several showing improved potency, selectivity, and activity, leading to the prioritization of three lead compounds: **C-8**, **PMZ-6** and **S-17**.

First, **C-8** (i) was effective *in vivo* against *B. pahangi*, showing adulticidal activity in addition to reducing fecundity and disrupting embryogenesis, (ii) showed increase *in vitro* potency (motility $IC_{50}$) compared to **CLE**, including a 4.1-fold improvement in adult male *B. pahangi* and a > 85.7-fold and


https://doi.org/10.1021/acs.jmedchem.6c01435
J. Med. Chem. XXXX, XXX, XXX−XXX

>5.9-fold improvement in adult female and male *O. ochengi*, respectively; (iii) in *B. pahangi in vitro* ultrastructural analysis, caused embryo deformation and vacuolization of embryos (a more severe phenotype than the **CLE**-induced necrosis), and destroyed adult female hypodermal chords, which were unaffected by **CLE,** (iv) had similar rodent pharmacokinetics to **CLE**, but a 2.9-fold decrease in intrinsic clearance from mouse liver microsomes, indicating slower liver metabolism; (v) showed a 316-fold reduction in affinity to human H1, the known GPCR target for **CLE**,[45] (vi) among **CLE** analogs, had the highest scoring physical compound properties associated with activity from the RF analysis (score = 0.916, vs 0.775 for **CLE**); (vii) transcriptionally upregulated stress responses and downregulated potential target GPCRs in **C-8** treated worms, and (viii) potentially targets the *C. elegans ser-7* receptor based on a reverse genetic screen.

Next, **PMZ-6** (i) did not significantly reduce adult worm burden, but affected *B. pahangi* fecundity *in vivo* and significantly increased deformed embryos; (ii) was more effective than **PMZ** *in vitro* against *B. pahangi*, increasing potency while decreasing cytotoxicity, resulting in a 1.5-fold and 2.9-fold increase in selectivity index for adult female and male *B. pahangi* (respectively); (iii) induced a 91% reduction in *O. volvulus* L4 viability, while **PMZ** showed no measurable activity; (iv) maintained a similar human GPCR inhibition profile to **PMZ** and (v) had the highest scoring physical compound properties associated with activity from the RF analysis among **PMZ** analogs (score = 0.950, vs 0.675 for **PMZ**).

Finally, **S-17** (i) had a significant effect on *B. pahangi* fecundity and embryogenesis *in vivo*; (ii) maintained a similar potency to **SUL** against *B. pahangi in vitro*, but reduced cytotoxicity by 3.9-fold, resulting in a 4.8-fold and 2.8-fold increase in selectivity index for adult female and adult male worms, respectively; (iii) showed a 6.2-fold increase in potency against adult female *O. ochengi in vitro* compared to **SUL**; (iv) had an 18.7-fold slower intrinsic clearance compared to **SUL** in mouse liver microsomes, indicating reduced liver metabolism; (v) showed substantially better PK characteristics compared to **SUL**, including a 53.9-fold higher exposure ($AUC_{inf}$), a 143.1-fold higher peak concentration and a 64.3-fold slower apparent clearance; (vi) had a 3.1-fold reduced affinity to human H2, the known target for **SUL**[49] and (vii) was among the top scoring compounds based on physical properties associated with activity from the RF analysis (score = 0.951).

Collectively, these improved properties for these three lead compounds highlights their value as highly promising, parasite-selective candidates for continued development. While specific target identification in filarial worms is yet to be performed, our findings validate this multidimensional approach for antifilarial drug discovery. We have used the standard concentrations for filarial nematodes *in vitro* testing,[33,90−92] however potential pleiotropic or off-target effects remain an important consideration that warrants further investigation. Also, while the cytotoxicity assay used serves as an essential preliminary screen, downstream evaluations of neurofunctional safety, blood-brain barrier compatibility, and off-target CNS interactions will be important to evaluate therapeutic viability. For example, limiting blood-brain barrier penetration for the clemizole class could help prevent CNS side effects,[83] and managing the risk of QT prolongation could be needed for the pimozide analogs.[46] Future work could prioritize validating molecular targets in the filarial species, initiating dedicated medicinal chemistry campaigns around these advanced lead compounds to maximize parasite selectivity, and enhance their bioavailability.

## 4. EXPERIMENTAL SECTION

In addition to the detailed methods below, the $^1$H NMR and HPLC/MS spectra of all compounds (**C-1** to **C-9**, **PMZ-1** to **PMZ-9**, **PRO-1** to **PRO-6** and **SUL-1** to **SUL-17**) are provided in Supporting Information. All compounds are >95% pure by HPLC.

### 4.1. Chemistry

**4.1.1. General.** Starting materials, reagents, and solvents were purchased from commercial vendors unless otherwise noted. $^1$H NMR spectra were measured on a Varian 400 MHz NMR instrument. The chemical shifts were reported as $\delta$ ppm relative to TMS using residual solvent peak as the reference unless otherwise noted. The following abbreviations were used to express the multiplicities: s = singlet; d = doublet; t = triplet; q = quartet; m = multiplet; br = broad. All reactions were monitored by thin layer chromatography (TLC) carried out on Merck silica gel plates (0.25 mm thick, 60F254), or by Hewlett-Packard Series 1100 HPLC or Waters 2695 HPLC, using a Sunfire C18 3.5 $\mu$m, 4.6 × 50 mm column eluted with a gradient system of 5:95 to 95:5 acetonitrile:water, with a buffer consisting of 0.05% TFA. Peak detection was monitored by 210 and 254 nm UV-absorption (HP Series 1100) or 210 ∼ 400 nm absorption (Waters 2695) and mass spectra (MS). MS were performed on HP LC/MSD (connected with HP Series 1100) or Waters Micromass (connected with Waters 2695) using electrospray ionization (ESI) for detection. TLC was visualized by using UV (254 nm) or staining with KMnO4, p-anisaldehyde, and cerium ammonium molybdate (CAMA or Hanessian's Stain). High performance liquid chromatography (HPLC) was carried out on GILSON GX-281 using Sunfire C18 5 $\mu$m, 19 mm × 150 mm reverse phase columns, eluted with a gradient system of 5:95 to 95:5 acetonitrile:water over 20 min, with a buffer consisting of 0.05% TFA. If products containing basic amines are purified by reverse-phase HPLC, they will form TFA salts. Unless otherwise noted, the yields are calculated based on the salt form. Silica gel chromatography was carried out on a Teledyne ISCO CombiFlash purification system using prepacked silica gel columns (4−330 g sizes). All compounds used for biological assays are greater than 95% purity based on NMR and LCMS.

**4.1.2. Synthesis.** *4.1.2.1. Clemizole (CLE) and Analogs. 2-(Pyrrolidin-1-ylmethyl)-1H-benzo[d]imidazole* (**C-1**)

The mixture of 2-chloromethylbenzimidazole (0.50 g, 3 mmol) in pyrrolidine (5 mL) was heated at 95 °C for 2 h. The solvent was removed and the residue was purified by silica gel chromatography with MeOH (1 N $NH_3$)/$CH_2Cl_2$ combination (0 ∼ 10% gradient) as eluent to give **C-1** (0.475 g) as beige solid in 79% yield. $^1$H NMR (400 MHz, METHANOL-$d_4$) $\delta$ ppm 1.70−1.95 (m, 4H) 2.66−2.92 (m, 4H) 4.03 (s, 2H) 7.20 (dd, $J$ = 6.23, 3.11 Hz, 2H) 7.54 (dd, $J$ = 5.84, 3.11 Hz, 2H). MS(ESI): found: $[M + H]^+$, 202.2.

*2-(Piperidin-1-ylmethyl)-1H-benzo[d]imidazole* (**C-2**)

**C-2** was synthesized in the same procedure as for **C-1**. Yield: 82% (beige solid). $^1$H NMR (400 MHz, METHANOL-$d_4$) $\delta$ ppm 1.37−1.53 (m, 4H) 1.64 (quin, $J$ = 5.64 Hz, 7H) 2.42−2.75 (m, 4H) 3.84 (s, 2H) 7.15−7.32 (m, 2H) 7.48−7.62 (m, 2H). MS(ESI): found: $[M + H]^+$, 216.4.

*1-(4-Bromobenzyl)-2-(pyrrolidin-1-ylmethyl)-1H-benzo[d]imidazole* (**C-3**)

Under $N_2$ atmosphere NaH (60%) (0.012 g, 0.3 mmol) was added to **C-1** (0.040 g, 0.2 mmol) in DMF (2 mL) at 0 °C. The mixture was stirred for 15 min, followed by the addition of 4-bromobenzyl bromide (0.050 g, 0.2 mmol). The mixture was stirred overnight at room temperature. The solvent was removed and the residue was purified by HPLC (C18, 15 × 150 mm column; eluent: acetonitrile/water (0.05% TFA)) to give **C-3** (0.063 g) as viscous solid in 53% yield along with **C-5** (0.025 g) as off-white solid in 26% yield. **C-3**: $^1$H NMR (400 MHz, METHANOL-$d_4$) $\delta$ ppm 2.05−2.23 (m, 4H) 3.43−3.72 (m, 4H) 4.78 (s, 2H) 5.54 (s, 2H) 7.05 (d, $J$ = 8.56 Hz,


https://doi.org/10.1021/acs.jmedchem.6c01435
J. Med. Chem. XXXX, XXX, XXX−XXX

2H) 7.26−7.37 (m, 2H) 7.40−7.57 (m, 3H) 7.67−7.81 (m, 1 H). MS(ESI): found: $[M + H]^+$, 370.3.

*1-Octyl-2-(pyrrolidin-1-ylmethyl)-1H-benzo[d]imidazole* (**C-4**)

**C-4** was synthesized in the same procedure as for **C-3**. Yield: 60% (viscous oil). $^1$H NMR (400 MHz, METHANOL-$d_4$) $\delta$ ppm 0.88 (t, $J$ = 7.20 Hz, 3H) 1.18−1.46 (m, 10H) 1.84 (quin, $J$ = 7.40 Hz, 2H) 2.08−2.25 (m, 4H) 3.60 (br. s., 4H) 4.32 (t, $J$ = 7.59 Hz, 2H) 4.95 (s, 2H) 7.22−7.44 (m, 2H) 7.60 (d, $J$ = 7.79 Hz, 1H) 7.72 (d, $J$ = 7.79 Hz, 1H). MS(ESI): found: $[M + H]^+$, 314.4.

*1-((1H-Benzo[d]imidazol-2-yl)methyl)-1-(4-bromobenzyl)pyrrolidin-1-ium bromide* (**C-5**)

**C-5**: See synthesis details for **C-3**, above. $^1$H NMR (400 MHz, METHANOL-$d_4$) $\delta$ ppm 2.11−2.38 (m, 4H) 3.71 (t, $J$ = 5.06 Hz, 4H) 4.70 (s, 2H) 4.86 (s, 2H) 7.29−7.42 (m, 2H) 7.64−7.80 (m, 6H). MS(ESI): found: $[M + H]^+$, 370.3.

*1-(4-Chlorobenzyl)-2-(piperidin-1-ylmethyl)-1H-benzo[d]imidazole* (**C-6**)

**C-6** was synthesized in the same procedure as for **C-3** except that **C-2** was used instead. Yield: 70% (viscous solid). $^1$H NMR (400 MHz, METHANOL-$d_4$) $\delta$ ppm 1.58−1.77 (m, 2H) 1.90 (quin, $J$ = 5.64 Hz, 4H) 3.43 (br. s., 4H) 4.66 (s, 2H) 5.61 (s, 2H) 7.12 (d, $J$ = 8.56 Hz, 2H) 7.27−7.41 (m, 4H) 7.43−7.55 (m, 1H) 7.69−7.83 (m, 1H). MS(ESI): found: $[M + H]^+$, 340.3.

*1-Octyl-2-(piperidin-1-ylmethyl)-1H-benzo[d]imidazole* (**C-7**)

**C-7** was synthesized in the same procedure as for **C-3** except that **C-2** was used instead. Yield: 70% (viscous solid). $^1$H NMR (400 MHz, METHANOL-$d_4$) $\delta$ ppm 0.88 (t, $J$ = 7.20 Hz, 3H) 1.16−1.46 (m, 10H) 1.59−1.76 (m, 2H) 1.77−2.00 (m, 6H) 3.40 (br. s., 4H) 4.36 (t, $J$ = 7.40 Hz, 2H) 4.67 (s, 2H) 7.30−7.48 (m, 2H) 7.64 (d, $J$ = 8.17 Hz, 1H) 7.74 (d, $J$ = 7.79 Hz, 1H). MS(ESI): found: $[M + H]^+$, 328.4.

*1-((3″,5′-Difluoro-[1,1″-biphenyl]-4-yl)methyl)-2-(pyrrolidin-1-ylmethyl)-1H-benzo[d]imidazole* (**C-8**)

**C-8** was synthesized in the same procedure as described below for **PMZ-3** except that **C-3** and 3,5-difluorophenylboronic acid were used instead. Yield: 95% (white solid). $^1$H NMR (400 MHz, METHANOL-$d_4$) $\delta$ ppm 2.07−2.21 (m, 4H) 3.60 (br. s., 4H) 4.81 (s, 2H) 5.63 (s, 2H) 6.91 (tt, $J$ = 9.15, 2.34 Hz, 1H) 7.15−7.27 (m, 4H) 7.28−7.38 (m, 2H) 7.47−7.55 (m, 1H) 7.63 (d, $J$ = 8.56 Hz, 2H) 7.71−7.81 (m, 1H). MS(ESI): found: $[M + H]^+$, 404.4.

*2-(Phenoxymethyl)-1H-benzo[d]imidazole* (**C-9**)

Under $N_2$ atmosphere, 2-chloromethylbenzimidazole (0.200 g, 1.2 mmol) was added to the solution of phenol (0.565 g, 6 mmol) and NaH (60%) (0.217 g, 5.4 mmol) in DMF (4 mL). The mixture was stirred for 3 h at RT. The residue was suspended between $CH_2Cl_2$ and water. The organic phase was separated, dried with $Na_2SO_4$, then concentrated. The residue was purified by silica gel chromatography with AcOEt/hexane combination as eluent (0 ∼ 60% gradient) to give **C-9** (0.075 g) as viscous oil in 28% yield. $^1$H NMR (400 MHz, METHANOL-$d_4$) $\delta$ ppm 5.26 (s, 2H) 6.93 (t, $J$ = 7.40 Hz, 1H) 7.01 (d, $J$ = 8.17 Hz, 2H) 7.15−7.32 (m, 4H) 7.54 (dd, $J$ = 5.06, 3.11 Hz, 2H). MS(ESI): found: $[M + H]^+$, 226.3.

*1-(4-Bromobenzyl)-2-(phenoxymethyl)-1H-benzo[d]imidazole* (**C-10**)

Under $N_2$ atmosphere, NaH (60%) (0.020 g, 0.5 mmol) was added to the solution of **C-9** (0.075 g, 0.3 mmol) in DMF (2 mL) at 0 °C. The mixture was stirred at 0 °C for 15 min, followed by addition of 4-bromobenzyl bromide (0.100 g, 0.4 mmol). The mixture was stirred for 2 h while being stirred at room temperature and ambient atmosphere. The residue was suspended between $CH_2Cl_2$ and water. The organic phase was separated, dried with $Na_2SO_4$, then concentrated. The residue was purified by silica gel chromatography with AcOEt/hexane combination (0 ∼ 50% gradient) as eluent to give **C-10** (0.100 g) as transparent solid in 77% yield. $^1$H NMR (400 MHz, CHLOROFORM-*d*) $\delta$ ppm 5.33 (s, 2H) 5.45 (s, 2H) 6.82−7.06 (m, 5H) 7.10−7.50 (m, 7H) 7.83 (d, $J$ = 7.40 Hz, 2H). MS(ESI): found: $[M + H]^+$, 394.2.

*1-((3″,5′-Difluoro-[1,1″-biphenyl]-4-yl)methyl)-2-(phenoxymethyl)-1H-benzo[d]imidazole* (**C-11**)

Under $N_2$ atmosphere palladium-tetrakis(triphenylphosphine) (0.015 g, 0.01 mmol) was added to the mixture of **C-10** (0.050 g, 0.1 mmol), 3,5-difluorophenylboronic acid (0.041 g, 0.3 mmol) and $Cs_2CO_3$ (0.124 g, 0.4 mmol) in dioxane/water (5 mL/1 mL). The vial was evacuated and purged with $N_2$ gas 3 times. The mixture was stirred at 80 °C for 2 h. The residue was suspended between $CH_2Cl_2$ and water. The organic phase was separated, dried with $Na_2SO_4$, then concentrated. The residue was purified by silica gel chromatography with AcOEt/hexane combination as eluent to give **C-11** (0.042 g) as off-white solid in 76% yield. $^1$H NMR (400 MHz, CHLOROFORM-*d*) $\delta$ ppm 5.37 (s, 2H) 5.57 (s, 2H) 6.78 (t, $J$ = 8.76 Hz, 1H) 6.91−7.09 (m, 5H) 7.15 (d, $J$ = 7.79 Hz, 2H) 7.21−7.36 (m, 5H) 7.43 (d, $J$ = 7.40 Hz, 2H) 7.85 (d, $J$ = 7.40 Hz, 1H). MS(ESI): found: $[M + H]^+$, 428.2.

*1-(4-Bromobenzyl)-1H-benzo[d]imidazole* (**C-12**)

Under $N_2$ atmosphere, NaH (60%) (0.104 g, 2.6 mmol) was added to the solution of benzimidazole (0.200 g, 1.7 mmol) in DMF (3 mL). The mixture was stirred at RT for 40 min, followed by addition of 4-bromobenzyl bromide (0.525 g, 2.1 mmol). The mixture was stirred for 2 h. The residue was suspended between $CH_2Cl_2$ and water. The organic phase was separated, dried with $Na_2SO_4$, then concentrated. The residue was purified by silica gel chromatography with AcOEt/hexane combination as eluent to give **C-12** (0.400 g) as transparent solid in 82% yield. $^1$H NMR (400 MHz, CHLOROFORM-*d*) $\delta$ ppm 5.30 (s, 2H) 7.03 (d, $J$ = 7.79 Hz, 2H) 7.18−7.36 (m, 3H) 7.45 (d, $J$ = 7.79 Hz, 2H) 7.83 (d, $J$ = 7.40 Hz, 1H) 7.94 (s, 1H). MS(ESI): found: $[M + H]^+$, 288.2.

*1-((3″,5′-Difluoro-[1,1″-biphenyl]-4-yl)methyl)-1H-benzo[d]-imidazole* (**C-13**)

Under $N_2$ atmosphere palladium-tetrakis(triphenylphosphine) (0.020 g, 0.02 mmol) was added to the mixture of **C-12** (0.050 g, 0.2 mmol), 3,5-difluorophenylboronic acid (0.055 g, 0.4 mmol) and $Cs_2CO_3$ (0.163 g, 0.5 mmol) in dioxane/water (5 mL/1 mL). The vial was evacuated and purged with $N_2$ gas 3 times. The mixture was stirred at 80 °C for 2 h. The residue was suspended between $CH_2Cl_2$ and water. The organic phase was separated, dried with $Na_2SO_4$, then concentrated. The residue was purified by silica gel chromatography with AcOEt/Hex combination as eluent. The fractions containing the product were pooled and concentrated. The residue was purified by HPLC (C18, 15 × 150 mm column; eluent: acetonitrile/water (0.05% TFA)) to give **C-13** (0.034 g) as white solid in 46% yield. $^1$H NMR (400 MHz, METHANOL-$d_4$) $\delta$ ppm 5.80 (s, 2H) 6.88−6.96 (m, 1H) 7.18−7.26 (m, 2H) 7.53 (d, $J$ = 8.17 Hz, 2H) 7.56−7.65 (m, 2H) 7.68 (d, $J$ = 8.17 Hz, 2H) 7.81 (d, $J$ = 7.79 Hz, 1H) 7.86 (d, $J$ = 7.79 Hz, 1H) 9.50 (s, 1H). MS(ESI): found: $[M + H]^+$, 321.2.

*4.1.2.2. Pimozide (PMZ) and Analogs. 1-(4-Bromobenzyl)-1,3-dihydro-2H-benzo[d]imidazol-2-one* (**PMZ-1**) and *1,3-Bis(4-bromobenzyl)-1,3-dihydro-2H-benzo[d]imidazol-2-one* (**PMZ-2**).

Under $N_2$ atmosphere, NaH (60%) (0.220 g, 5.5 mmol) was added to the solution of benzimidazolone (0.671 g, 5 mmol) in DMF (28 mL) at 0 °C. The mixture was stirred at 0 °C for 5 min then at RT for 40 min, followed by addition of 4-bromo-benzyl bromide (1.375 g, 5.5 mmol). The mixture was stirred overnight. The precipitate was filtered, washed with DMF. The filtrate was concentrated and the residue was purified by silica gel chromatography with AcOEt/$CH_2Cl_2$ combination (0 ∼ 30% gradient) as eluent to afford **PMZ-2** (0.856 g, together with the precipitate isolated before) as white solid in 36% yield along with **PMZ-1** (0.15 g) as white solid in 10% yield.

**PMZ-1**: $^1$H NMR (400 MHz, CHLOROFORM-*d*) $\delta$ ppm 5.05 (s, 2H) 6.84 (d, $J$ = 7.79 Hz, 1H) 6.97−7.10 (m, 2H) 7.10−7.16 (m, 1H) 7.21 (d, $J$ = 8.17 Hz, 2H) 7.44 (d, $J$ = 8.17 Hz, 2H) 10.44 (br s, 1H). MS(ESI): found: $[M + H]^+$, 303.4.

**PMZ-2**: $^1$H NMR (400 MHz, CHLOROFORM-*d*) $\delta$ ppm 5.05 (s, 4H) 6.81−6.89 (m, 2H) 6.96−7.04 (m, 2H) 7.21 (d, $J$ = 8.56 Hz, 4H) 7.45 (d, $J$ = 8.17 Hz, 4H). MS(ESI): found: $[M + Na]^+$, 495.1.

*1-(4-(Pyridin-4-yl)benzyl)-1,3-dihydro-2H-benzo[d]imidazol-2-one* (**PMZ-3**).

Under $N_2$ atmosphere palladium-tetrakis(triphenylphosphine) (0.012 g, 0.01 mmol) was added to the mixture of **PMZ-1** (0.030 g, 0.1 mmol), 4-pyridineboronic acid (0.027 g, 0.2 mmol) and


https://doi.org/10.1021/acs.jmedchem.6c01435
J. Med. Chem. XXXX, XXX, XXX−XXX

$Cs_2CO_3$ (0.130 g, 0.4 mmol) in dioxane/water (5 mL/1 mL). The mixture was stirred at 80 °C for 2 h. The solvent was removed and the residue was purified by HPLC (C18, 15 × 150 mm column; eluent: acetonitrile/water (0.05% TFA)) to give **PMZ-3** (0.030 g) as viscous solid in 72% yield. $^1$H NMR (400 MHz, METHANOL-$d_4$) $\delta$ ppm 5.20 (s, 2H) 6.89−7.20 (m, 4H) 7.55 (d, $J$ = 8.17 Hz, 2H) 7.92 (d, $J$ = 8.17 Hz, 2H) 8.26 (d, $J$ = 6.62 Hz, 2H) 8.79 (d, $J$ = 6.62 Hz, 2H). MS(ESI): found: $[M + H]^+$, 302.3.

*1-(4,4-Bis(4-fluorophenyl)butyl)-1-methyl-4-(3-methyl-2-oxo-2,3-dihydro-1H-benzo[d]imidazol-1-yl)piperidin-1-ium iodide* (**PMZ-4**).

Under $N_2$ atmosphere NaH (60%) (0.008 g, 0.2 mmol) was added to pimozide (0.046 g, 0.1 mmol) in DMF (2 mL) at 0 °C. The mixture was stirred for 15 min, followed by the addition of MeI (0.2 mL). The mixture was stirred overnight at room temperature. The solvent was removed and the residue was purified by HPLC (C18, 15 × 150 mm column; eluent: acetonitrile/water (0.05% TFA)) to give **PMZ-4** (0.059 g, mixture of isomer (ratio: 68/32)) as white powder in 95% yield. $^1$H NMR (400 MHz, METHANOL-$d_4$) $\delta$ ppm 1.66−1.89 (m, 2H) 1.91−2.06 (m, 2H) 2.14 (q, $J$ = 8.05 Hz, 1.36H) 2.24 (q, $J$ = 7.79 Hz, 0.64H) 2.87−3.05 (m, 2H) 3.07 (s, 1H) 3.18 (s, 2H) 3.40 (s, 2H) 3.42−3.71 (m, 7H) 4.07 (t, $J$ = 7.98 Hz, 0.68H) 4.14 (t, $J$ = 7.98 Hz, 0.32H) 4.46−4.61 (m, 1H) 6.99−7.09 (m, 4H) 7.12−7.20 (m, 3H) 7.21−7.28 (m, 1H) 7.28−7.41 (m, 4H). MS(ESI): found: $[M - I]^+$, 490.4.

*Benzyl-3-(1-(4,4-bis(4-fluorophenyl)butyl)piperidin-4-yl)-1,3-dihydro-2H-benzo[d]imidazol-2-one* (**PMZ-5**).

Under $N_2$ atmosphere NaH (60%) (0.008 g, 0.2 mmol) was added to pimozide (0.046 g, 0.1 mmol) in DMF (2 mL) at 0 °C. The mixture was stirred for 15 min, followed by the addition of benzyl bromide (0.018 mL, 0.15 mmol). The mixture was stirred for 1 h at room temperature. The solvent was removed and the residue was purified by HPLC (C18, 15 × 150 mm column; eluent: acetonitrile/water (0.05% TFA)) to give **PMZ-5** (0.054 g) as white powder in 81% yield. $^1$H NMR (400 MHz, METHANOL-$d_4$) $\delta$ ppm 1.59−1.85 (m, 2H) 1.91−2.29 (m, 4H) 2.67−2.94 (m, 2H) 3.05−3.27 (m, 4H) 3.67 (d, $J$ = 12.07 Hz, 2H) 4.02 (t, $J$ = 7.79 Hz, 1H) 4.61 (ddd, $J$ = 12.26, 8.17, 4.09 Hz, 1H) 5.06 (s, 2H) 6.89−7.16 (m, 7H) 7.18−7.41 (m, 10H). MS(ESI): found: $[M + H]^+$, 552.5.

*1-(1-(4,4-Bis(4-fluorophenyl)butyl)piperidin-4-yl)-3-methyl-1,3-dihydro-2H-benzo[d]imidazol-2-one* (**PMZ-6**).

Under $N_2$ atmosphere NaH (60%) (0.012 g, 0.3 mmol) was added to pimozide (0.092 g, 0.2 mmol) in DMF (2 mL) at 0 °C. The mixture was stirred for 15 min, followed by the addition of MeI (0.012 mL, 0.2 mmol). The mixture was stirred at 0 °C for 30 min. The solvent was removed and the residue was purified by HPLC (C18, 15 × 150 mm column; eluent: acetonitrile/water (0.05% TFA)) to give **PMZ-6** (0.097 g) as white powder in 82% yield. $^1$H NMR (400 MHz, METHANOL-$d_4$) $\delta$ ppm 1.66−1.80 (m, 2H) 1.99−2.09 (m, 2H) 2.09−2.20 (m, 2H) 2.66−2.91 (m, 2H) 3.04−3.28 (m, 4H) 3.39 (s, 3H) 3.67 (d, $J$ = 12.85 Hz, 2H) 4.03 (t, $J$ = 7.98 Hz, 1H) 4.57 (tt, $J$ = 12.36, 3.99 Hz, 1H) 6.98−7.07 (m, 4H) 7.08−7.19 (m, 3H) 7.23−7.37 (m, 5H). MS(ESI): found: $[M + H]^+$, 476.4.

**PMZ-7** was purchased from commercial supply.

*1-(1-Octylpiperidin-4-yl)-1,3-dihydro-2H-benzo[d]imidazol-2-one* (**PMZ-8**).

The mixture of 4-(2-Keto-1-benzimidazolinyl)piperidine (0.065 g, 0.3 mmol), 1-octyl iodide (0.054 mL, 0.3 mmol) and triethylamine (0.184 mL, 1.32 mmol) in THF (2 mL) was stirred at 55 °C for 2 days. The solvent was removed and the residue was purified by HPLC (C18, 15 × 150 mm column; eluent: acetonitrile/water (0.05% TFA)) to give **PMZ-8** (0.085 g) as viscous solid in 64% yield. $^1$H NMR (400 MHz, METHANOL-$d_4$) $\delta$ ppm 0.91 (t, $J$ = 6.80 Hz, 3H) 1.19−1.56 (m, 10H) 1.64−1.91 (m, 2H) 2.07 (d, $J$ = 14.01 Hz, 2H) 2.83 (qd, $J$ = 13.37, 3.89 Hz, 2H) 3.06−3.28 (m, 4H) 3.75 (d, $J$ = 12.46 Hz, 2H) 4.59 (tt, $J$ = 12.36, 3.99 Hz, 1H) 6.96−7.15 (m, 3H) 7.17−7.39 (m, 1H). MS(ESI): found: $[M + H]^+$, 330.4.

*1-(1-(3,5-Dimethoxybenzyl)piperidin-4-yl)-1,3-dihydro-2H-benzo[d]-imidazol-2-one* (**PMZ-9**).

The mixture of 4-(2-keto-1-benzimidazolinyl)piperidine (0.065 g, 0.3 mmol), 3,5-dimethoxybenzyl bromide (0.069, 0.3 mmol) and triethylamine (0.084 mL, 0.6 mmol) in THF (2 mL) was stirred at RT overnight. The solvent was removed and the residue was purified by HPLC (C18, 15 × 150 mm column; eluent: acetonitrile/water (0.05% TFA)) to give **PMZ-9** (0.136 g) as off-white solid in 94% yield. $^1$H NMR (400 MHz, METHANOL-$d_4$) $\delta$ ppm 2.04 (d, $J$ = 13.24 Hz, 2H) 2.70−2.91 (m, 2H) 3.23 (t, $J$ = 12.26 Hz, 2H) 3.65 (d, $J$ = 12.07 Hz, 2H) 3.81 (s, 6H) 4.29 (s, 2H) 4.59 (ddt, $J$ = 12.21, 8.13, 4.23, 4.23 Hz, 1H) 6.58 (t, $J$ = 2.14 Hz, 1H) 6.71 (d, $J$ = 1.95 Hz, 2H) 6.96−7.17 (m, 3H) 7.22−7.40 (m, 1H). MS(ESI): found: $[M + H]^+$, 368.4.

*4.1.2.3. Proroxan (PRO) and Analogs. 1-(2,3-Dihydrobenzo[b]-[1,4]dioxin-6-yl)-3-(4-phenylpiperidin-1-yl)propan-1-one* (**PRO-1**)

In a round-bottom flask, 3-bromopropanoyl chloride (200 $\mu$L, 2.41 mmol) was dissolved in DCM (3 mL) at 0 °C. While stirring, benzo(1,4)-dioxane (141 $\mu$L, 1.40 mmol) was added slowly, followed by aluminum chloride (0.597 g, 4.48 mmol). The reaction was allowed to warm to room temperature, then was stirred overnight. The crude reaction mixture was poured over crushed ice, and was extracted with DCM (2 × 100 mL). The organic phase was washed with water (300 mL), $NaHCO_3$ (300 mL), and brine (300 mL), and then was dried over $Na_2SO_4$. The mixture was filtered and concentrated to give 220 mg as a purple-crystalline oil in crude yield (58%). 4-Phenyl-1-piperidine (62 $\mu$L, 0.406 mmol) was dissolved in DCM, then DMAP (0.009 g, 0.074 mmol) and DIPEA (193 $\mu$L, 1.11 mmol) were added and reaction was stirred for 5 min. The product from the previous reaction (0.100 g, 0.369 mmol) was added, and reaction was stirred for 2 h at room temperature. Once reaction was complete, and then solvent was removed. Crude reaction mixture was purified by rev. phase HPLC (10% acetonitrile/water (0.05% TFA)-70% acetonitrile/water (0.05% TFA) over 18 min) to give **PRO-1** (0.029 g) as a white powder in 22% yield. $^1$H NMR (400 MHz, $CD_3OD$) $\delta$ 7.62−7.56 (m, 2H), 7.37−7.31 (m, 2H), 7.28−7.21 (m, 3H), 6.97 (d, J = 8.3 Hz, 1H), 4.35−4.32 (m, 2H), 4.31−4.27 (m, 2H), 3.76 (d, J = 12.6 Hz, 2H), 3.58−3.54 (m, 3H), 3.21 (t, J = 12.5 Hz, 2H), 2.92 (t, J = 12.4 Hz, 1H), 2.14 (d, J = 14.4 Hz, 2H), 2.01 (t, J = 12.7 Hz, 2H). MS(ESI): found: $[M + H]^+$, 352.4.

*N-(2,3-Dihydrobenzo[b][1,4]dioxin-6-yl)-3-(3-phenylpyrrolidin-1-yl)-propanamide* (**PRO-2**)

In a round-bottom flask, 3.4-ethylenedioxyaniline (200 $\mu$L, 1.63 mmol) was dissolved in dioaxane (3.4 mL). While stirring, 3-bromopropanoyl chloride (137 $\mu$L, 1.36 mmol) and NaOH (49 $\mu$L, 0.15 mmol) were added simultaneously. The reaction was stirred at room temperature for 30 min. After full conversion to the product, the reaction was poured into water (34 mL) and the resulting purple precipitate was collected. The solid was recrystallized in EtOH, and was collected to give 143.6 mg of a light purple solid (37% crude yield). In a round-bottom flask, 3-phenyl-1-pyrrolidine (42 $\mu$L, 0.293 mmol) was dissolved in DCM, then DMAP (0.006 g, 0.049 mmol) and DIPEA (51 $\mu$L, 0.293 mmol) were added and reaction was stirred for 10 min. The product from the previous reaction (0.070 g, 0.245 mmol) was added, and reaction was stirred for 4 h at room temperature. MeOH was added until all solids were dissolved, then reaction was stirred for 2 days. Once reaction was complete, and then solvent was removed. Crude reaction mixture was purified by rev. phase HPLC (10% acetonitrile/water (0.05% TFA)-70% acetonitrile/water (0.05% TFA) over 18 min) to give **PRO-2** (0.0854 g) as a white powder in 37% yield over 2 steps. $^1$H NMR (400 MHz, $CD_3OD$) $\delta$ 7.36 (d, J = 6.4 Hz, 4H), 7.28 (td, J = 5.8, 2.9 Hz, 1H), 7.21 (d, J = 2.5 Hz, 1H), 6.93 (ddd, J = 8.7, 2.5, 1.4 Hz, 1H), 6.80−6.73 (m, 1H), 4.26−4.15 (m, 4H), 4.09−3.70 (m, 3H), 3.64 (t, J = 6.6 Hz, 3H), 3.49 (s, 1H), 3.22 (t, J = 11.5 Hz, 1H), 2.91−2.84 (m, 2H), 2.52 (d, J = 10.0 Hz, 1H), 2.24 (d, J = 36.4 Hz, 1H). MS(ESI): found: $[M + H]^+$, 353.4.

*1-(2,3-Dihydrobenzo[b][1,4]dioxin-6-yl)-2-(3-phenylpyrrolidin-1-yl)-ethan-1-one* (**PRO-3**)

**PRO-3:** Synthesized by same method as **PRO-1** with 2-bromoacetyl chloride (200 $\mu$L, 2.41 mmol) and 3-phenyl-1-pyrrolidine (92 $\mu$L, 0.64 mmol). 1.7 mg of a clear oil in 40% yield; $^1$H NMR (400 MHz, $CD_3OD$) $\delta$ 7.56−7.48 (m, 2H), 7.33−7.24 (m, 4H), 7.16 (tt, J = 5.7, 3.0 Hz, 1H), 6.90 (d, J = 8.3 Hz, 1H), 4.31−


https://doi.org/10.1021/acs.jmedchem.6c01435
J. Med. Chem. XXXX, XXX, XXX−XXX

4.27 (m, 2H), 4.27−4.21 (m, 2H), 4.10−3.93 (m, 1H), 3.44−3.33 (m, 1H), 3.18 (td, J = 8.2, 3.8 Hz, 1H), 3.10−3.01 (m, 1H), 2.79 (td, J = 9.1, 5.8 Hz, 1H), 2.67 (td, J = 9.0, 4.2 Hz, 1H), 2.36−2.23 (m, 1H), 1.96−1.83 (m, 1H). MS(ESI): found: $[M + H]^+$, 324.2.

*1-(2,3-Dihydrobenzo[b][1,4]dioxin-6-yl)-4-(3-phenylpyrrolidin-1-yl)-butan-1-one* (**PRO-4**)

**PRO-4:** Synthesized by same method as **PRO-1** with 4-bromobutanoyl chloride (200 μL, 1.73 mmol) and 3-phenyl-1-pyrrolidine (83 μL, 0.58 mmol). 134.9 mg of a white powder in 73% yield; $^1$H NMR (400 MHz, $CD_3OD$) δ 7.46 (dddt, J = 15.5, 7.2, 5.1, 2.4 Hz, 2H), 7.37−7.29 (m, 4H), 7.26 (h, J = 3.5 Hz, 1H), 6.91−6.83 (m, 1H), 4.99 (d, J = 13.2 Hz, 2H), 4.31−4.10 (m, 5H), 4.05−3.79 (m, 2H), 3.64 (dddd, J = 29.2, 22.8, 16.8, 9.3 Hz, 2H), 3.44 (tt, J = 8.8, 4.0 Hz, 1H), 3.16−3.05 (m, 2H), 2.48 (dq, J = 17.2, 5.3 Hz, 1H), 2.30−2.07 (m, 3H). MS(ESI): found: $[M + H]^+$, 352.3.

*N-(2,3-Dihydrobenzo[b][1,4]dioxin-6-yl)-2-(3-phenylpyrrolidin-1-yl)-acetamide* (**PRO-5**)

**PRO-5:** Synthesized by same method as **PRO-2** with 2-bromoacetyl chloride (140 μL, 1.70 mmol). 125.8 mg of a clear oil in 40% yield; $^1$H NMR (400 MHz, $CD_3OD$) δ 7.37 (d, J = 7.0 Hz, 5H), 7.33−7.27 (m, 1H), 7.21 (dt, J = 2.7, 1.2 Hz, 1H), 6.95 (ddt, J = 8.8, 2.6, 1.3 Hz, 1H), 6.79 (d, J = 8.7 Hz, 1H), 4.29−4.20 (m, 8H), 3.69 (s, 2H), 2.53 (d, J = 11.6 Hz, 1H), 2.26 (s, 1H). MS(ESI): found: $[M + H]^+$, 339.3.

*N-(2,3-Dihydrobenzo[b][1,4]dioxin-6-yl)-4-(3-phenylpyrrolidin-1-yl)-butanamide* (**PRO-6**)

**PRO-6:** Synthesized by same method as **PRO-2** with 4-bromobutanoyl chloride (196 μL, 1.70 mmol). 60.7 mg of a clear oil in 50% yield; $^1$H NMR (400 MHz, $CD_3OD$)δ 7.35 (d, J = 6.4 Hz, 4H), 7.27 (td, J = 6.1, 2.9 Hz, 1H), 7.22−7.18 (m, 1H), 6.91 (dd, J = 8.8, 2.5 Hz, 1H), 6.75 (dd, J = 8.7, 1.4 Hz, 1H), 4.25−4.14 (m, 4H), 4.03−3.39 (m, 4H), 3.38−3.32 (m, 2H), 3.28−3.10 (m, 1H), 2.52 (q, J = 10.2 Hz, 3H), 2.09 (h, J = 7.2 Hz, 2H). MS(ESI): found: $[M + H]^+$, 367.4.

*1-(2,3-Dihydrobenzo[b][1,4]dioxin-6-yl)-3-[(R)-3-phenylpyrrolidin-1-yl]propan-1-one* (**PRO-R**)

**PRO-R:** Synthesized by same method as **PRO-1** with (R)-3-phenyl-1-pyrrolidine. 139.0 mg of a yellow oil in 83% yield; $^1$H NMR (400 MHz, METHANOL- $d_4$) δ 7.56 (ddd, J = 8.4, 2.1 Hz, 2H), 7.40−7.33 (m, 4H), 7.32−7.24 (m, 1H), 6.95 (d, J = 8.4 Hz, 1H), 4.34−4.30 (m, 2H), 4.30−4.25 (m, 2H), 4.07−3.44 (m, 8H), 3.28−3.17 (m, 1H), 2.58−2.45 (m, 1H), 2.36 − 2.10 (m, 1H). MS(ESI): found: $[M + H]^+$, 338.20.

*1-(2,3-Dihydrobenzo[b][1,4]dioxin-6-yl)-3-[(S)-3-phenylpyrrolidin-1-yl]propan-1-one* (**PRO-S**)

**PRO-S**: Synthesized by same method as **PRO-1** with (S)-3-phenyl-1-pyrrolidine. 50.0 mg of a clear oil in 30% yield; 1H NMR (400 MHz, METHANOL- $d_4$) δ 7.56 (ddd, J = 8.4, 5.8, 2.1 Hz, 2H), 7.40−7.32 (m, 4H), 7.32−7.24 (m, 1H), 6.94 (d, J = 8.4 Hz, 1H), 4.34−4.30 (m, 2H), 4.29−4.25 (m, 2H), 4.07−3.44 (m, 8H), 3.27−3.17 (m, 1H), 2.58−2.44 (m, 1H), 2.36−2.09 (m, 1H). MS(ESI): found: $[M + H]^+$, 338.20.

*4.1.2.4. Suloctidil (SUL) and Analogs. Methyl 4-(3-((1R,2S)-1-hydroxy-1-(4-isopropoxyphenyl)-3-phenylpropan-2-yl)ureido)benzoate* (**S-1**)

Under nitrogen atmosphere THF (4 mL) was added to the reaction vial containing **S-3** (0.040g, 0.14 mmol) and 4-methoxycarbonylphenyl isocyanate (0.030 g, 0.17 mmol) at room temperature, followed by the addition of $iPr_2NEt$ (0.024 mL, 0.14 mmol). The mixture was stirred overnight. A few drops of water were added and the mixture was stirred for 30 min. The solvent was removed and the residue was purified by silica gel chromatography with AcOEt/$CH_2Cl_2$ combination (0 ∼ 30% gradient) as eluent to afford **S-1** (0.038 g) as white solid in 59% yield. $^1$H NMR (400 MHz, METHANOL-$d_4$) δ ppm 1.27 (d, J = 6.23 Hz, 6H) 2.70 (dd, J = 14.01, 10.12 Hz, 1H) 2.89 (dd, J = 14.21, 3.31 Hz, 1H) 4.18−4.30 (m, 1H) 4.55 (dt, J = 12.07, 6.03 Hz, 1H) 4.77 (d, J = 4.67 Hz, 1H) 6.89 (d, J = 8.17 Hz, 2H) 7.06−7.25 (m, 5H) 7.33 (dd, J = 17.91, 8.56 Hz, 4H) 7.83 (d, J = 8.56 Hz, 2H). MS(ESI): found: $[M + Na]^+$, 485.4.

*(1S,2S)-1-(4-Isopropoxyphenyl)-2-(octylamino)-3-phenylpropan-1-ol* (**S-2**)

It was synthesized in the same procedure as for **S-4** except that syn-adduct **A** was used as the starting material instead. Yield: 33% (viscous solid). $^1$H NMR (400 MHz, METHANOL-$d_4$) δ ppm 0.91 (t, J = 8.00 Hz, 3H) 1.15−1.38 (m, 16H) 1.43−1.64 (m, 2H) 2.70−3.09 (m, 4H) 3.54−3.74 (m, 2H) 4.55−4.63 (m, 1H) 4.65 (d, J = 7.01 Hz, 1H) 6.90 (d, J = 8.00 Hz, 2H) 7.16 (d, J = 7.40 Hz, 2H) 7.20−7.33 (m, 5H). MS(ESI): found: $[M + H]^+$- $H_2O$, 380.5.

*(1R,2S)-2-Amino-1-(4-isopropoxyphenyl)-3-phenylpropan-1-ol* (**S-3**)

Under $N_2$ atmosphere and at −78 °C, oxalyl chloride (0.20 mL, 2.4 mmol) was added dropwise to the solution of DMSO (0.28 mL, 4 mmol) in $CH_2Cl_2$ (20 mL). After 5 min of stirring, N,N-dibenzyl-L-phenylalaninol (0.663 g, 2 mmol) in $CH_2Cl_2$ (2 mL) was added. The mixture was stirred for 30 min, followed by the addition of $Et_3N$ (1.1 mL, 8 mmol). The mixture was allowed to warm to room temperature over 30 min. Water (20 mL) was added and the product was extracted with Hex/AcOEt (3/1). The organic layer was washed with 5% $NaHCO_3$ aqueous solution and brine sequentially, then filtered through a plug of silica gel. The filtrate was concentrated, dried in vacuo to afford N,N-dibenzyl-L-phenylalaninal (0.64 g) in 97% yield. Under $N_2$ atmosphere and at 0 °C, $Et_2Zn$/Hex (1 M, 24 mL) was added slowly to the suspension of 4-isopropoxyphenylboronic acid (1.44 g, 8 mmol) in toluene (20 mL). The mixture was heated at 60 °C for 1 h then cooled at °C when N,N-dibenzyl-L-phenylalaninal (0.64 g, 1.94 mmol) in toluene (5 mL) was added. The mixture was stirred at 0 °C for 24 h, then water (6 mL) was slowly added. Hex/AcOEt (3/1) was used for extraction. The organic phase was washed with brine, dried with $Na_2SO_4$, then concentrated. The residue was purified by silica gel chromatography with AcOEt/Hex (1/10) combination as eluent to give syn-adduct **A** as viscous oil (0.154 g, yield: 16%, with a higher Rf value of 0.3) and antiadduct **B** as viscous oil (0.186 g, yield: 37%, with a lower Rf value of 0.25). Antiadduct **B** (0.065 g, 0.14 mmol) and $Pd(OH)_2$/C (20 wt % loading, 0.030 g) in MeOH/THF (v/v: 2/1, 5 mL) was stirred under $H_2$ atmosphere overnight. The mixture was filtered, and the filtrate was concentrated, dried in vacuo to afford **S-3** (0.040 g) as viscous oil in quantitative yield. $^1$H NMR (400 MHz, METHANOL-$d_4$) δ ppm 1.30 (d, J = 5.84 Hz, 6H) 2.47 (dd, J = 13.62, 9.73 Hz, 1H) 3.07 (dd, J = 13.62, 2.72 Hz, 1H) 3.13−3.23 (m, 1H) 4.46 (d, J = 6.23 Hz, 1H) 4.59 (dt, J = 11.97, 5.89 Hz, 1H) 6.91 (d, J = 8.56 Hz, 2H) 7.09−7.44 (m, 7H). MS(ESI): found: $[M + H]^+$ - $H_2O$, 268.2.

*(1R,2S)-1-(4-Isopropoxyphenyl)-2-(octylamino)-3-phenylpropan-1-ol* (**S-4**)

At room temprature, the mixture of **S-3** (0.045 g, 0.16 mmol) and octanal (0.021 g, 0.16 mmol) in MeOH (3 mL, dried with MS 4A) was stirred for 5 min. $NaBH_3CN$ (0.028 g, 0.45 mmol) was added and the mixture was stirred overnight. Water was added and the mixture was concentrated. The residue was purified by HPLC (C18, 15 × 150 mm column; eluent: acetonitrile/water (0.05% TFA)) to give **S-4** (0.049 g) as viscous solid in 60% yield. $^1$H NMR (400 MHz, METHANOL-$d_4$) δ ppm 0.81−0.98 (m, 3H) 1.14−1.40 (m, 16H) 1.60 (br. s., 2H) 2.72−3.01 (m, 4H) 3.72 (d, J = 2.72 Hz, 1H) 4.60 (dt, J = 11.87, 6.13 Hz, 1H) 5.15 (br. s., 1H) 6.93 (d, J = 7.01 Hz, 2H) 7.07 (d, J = 7.40 Hz, 2H) 7.14−7.31 (m, 3H) 7.37 (d, J = 7.01 Hz, 2H). MS(ESI): found: $[M + H]^+$-$H_2O$, 380.4.

*(1R,2S)-1-(4-Isopropoxyphenyl)-2-((4-methoxybenzyl)amino)-3-phenylpropan-1-ol* (**S-5**)

It was synthesized in the same procedure as for **S-4**. Yield: 65% (white powder). $^1$H NMR (400 MHz, METHANOL-$d_4$) δ ppm 1.30 (d, J = 8.00 Hz, 6H) 2.90 (d, J = 6.23 Hz, 2H) 3.64 (br. s., 1H) 3.82 (s, 3H) 3.97−4.15 (m, 2H) 4.53−4.66 (m, 1H) 5.12 (br. s., 1H) 6.85−7.06 (m, 6H) 7.16−7.37 (m, 7H). MS(ESI): found: $[M + H]^+$, 406.8.

*(1S,2R)-2-Amino-1-(4-isopropoxyphenyl)propan-1-ol* (**S-6**)

Under $N_2$ atmosphere and at −78 °C, oxalyl chloride (0.41 mL, 4.8 mmol) was added dropwise to the solution of DMSO (0.57 mL, 8.0 mmol) in $CH_2Cl_2$ (30 mL). After 5 min of stirring, N,N-dibenzyl-D-alaninol (1.022 g, 4 mmol) in $CH_2Cl_2$ (5 mL) was added. The mixture was stirred for 30 min, followed by the addition of $Et_3N$ (2.23


https://doi.org/10.1021/acs.jmedchem.6c01435
J. Med. Chem. XXXX, XXX, XXX−XXX

mL, 16 mmol). The mixture was allowed to warm to room temperature over 30 min. Water (30 mL) was added and the product was extracted with Hex/AcOEt (2/1). The organic layer was washed with 1% HCl aqueous solution, water, 5% $NaHCO_3$ aqueous solution and brine sequetially, then filtered through a plug of silica gel. The filtrate was concentrated, dried in vacuo to afford N,N-dibenzyl-D-alaninal (0.965 g) in 95% yield. At 0 °C N,N-dibenzyl-D-alaninal (0.945 g, 3.73 mmol) in THF (6 mL) was added slowly to the RB flask containing 4-isopropoxyphenylmagnesium bromide (0.5 M in THF, 12 mL). The mixture was stirred at room temperature over 1 h, then quenched with water. The product was extracted with Hex/AcOEt (2/1) and the organic layer was dried with $Na_2SO_4$, then concentrated. The residue was purified by silica gel chromatography with AcOEt/Hex (1/5) combination as eluent to afford antiadduct **D** as viscous oil (0.090 g, yield: 6.2%). $Pd(OH)_2/C$ (20 wt % loading, 0.052 g) was added to the solution of antiadduct **D** (0.090 g, 0.23 mmol) in EtOH (5 mL). The mixture was stirred at room temperature under $H_2$ atmosphere overnight then filtered. The filtrate was concentrate and dried in vacuo to give **S-6** (0.046 g) as viscous oil in 95% yield. $^1$H NMR (400 MHz, METHANOL-$d_4$) $\delta$ ppm 1.07 (d, $J$ = 6.60 Hz, 3H) 1.30 (d, $J$ = 5.84 Hz, 6H) 2.99−3.18 (m, 1H) 4.46 (d, $J$ = 5.06 Hz, 1H) 4.59 (dt, $J$ = 11.97, 5.89 Hz, 1H) 6.90 (d, $J$ = 7.40 Hz, 2H) 7.26 (d, $J$ = 7.40 Hz, 2H). MS(ESI): found: $[M + H]^+$-$H_2O$, 192.2.

*(1S,2R)-1-(4-Isopropoxyphenyl)-2-(octylamino)propan-1-ol* (**S-7**)

It was synthesized via reductive amination from **S-6** following the same procedure as for **S-4**. Yield: 60% (viscous solid). $^1$H NMR (400 MHz, METHANOL-$d_4$) $\delta$ ppm 0.91 (t, $J$ = 6.62 Hz, 3H) 1.08 (d, $J$ = 6.62 Hz, 3H) 1.20−1.51 (m, 16H) 1.64−1.81 (m, 2H) 3.08 (t, $J$ = 8.17 Hz, 2H) 3.35−3.47 (m, 1H) 4.59 (dt, $J$ = 11.97, 5.89 Hz, 1H) 5.06 (d, $J$ = 2.72 Hz, 1H) 6.92 (d, $J$ = 8.56 Hz, 2H) 7.30 (d, $J$ = 8.56 Hz, 2H). MS(ESI): found: $[M + H]^+$, 322.7.

*tert-Butyl ((1R,2R)-1-hydroxy-1-(4-(isopropylthio)phenyl)propan-2-yl)carbamate* (**S-8**)

Under $N_2$ atmosphere and at 0 °C, (R)-Boc-alaninal (0.260 g, 1.5 mmol) in THF (5 mL) was added slowly to the RB flask containing 4-(isopropylthio)phenylmagnesium bromide (0.5 M in THF, 7 mL). The mixture was stirred at 0 °C for 1 h, then quenched with water. The solvent was removed and the residue was suspended between Hex/AcOEt (2/1) and $NH_4Cl$ aqueous solution. The organic layer was separated, dried with $Na_2SO_4$, then concentrated. The residue was purified by silica gel chromatography with AcOEt/Hex combination (0 ∼ 30% gradient) as eluent to afford syn-adduct **S-8** as the major isomer (0.120 g, yield: 25%, lower part of spot on TLC with AcOEt/Hex (1/3) as eluent: Rf = 0.28). $^1$H NMR (400 MHz, METHANOL-$d_4$) $\delta$ ppm 1.06 (d, $J$ = 6.23 Hz, 3H) 1.25 (d, $J$ = 6.62 Hz, 6H) 1.38 (s, 9H) 3.37 (dt, $J$ = 13.53, 6.67 Hz, 1H) 3.70−3.87 (m, 1H) 4.58 (d, $J$ = 4.67 Hz, 1H) 7.26−7.32 (m, 2H) 7.33−7.38 (m, 2H). MS(ESI): found: $[M + Na]^+$, 348.6.

*(1R,2R)-1-(4-(Isopropylthio)phenyl)-2-(octylamino)propan-1-ol* (**S-9**)

**S-8** (0.120 g, 0.37 mmol) was added to HCl/dioxane (2 M, 6 mL) at rt. The mixture was stirred for 3 h, then concentrated and dried in vacuo to afford the de-Boc intermediate (0.093 g) quantitatively. At rt, the de-Boc intermediate (0.025 g, 0.1 mmol) was added to the solution of octanal (0.017 mL, 0.11 mmol) and $Et_3N$ (0.015 mL, 1.1 mmol) in MeOH (2 mL, dried with MS 4A). The mixture was stirred for 5 min. $NaBH_3CN$ (0.030 g, 0.48 mmol) was added and the mixture was stirred overnight. Water was added and the mixture was concentrated. The residue was purified by HPLC (C18, 15 × 150 mm column; eluent: acetonitrile/water (0.05% TFA)) to give **S-9** (0.027 g) as viscous solid in 62% yield. $^1$H NMR (400 MHz, METHANOL-$d_4$) $\delta$ ppm 0.91 (t, $J$ = 7.20 Hz, 3H) 1.10 (d, $J$ = 7.01 Hz, 3H) 1.28 (d, $J$ = 6.62 Hz, 6H) 1.30−1.48 (m, 10H) 1.59−1.85 (m, 2H) 2.95−3.15 (m, 2H) 3.33−3.51 (m, 2H) 4.54 (d, $J$ = 8.95 Hz, 1H) 7.30−7.48 (m, 4H). MS(ESI): found: $[M + H]^+$- $H_2O$, 320.6.

*(1R,2R)-2-(Hexylamino)-1-(4-(isopropylthio)phenyl)propan-1-ol* (**S-10**)

**S-10** was synthesized following the same procedure as for **S-9**. Yield: 49% (viscous solid). $^1$H NMR (400 MHz, METHANOL-$d_4$) $\delta$ ppm 0.93 (t, $J$ = 6.80 Hz, 3H) 1.10 (d, $J$ = 6.80 Hz, 3H) 1.27 (d, $J$ = 6.60 Hz, 6H) 1.32−1.49 (m, 6H) 1.72 (dt, $J$ = 16.54, 8.47 Hz, 2H) 2.97−3.14 (m, 2H) 3.33−3.50 (m, 2H) 4.54 (dd, $J$ = 8.00, 2.00 Hz, 1H) 7.27−7.48 (m, 4H). MS(ESI): found: $[M + H]^+$, 310.7.

*(1R,2R)-2-(Decylamino)-1-(4-(isopropylthio)phenyl)propan-1-ol* (**S-11**)

**S-11** was synthesized following the same procedure as for **S-9**. Yield: 56% (viscous solid). $^1$H NMR (400 MHz, METHANOL-$d_4$) $\delta$ ppm 0.90 (t, $J$ = 8.00 Hz, 3H) 1.10 (d, $J$ = 7.01 Hz, 3H) 1.21−1.47 (m, 20H) 1.59−1.83 (m, 2H) 3.05 (ddt, $J$ = 16.30, 12.60, 6.18, 6.18 Hz, 2H) 3.33−3.50 (m, 2H) 4.54 (d, $J$ = 8.95 Hz, 1H) 7.39 (t, $J$ = 8.00 Hz, 4H). MS(ESI): found: $[M + H]^+$, 366.7.

*(1S,2S)-1-(4-(Isopropylthio)phenyl)-2-(octylamino)propan-1-ol* (**S-12**)

**S-12** was synthesized following the same procedure as for **S-9** except that syn-adduct **F** was used, which was prepared from (S)-Boc-alaninal in the same procedure as for **S-8**. Yield: 32% (viscous solid). Since **S-12** is the enantiomer of **S-9**, it has the same NMR and LCMS as **S-9**.

*(1S,2S)-2-((Cyclohexylmethyl)amino)-1-(4-(isopropylthio)phenyl)-propan-1-ol* (**S-13**)

**S-13** was synthesized following the same procedure as for **S-12** except that cyclohexanecarboxaldehyde was used in the final step of reductive amination. Yield: 60% (viscous solid). $^1$H NMR (400 MHz, METHANOL-$d_4$) $\delta$ ppm 1.02−1.13 (m, 2H) 1.10 (d, $J$ = 6.62 Hz, 3H) 1.24−1.44 (m, 3H) 1.27 (d, $J$ = 6.62 Hz, 6H) 1.65−1.94 (m, 6H) 2.94 (d, $J$ = 7.01 Hz, 2H) 3.33−3.51 (m, 2H) 4.57 (d, $J$ = 9.34 Hz, 1H) 7.32−7.49 (m, 4H). MS(ESI): found: $[M + H]^+$, 322.6.

*(1S,2S)-1-(4-(Isopropylthio)phenyl)-2-((pyridin-4-ylmethyl)amino)-propan-1-ol* (**S-14**)

**S-14** was synthesized following the same procedure as for **S-12** except that 4-pyridinecarboxaldehyde was used in the final step of reductive amination. Yield: 23% (viscous solid). $^1$H NMR (400 MHz, METHANOL-$d_4$) $\delta$ ppm 1.21 (d, $J$ = 7.01 Hz, 3H) 1.28 (d, $J$ = 6.62 Hz, 6H) 3.40−3.52 (m, 2H) 4.54 (q, $J$ = 14.40 Hz, 2H) 4.66 (d, $J$ = 9.34 Hz, 1H) 7.26−7.51 (m, 4H) 7.74−7.93 (m, 2H) 8.66−8.89 (m, 2H). MS(ESI): found: $[M + H]^+$, 317.5.

*(1R,2S)-1-(4-(Isopropylthio)phenyl)-2-(octylamino)propan-1-ol* (**S-15**)

**S-15** was synthesized following the same procedure as for **S-12** except that antiadduct **G**, which was prepared from (S)-Boc-alaninal in the same procedure as for **S-8**, was used. Yield: 47% (viscous solid). $^1$H NMR (400 MHz, METHANOL-$d_4$) $\delta$ ppm 0.92 (t, $J$ = 8.00 Hz, 3H) 1.07 (d, $J$ = 6.62 Hz, 3H) 1.27 (d, $J$ = 6.62 Hz, 6H) 1.30−1.51 (m, 10H) 1.67−1.81 (m, 2H) 3.10 (t, $J$ = 8.00 Hz, 2H) 3.36−3.52 (m, 2H) 5.12 (d, $J$ = 3.11 Hz, 1H) 7.29−7.47 (m, 4H). MS(ESI): found: $[M + H]^+$, 338.6.

*(S)-N-(1-(4-Isopropoxyphenyl)-3-phenylpropan-2-yl)octan-1-amine* (**S-16**)

Trifluoroacetic acid (2 mL) was added to the solution of **S-4** (0.028 g, 0.056 mmol) in $CH_2Cl_2$ (1.5 mL) at rt, followed by the addition of $Et_3SiH$ (0.3 mL, 1.88 mmol). The mixture was heated at 60 °C for 3 h, then concentrated. The residue was purified by HPLC (C18, 15 × 150 mm column; eluent: acetonitrile/water (0.05% TFA)) to give **S-16** (0.021 g) as viscous oil in 77% yield. $^1$H NMR (400 MHz, METHANOL-$d_4$) $\delta$ ppm 0.90 (t, $J$ = 7.01 Hz, 3H) 1.17−1.40 (m, 16H) 1.49−1.65 (m, 2H) 2.82−3.00 (m, 5H) 3.02−3.09 (m, 1H) 3.76 (t, $J$ = 6.81 Hz, 1H) 4.50−4.63 (m, 1H) 6.86 (d, $J$ = 8.56 Hz, 2H) 7.13 (d, $J$ = 8.56 Hz, 2H) 7.20−7.40 (m, 5H). MS(ESI): found: $[M + H]^+$, 382.5.

*N-((1R,2S)-1-Ethoxy-1-(4-isopropoxyphenyl)-3-phenylpropan-2-yl)-octan-1-amine* (**S-17**)

At 0 °C, NaH (0.017 g, 0.4 mmol) was added to the solution of antiadduct **B** (0.096g, 0.2 mmol) in DMF (2.5 mL). The mixture was stirred for 15 min then EtBr (0.016 mL, 0.2 mmol) was added. The reaction vial was sealed and heated at 50 °C for 10 h. NaH (0.010 g, 0.24 mmol) was added at 0 °C, followed by the addition of EtBr (0.010 mL, 0.13 mmol). The mixture was heated at 50 °C for additional 6 h. The mixture was concentrated and the residue was suspended between Hex/AcOEt (10/1) and water. The organic layer


https://doi.org/10.1021/acs.jmedchem.6c01435
J. Med. Chem. XXXX, XXX, XXX−XXX

was washed with water, dried with $Na_2SO_4$, then concentrated. The residue was purified by silica gel chromatography with AcOEt/Hex (0 ~ 5% gradient) combination as eluent to afford intermediate **H** (0.070 g) as viscous oil in 70% yield. $Pd(OH)_2/C$ (20 wt % loading, 0.014 g) was added to the solution of **H** (0.070 g, 0.14 mmol) in EtOH (8 mL) at rt. The mixture was stirred under $H_2$ atmosphere overnight then filtered. The filtrate was concentrated and dried in vacuo to give intermediate **I**. **I** was subjected to the reductive amination following the same procedure as for **S-4** to afford **S-17** (0.022 g) as viscous solid in 29% yield. $^1$H NMR (400 MHz, METHANOL-$d_4$) $\delta$ ppm 0.90 (t, $J$ = 6.62 Hz, 3H) 1.14−1.39 (m, 19H) 1.50−1.65 (m, 2H) 2.70−2.90 (m, 3H) 3.02 (dd, $J$ = 15.38, 4.09 Hz, 1H) 3.41−3.52 (m, 1H) 3.60 (quin, $J$ = 7.69 Hz, 1H) 3.67−3.76 (m, 1H) 4.62 (dt, $J$ = 11.97, 5.89 Hz, 1H) 4.80 (d, $J$ = 2.72 Hz, 1H) 6.96 (d, $J$ = 8.17 Hz, 2H) 7.06 (d, $J$ = 7.40 Hz, 2H) 7.16−7.37 (m, 5H). MS(ESI): found: $[M + H]^+$, 427.4.

## 4.2. ADMET Screening Assays

**4.2.1. Optical Density Solubility Assay.** FaSSIF (Fasted State Simulated Intestinal Fluid (Biorelevant cat#: FF01)), FeSSIF (Fed State Simulated Intestinal Fluid (Biorelevant cat#: FASBUF)), FaSSGF (Fasted State Simulated Gastric Fluid (Biorelevant cat#: FASGUF)), PBS (Phosphate Buffered Saline, pH 7.4 (Sigma cat#: P3813)) solutions were made according to the manufacturer's specifications. Compounds to be tested were dissolved in DMSO to make 10 mM stock solutions. For each compound, 4 tubes were prepared; for the simulated fluids, 490 $\mu$L of fluid was combined with 10 $\mu$L of compound stock solution in DMSO and for the PBS solution, 497.5 $\mu$L of PBS solution was combined with 2.5 $\mu$L of compound stock solution in DMSO. DMSO controls for all fluids were prepared by adding either 2.5 or 10 $\mu$L of DMSO to the respective fluids. All vials were vortexed for 5 to 10 s, then were placed on an orbital shaker at 250 rpm overnight at room temperature. A total of 200 $\mu$L of each sample was added to two technical replicate wells on a 96-well flat bottom plate (Corning #3370), with DMSO control cells as blanks for each media/buffer. The plate was shaken for 5 s on the plate reader, and samples were read at $OD_{600}$ nm wavelength. Higher OD's mean lower solubility (OD < 0.010 is considered fully or near fully soluble; between 0.010 and 0.100 is considered partly/moderately soluble; and over 0.100 is considered insoluble). We have run Q203 as control in our kinetic solubility assay starting at 200 $\mu$M five times previously and the running O.D averages are 0.043 (FaSSIF), 0.035 (FeSSIF), and 0.007 (FaSSGF), and the OD average in this experiment is within historical range for the biorelevant buffers. The data was exported to Excel and average $OD_{600}$ values were calculated in the spreadsheet.

**4.2.2. Metabolic Stability of Compounds.** To evaluate compounds' metabolic stability, we calculated their half-life ($t_{1/2}$; in minutes) by measuring how quickly the compounds were metabolized by liver enzymes using mouse liver microsomes, which mediate Phase I metabolism (i.e., oxidation), the first step in liver clearance of xenobiotics. The half-life ($t_{1/2}$) in minutes provides insight into a drug's metabolic stability, along with the calculation of intrinsic clearance ($CL_{int}$), i.e., theoretical clearance of a drug by liver enzymes mediating Phase I metabolism in the absence of blood flow limitations. Verapamil was used as positive control and tolbutamide was used as an internal standard, the latter to account for variations in extraction and ionization efficiency. Compounds had a wide range of short $t_{1/2}$ in mouse liver microsomes, indicating they undergo rapid hepatic metabolism, potentially leading to low bioavailability *in vivo*.

**4.2.3. Cytotoxicity Assay.** HepG2 (human hepatoma) cells were routinely subcultured in DMEM low glucose medium with 10% fetal bovine serum (FBS), 100U/mL: penicillin and 100U/mL streptomycin incubated at 37 °C with 5% $CO_2$. The cytotoxicity activities of compounds were determined using MTT (3-(4,5-dimethylthiazol-2-yl)-2,5-diphenyl tetrazolium bromide) reduction assay. $1 \times 10^4$ HepG2 cells/well were seeded in 100 $\mu$L DMEM low glucose (Dulbecco's Modified Eagle's Medium) supplemented with 10% FBS in each well of 96-well microculture plates and incubated for 24 h at 37 °C in $CO_2$ incubator. Compound stock solutions were prepared in DMSO and were diluted to the desired concentrations in culture medium. Cells cultured in 96-well plate were treated with various concentrations of test compounds in four replicates for 24 h. After the period of incubation, 10 $\mu$L of MTT (5 mg/mL) was added in each well and the plates were further incubated for 2 h. Supernatant from each well was carefully removed, formazan crystals were dissolved in 100 $\mu$L of DMSO and absorbance at 630 nM wavelength was recorded. Cells treated with 0.1% and 1% Triton X-100 were positive control. Percentage cell inhibition was calculated by linearly normalizing compound absorbance between DMSO-treated control group absorbance (0% cytotoxicity) and 1% Triton X-100 absorbance (100% cytotoxicity). For all experiments, N = 12 for DMSO-only controls, and N = 4 for all test groups. Dose−response relationships for HepG2 cell $CC_{50}$ values and all associated statistics were analyzed using a four-parameter log−logistic (LL.4) model implemented in the drc package in R, using 5−6 concentrations.

**4.2.4. Human GPCR Binding Affinity.** Primary receptor binding profiles and $K_i$ determinations for parent drugs and selected analogs with human GPCRs was done by the National Institute of Mental Health's Psychoactive Drug Screening Program, contract #75N95023C00021 (NIMH PDSP). As previously described,[93] the affinity of compounds for human GPCRs was tested by a radioligand competition binding assay. Briefly, the approach tests the ability of compounds to displace a known, high-affinity radioactive tracer (radioligand) from the receptor's active site. The assay is performed using membrane fractions derived from transfected cell lines (typically HEK293 or CHO) stably expressing the target human recombinant receptor. Total binding is defined using the radioligand alone, while nonspecific binding (NSB) is determined in the presence of a high concentration of a reference saturating antagonist. First, compounds were tested at a single concentration (10 $\mu$M) in quadruplicate, and results were expressed as a percentage of inhibition of specific radioligand binding. Compounds exhibiting ≥50% inhibition in the primary screen were progressed to secondary assays to determine equilibrium dissociation constants ($K_i$). These assays used 11 concentrations of the test compound (ranging from 0.1 nM to 10 $\mu$M) to generate a full competition curve. Radiometric data (measured in counts per minute, CPM) were processed to calculate specific binding by subtracting nonspecific binding from total binding. Dose−response data were analyzed using nonlinear least-squares regression in GraphPad Prism to determine the $IC_{50}$ (the concentration of test compound required to displace 50% of the specific radioligand binding). The $IC_{50}$ value was converted to the absolute inhibition constant ($K_i$) using the Cheng-Prusoff equation: $K_i = IC_{50}/(1 + [L/K_d])$, where L is the concentration of free radioligand used in the assay and $K_d$ is the equilibrium dissociation constant for each receptor, predetermined through saturation binding experiments.

## 4.3. *In Vitro* Worm Experiments

**4.3.1. *B. Pahangi.*** *4.3.1.1. In Vitro Motility Assays with Adult and L4 B. Pahangi.* Individual adult male and female *Brugia pahangi* worms (100−120 dpi) were placed in media (RPMI-1640 with 1 M HEPES, 7.5% $NaHCO_3$, 5% heat inactivated fetal bovine serum (FBS), and 1X Antibiotic and Antimycotic solution) in 24-well plates. Each well contained one female or one male worm in 500 $\mu$L media. Two female and three male L4 worms (42 dpi) were used for assays under the same conditions. Compounds dissolved in DMSO were added to each well at a concentration of 10 $\mu$M, with 4 replicates per compound and eight replicates of 1% DMSO, used as a vehicle control. Cultures were maintained at 5% $CO_2$ in a 37 °C humidified incubator. Movement of worms was recorded using "*QuickTime Player*" on Mac by recording apparatus and 1080p digital camcorder on at interval of 4 h, 1 day, 2 days, 3 days, and 6 days. Three videos were recorded as technical replicates of a plate. Thirty second of each video was trimmed using iMovie' tool to calculated Mean Movement Unit (MMU). MMU was calculated using setup "*Bottom-Read Rotated 180°*" on Plate Orientation setting and "*Lucas-Kanade Optical Flow (Velocity, 1 organism per well)*" on Assay Analyzer setting of the "*WormAssay*" tool.[94] Statistical procedures were used to minimize


https://doi.org/10.1021/acs.jmedchem.6c01435
J. Med. Chem. XXXX, XXX, XXX−XXX

noise resulting from worms that occasionally would be at the edge of the well, resulting in low MMU detection values by WormAssay. First, of the eight DMSO replicates, any values less than 70% of the average MMU value were excluded as outliers. Second, for the four replicates of the test compounds, MMU values were excluded that were *both* (a) above or below 1 standard deviation of the average MMU value and (b) were more than 20% above or below the average MMU value of the four replicates, with no bias toward increasing or decreasing the resulting motility inhibition values.

Compounds that caused 75% or greater inhibition of motility by day 3 were considered hits and were then tested in $IC_{50}$ assays, using a serial dilution ranging from 30 $\mu$M to 0.1 $\mu$M (with the same filtering and sample numbers as described above), at 6 concentrations (with only 5, omitting the 0.1 $\mu$M concentration, for several adult male tests due to fewer male worms being available for testing). Dose−response relationships for $IC_{50}$ values and all associated statistics were analyzed using a four-parameter log−logistic (LL.4) model implemented in the drc package in R. For the drc calculation, the lower asymptote was fixed at 0% and the upper asymptote was fixed at 100%. The model estimation was performed using maximum likelihood, with the delta method for confidence interval calculation. This parametrization allows for sigmoidal curve fitting with asymmetric responses around the inflection point, which is particularly suitable for cytotoxicity and inhibition assays where complete response ranges from 0% to 100%. *P* values for each $IC_{50}$ curve were calculated from the F-statistic of the overall four-parameter log−logistic model fit (df_model = 4, df_residual = n−4), using the upper-tail probability of the F distribution, with no correction for multiple testing across compounds. Detailed statistics for motility and $IC_{50}$ values are provided for all compounds in Table S1.

*4.3.1.2. Adult Female B. Pahangi Bioaccumulation Assay.* Individual adult female *Brugia pahangi* were placed in 24 well plate containing media. Compounds dissolved in DMSO were added to each well at a concentration of 30 $\mu$M, with 4 replicates per compound and 1% DMSO was used as a vehicle control. Movement of treated worms was observed until the worms became morbid but not completely dead. Worms were collected in saline and washed two times using 0.1% SDS to remove drug from the surface. One more washing was done using media and 4 worms collected in Eppendorf tube and store at −80 °C overnight. For lysis, worms were thawed on ice, crushed in liquid nitrogen using pestles and incubated with 100 $\mu$L of 1X lysis buffer with proteinase K (50 mM KCl, 10 mM Tris, pH 8.3, 0.2% SDS, 250 $\mu$g/mL proteinase K) for 5 h at 60 °C. Proteins were precipitated using 100 $\mu$L of acetonitrile and stored (∼180−200 $\mu$L) at −80 °C. Lysates were analyzed for level of each individual compound by HPLC/MS. DMSO was used as the negative control while the parent compound, which is known to be membrane permeable, was used as the positive control. Lysates were analyzed on a Hewlett-Packard Series 1100 HPLC, using a Sunfire $C_{18}$ 3.5 $\mu$m pore size, 4.6 × 50 mm column as previously described[56] with slight modifications; in short, samples were injected with 20 $\mu$L of volume with a flow rate of 1 mL/mins and solvent system of $H_2O$ (0.05% TFA) and acetonitrile (0.05% TFA). Gradient was 0→5 min: 5−95% linear increase acetonitrile; 5→6 min 95% acetonitrile hold; 6→7 min 95−5% linear decrease acetonitrile. Elution was monitored by 210 and 254 nm UV absorption and by MS. MS conditions were drying gas 12 L/mins, drying gas temperature 350 °C, nebulizer psig 55−60, and capillary voltage 4000 V. Compound presence was evaluated by extracting $[M + H]^+$ or $[M + Na]^+$ of parent compound mass.

*4.3.1.3. Embryogram to Assess In Vitro B. Pahangi Fitness.* The evaluation of the effect of treatment on female worm fitness was measured based on the microfilariae (mf) released from individual females (n = 4) after 6 days treatment, characterized and counted using a dissecting microscope. 500 $\mu$L media from treated and untreated wells containing female *Brugia pahangi* in a 24 well plate was pipetted up and down to disperse the mf equally. 5 $\mu$L of then placed on slide, and videos and images were captured twice using a Keyence microscope (Lens ×4 PlanApo NA 0.20, Zoom ×1.0, CH4 BF/Phase BF/Phase). Total, dead and live mf were counted and significant differences relative to DMSO for total active mf proportions were tested using two-tailed pooled student's *t* tests (equal variance), performed in MS Excel, with no correction for multiple testing. A Kolmogorov−Smirnov test[95] did not show a significant departure from normality for mf count data (using 64 DMSO total mf counts; D(64) = .089, *P* = 0.233, K = 0.7143, skewness = 0.3755), justifying the use of parametric statistics.

An additional embryogram procedure was used to determine total gonad contents, MF to embryo stage development and deformity from treated female *Brugia pahangi* worms. At the sixth day of treatment, 1 female worm was collected in an Eppendorf tube containing 1 mL of PBS and stored at 4 °C. 500 $\mu$L of PBS were removed and the worms were chopped vigorously for 2−3 min with small scissors, with vortexing every minute. Tubes were then placed on a rotator overnight at RT, to allow all contents of the worm to be released out into the PBS. Tubes were centrifuged at 500 × g for 5 min to pellet contents, and 400 $\mu$L of the PBS were removed. 10 $\mu$L from the bottom placed into a well of a 10-well 30−7H-Black slide. Multiple images from different fields were captured using a Keyence microscope (Lens ×20 PlanApo NA 0.75, Zoom ×1.0, CH4 BF/Phase BF/Phase). 200 events were counted that include all stages: eggs, embryos, premf, mf, stretch mf's and deformed stages. Counts were performed for four biological replicates per treatment condition, including DMSO. Significant differences in the proportions of each stage relative to DMSO were tested using two-tailed pooled student's *t* tests with equal variance with no correction for multiple testing, performed in MS Excel. Within each stage, Kolmogorov−Smirnov tests[95] did not show a significant departure from normality for proportion values in any of the stages count data (using 40 DMSO sample proportions; D(40) ≤ 0.1334, *P* ≥ 0.0706, K ≤ 0.8433, skewness ≤ 0.8433), justifying the use of parametric statistics.

Detailed student's *t* test results as described above for mf and embryogram results, including average values, standard error values, *t* test *P* values, t statistics, 95% confidence intervals of the t statistic, degrees of freedom and Cohen's *d* values for all compounds are provided in Table S1.

*4.3.1.4. Ex Vivo Adult Female B. Pahangi Fecundity.* To test the effects of the compounds on female worm fecundity, all surviving female worms were examined *ex vivo* to quantify the number of microfilariae (mf) released overnight in culture and to profile the various stages of embryonic development within the uteri of the individual female worms, as previously described.[91] One-tailed pooled Student's *t* tests (equal variance) were used to test for significant reduction in microfilariae secretion, with no correction applied for multiple testing. A Kolmogorov−Smirnov test[95] did not show a significant departure from normality for microfilariae secretion counts (using 84 vehicle-only control counts; D(84) = 0.1296, *P* = 0.1087, K = 1.1879, skewness = 0.434), justifying the use of parametric statistics. After necropsy, recovered female worms were incubated in individual wells of a 24-well plate with 2 mL complete media at 37 °C and 5% $CO_2$. After 24 h, the number of mf released by each adult female was determined by counting the number of mf in a 0.5 mL aliquot and multiplying by 4 to calculate the total number secreted by each worm. Additionally, embryogram analyses on the individual female worms were performed as described.[91] Briefly, each female worm was homogenized first in 0.5 mL PBS to release the uterine content. The suspension was then spun down, 0.4 mL of the PBS was removed, and the remaining 0.1 mL was used for analysis. The total gonad contents were determined in two 10 $\mu$L aliquots using a hemocytometer, while the distribution of the various embryonic developmental stages (eggs, embryos, premicrofilariae, and stretched mf) was determined in two separate aliquots containing at least 200 events each on a 30−7H-Black slide using a compound microscope. A minimum of 200 events were assessed from each female worm and at least six females per treated gerbil. The intrauterine embryogram was expressed as the relative proportions of the different stages of development: eggs, embryos, premicrofilariae (premf), stretched mf, and deformed embryos in the total number of events recorded. One-tailed pooled Student's *t* tests (equal variance) were used to test for significant reduction in total gonad contents, with no correction applied for multiple testing. A Kolmogorov−Smirnov test[95] did not show a


https://doi.org/10.1021/acs.jmedchem.6c01435
J. Med. Chem. XXXX, XXX, XXX−XXX

significant departure from normality for total gonad contents data (using 48 vehicle-only control counts; D(48) = 0.0904, $P$ = 0.8533, K = 0.5856, skewness = 0.261), justifying the use of parametric statistics. Significant differences in the proportions of each embryogram stage relative to vehicle-only controls were tested using two-tailed pooled Student's $t$ tests (equal variance), with no correction for multiple testing, performed in MS Excel. Within each stage, Kolmogorov–Smirnov tests[95] did not show a significant departure from normality for proportion values in any of the stages count data (using 40 DMSO sample proportions; D(40) $\leq$ 0.1334, $P \geq$ 0.0706, K $\leq$ 0.8433, skewness $\leq$ 0.8433), justifying the use of parametric statistics.

*4.3.1.5. Transmission Electron Microscopy of Female Brugia Pahangi.* Following treatment with compounds for 3 days at 30 $\mu$M concentrations as described above for *in vitro* assays, and 1 day after collection from *in vivo* experiments, adult female *B. pahangi* worms were fixed with 2.5% glutaraldehyde and 2% paraformaldehyde buffered with 0.1 M sodium cacodylate pH 7.3–7.4 as previously described.[50] After being submerged in fixative, the worms were cut into small pieces and kept for 2 h at room temperature before being stored at 4 °C. Following fixation, samples were washed with 0.1 M sodium cacodylate and postfixed with 1% osmium tetroxide for 1 h. Following another wash with 0.1 M sodium cacodylate, samples were dehydrated in increasing ethanol concentrations (30–100%), washed two times with propylene oxide, and then infiltrated with a 1:1 Spurr:propylene oxide solution. Samples were then embedded in size 00 BEEM capsules using Spurr's low viscosity embedding kit (Electron Microscopy Sciences, Hatfield, PA, USA). Blocks were polymerized at 60 °C overnight. Ultrathin sections were collected on nickel Formvar/carbon-coated 100 mesh grids or copper slot grids and contrasted with Uranyless (Electron Microscopy Sciences) and lead citrate. Sections were imaged on a Tecnai G2 Spirit TEM equipped with an AMT camera.

**4.3.2. *O. Ochengi In Vitro* Motility and Viability Assays.** Cows that had grazed in northern Cameroon where *O. ochengi* is highly endemic were brought to abattoirs located in Douala, Cameroon. Subcutaneous nodules containing adult *O. ochengi* worms were identified on the umbilical skin of infected cows. Adult worm masses containing one viable, adult female and zero to several adult males were carefully recovered by dissection of the nodule with a sterile razor blade. The masses were then incubated in 4 mL of complete culture medium (CCM), which was comprised of RPMI-1640 (Sigma-Aldrich), 5% newborn calf serum, 200 units/mL penicillin, 200 $\mu$g/mL streptomycin and 2.5 $\mu$g/mL amphotericin B (Sigma-Aldrich), in standard 12-well culture plates. Masses were maintained in the medium in a 37 °C, 5% $CO_2$ incubator overnight during which period most of the smaller and more agile adult males migrated out of the masses while the females remained in the nodules. Worm viability was checked microscopically by observing the movement of adult male worms or emergence of viable microfilariae from the nodular masses. The next day, 2 mL of the CCM was removed and replaced with 200 $\mu$M of the test drug in 2 mL CCM in each well to generate a final drug concentration of 100 $\mu$M. The compound and controls were tested in quadruplicate at each concentration and the experiments were repeated twice on different days. The negative control wells received only 1% DMSO. Cultures were terminated on day 7 post addition of drug. Adult male worm viability was visually scored on day 5 as percent reduction of motility ranging from 100% (complete inhibition of motility), 90% (only head or tail of worm moving or vibrating), 75% (worm very sluggish), 50% (worm sluggish), 25% (little change in motility), to 0% (no observable reduction in motility). Day 5 was selected for testing males because they were observed to not survive well in culture control conditions for more than 5 days. Adult female worm viability was assessed on day 7 by the standard MTT/formazan assay in which each nodular mass was placed in a well of a 48-well microtiter plate containing 500 $\mu$L of 0.5 mg/mL MTT (Sigma-Aldrich) in incomplete culture medium and then incubated in the dark at 37 °C for 30 min. Adult female worm viability was evaluated visually by the extent to which the female worm mass was stained with MTT. Mean percent inhibition of formazan formation was calculated relative to the negative control worm masses after 7 days in culture. Adult worm death positively correlated with inhibition of formazan formation. To calculate the $IC_{50}$ of the active drug, quadruplicate worm masses were incubated with final concentrations of 100 $\mu$M, 30 $\mu$M, 10 $\mu$M, 3 $\mu$M, 1 $\mu$M, 0.3 $\mu$M, and 0.1 $\mu$M, and assays were conducted as described above. $IC_{50}$ values were calculated using the "drc" R package, LL.4 function, as described for *B. pahangi*, and complete $IC_{50}$ statistical results are provided in Table S1.

**4.3.3. *O. Volvulus In Vitro* Assays.** Drug screening of *Onchocerca volvulus* L3 molting *in vitro*. L3 stage larvae previously collected and cryopreserved in Kumba, Cameroon, were rapidly thawed in a 37 °C water bath and washed in incomplete media comprised of a 1:1 ratio of Medium NCTC-109 and IMDM + GlutaMax-I containing 1X glutamine, penicillin, and streptomycin (all from Gibco by Life Technologies, Grand Island, NY). The number of L3s was adjusted to 10 worms per 50 $\mu$L, in complete medium containing 20% heat inactivated FCS. L3s were distributed into the wells of a 96-well plate containing 50 $\mu$L of 1.5 × $10^5$ normal human PBMCs. 100 $\mu$L of 2× tested drug at a final concentration of 30 $\mu$M was added. For $IC_{50}$ testing, drugs at final concentrations of 30 $\mu$M, 10 $\mu$M, 3 $\mu$M, 1 $\mu$M and 0.3 $\mu$M were added to each well for a final volume of 200 $\mu$L. Each concentration was tested in triplicate. Controls included 0.05% DMSO in complete medium and complete medium only with neither DMSO nor compound added. The 96-well plates were then incubated at 37 °C in a 5% $CO_2$ incubator for 6 days, then molting was assessed using an inverted microscope. Molting was determined in each well by counting the presence of fourth-stage larvae (L4) and empty casts of the molted L3. The percentage of inhibition of molting was calculated based on the number of treated larvae that were able to molt in comparison to the number of control larvae that had successfully molted. As described above for *B. pahangi*, $IC_{50}$ values were calculated using the "drc" R package, LL.4 function. Inhibition of *O. volvulus* L4 motility. L3 washed larvae were dispersed in a 96-well plate (10 larvae/well) containing 1.5 × $10^5$ PBMC per well in complete medium at 37 °C and in 5% $CO_2$ incubator until day 5. The highly motile L4s were then transferred into a Petri dish containing complete medium and L4 larvae were retrieved from the Petri dish and placed into a 96-well plate (8–10 larvae/well) in 100 $\mu$L of media. Tested compounds were dissolved in DMSO at a concentration of 10 mM and added to the L4s in 100 $\mu$L of complete media containing 2× the desired final concentration of 10 or 30 $\mu$M. Motility was evaluated manually every day under an inverted microscope until day 6 to 8. Each condition was tested in duplicates and repeated at least once. Motility was scored based on the following scale: 100% motility, constant coiling movement; 75% motility, slower coiling; 50% motility, slow and intermittent movement; 25% motility, very slow movement, or twitching; and 0% motility, no movement. The percentage inhibition of motility was calculated based on the % motility of the treated larvae in comparison to % motility of control larvae. $IC_{50}$ were calculated as described above.

**4.3.4. *C. Elegans* Reverse Genetic Screen.** *Caenorhabditis elegans* wild type (N2) and mutant strains were maintained on 6 cm plates seeded with *Escherichia coli* OP50 bacteria following standard protocols.[74] The following mutant strains were purchased: *gar-3 (gk305)*, *dop-5 (ok568)*, *dop-2 (vs105)*, *dop-1 (vs100)*, *ser-4 (ok512)*, *ser-2 (ok2103)*, *ser-1 (ok345)*, *ser-7 (vq2)*, *tyra-3 (ok325)*, and *gar-2 (ok520)*. These strains were provided by the *Caenorhabditis* Genetics Center (CGC). Whole organism phenotypes were compared across wild type and mutant strains using an established pipeline with development as the primary end point.[84,85] Worms were chunked from starved plates onto fresh 10 cm NGM plates seeded with *Escherichia coli OP50* bacteria and gravid worms and grown at 20 °C for 72 h. Gravid adults were bleach-synchronized and hatched overnight in K media (0.5 M NaCl, 30 mM KCl, 3 mM CaCl2, 3 mM MgSO4, MQ_H2O, 0.625 mg cholesterol). Populations of L1 larvae were seeded into 96-well plates (Fisher Scientific, 655180) at 50 worms per well in K media supplemented with *E. coli* HB101, kanamycin (25 $\mu$g/mL), and 1 $\mu$L of 100× test compound (**CLE**, **C-4**, **C-6**, **C-8**) or control solvent (final concentration 100 $\mu$M). After 48 h incubation at 20 °C with shaking at 180 rpm, excess bacteria was


https://doi.org/10.1021/acs.jmedchem.6c01435
J. Med. Chem. XXXX, XXX, XXX–XXX

removed using an AquaMax 2000 (Molecular Devices). Worms were then paralyzed with sodium azide (50 mM in M9) and imaged using an ImageXpress Nano (Molecular Devices). Images were analyzed using WrmXpress v.2.[96] Kolmogorov−Smirnov tests[95] did not show a significant departure from normality for development inhibition values (measured as the % reduction in worm length compared to the average length of untreated worms), for any of the four test compounds (using 40 WT sample proportions for each compound; $D(40) \leq 0.115$, $P \geq 0.1963$, $K \leq 0.7307$, skewness $\leq 0.7168$), justifying the use of parametric statistics. Differences in development inhibition values were tested compared to the WT values using (i) two-tailed student's $t$ tests for each mutant, with FDR correction for the number of strains tested, requiring FDR-adjusted $P \leq 10^{-10}$, and (ii) Cohen's $d$ effect size $\geq 1$. These stringent criteria were selected due to the large number of replicates, with each individual worm being computationally measured (average of 67.2 worms per strain per compound, standard deviation of 48.0).

## 4.4. *In Vivo* Animal Experiments

**4.4.1. Ethics Statement.** Animal studies were approved under New York Blood Center (NYBC) Institutional Animal Care and Use Committee (IACUC) Protocol 369 and adhered to the guidelines set forth in the NIH Guide for the Care and Use of Laboratory Animals in Research (see 18-F22) and the USDA Animal Care Policies, including regulations implementing the Animal Welfare Act (P.L. 89-544) as amended (see 18-*F*23). *O. volvulus* L3s were purified from black flies (*Simulium damnosum*) fed on consenting donors that were infected with *O. volvulus* (Institutional Review Board (IRB) protocol 320 approved by the New York Blood Center, USA and the Kumba, Cameroon IRB). After 7 days the fed flies were dissected to collect developed L3s, cleaned and cryopreserved in dimethyl sulfoxide and sucrose by using Biocool II computerized freezing equipment (FTS Systems Inc., Stone Ridge, NY, USA) as previously described.[97] Donors were not selected on the basis of sex or gender, race, ethnicity or other socially relevant groupings. Dr. Fidelis Cho-Ngwa from Cameroon was involved throughout the research and has been included among the authors. Local and regional research relevant to the study is cited frequently throughout the manuscript.

**4.4.2. Animal Infections and Efficacy of Treatment of *Brugia Pahangi*-Infected Gerbils.** Mongolian gerbils (*Meriones unguiculatus*) were sourced from the NIH/NIAID Filariasis Research Reagent Resource (FR3) Center, Athens, GA (BEI resources catalog #NR-48912). The source of gerbils for the FR3 is Charles River Laboratory, Wilmington, MA. Male gerbils 5−7 weeks old, weighing 50−60 g, were injected intraperitoneally with 200 *B. pahangi* third-stage larvae (FR3 strain, originally obtained from researchers in Malaysia by Dr. John Schacher) and then shipped to the NYBC, as previously described.[91] Infected gerbils, 5−7 months postinfection, were treated for 10 days as follows: (**1**) Gerbils were treated PO with 25 mg/kg BID 6 h apart for 10 days with either Clemizole ($n = 4$) or **C-8** ($n = 5$) dissolved in 10% DMSO + 90% Corn Oil (HY-Y1888, MCE, Monmouth Junction, NJ). All the treated animals were necropsied 30 days postlast dose. (**2**) Gerbils were treated PO with 50 mg/kg BID 6 h apart for 10 days with **C-8** (n = 3) dissolved in 10% DMSO + 90% Corn Oil (HY-Y1888, MCE, Monmouth Junction, NJ). All the treated animals were necropsied 30 days postlast dose. (**3**) Gerbils were treated with **PMZ-6** intraperitoneally (IP, BID x 2 days, QD x 7 days, 25 mg/kg, $n = 5$). The drug was dissolved in 5% DMSO, 40% PEG300 (HY-Y0873, MCE, Monmouth Junction, NJ), and 5% Tween- 80 (P1754, Sigma, St. Louis, MO) in 45% saline. All the treated animals were necropsied 48 days postlast dose. (**4**) Gerbils were treated PO with 50 mg/kg **S-17** BID 6 h apart for 10 days ($n = 3$). The drug was dissolved in 5% DMSO, 40% PEG300 (HY-Y0873, MCE, Monmouth Junction, NJ), and 5% Tween- 80 (P1754, Sigma, St. Louis, MO) in 45% saline. All the treated animals were necropsied 35 days postlast dose. The control groups ($n = 6−7$ per experiment) were treated with the vehicle solution only similarly to the experimental group. All the control animals were necropsied at the same time as the corresponding treated animals per each experiment. For all *in vivo* studies, as previously reported,[50] worms were collected from the gerbil's peritoneal cavity, counted, sexed, and examined under a dissecting microscope before being processed for analyses. Significant changes in adult worm burden were tested using one-tailed pooled student's $t$ tests (equal variance), relative to vehicle-only controls. Kolmogorov−Smirnov test[95] did not show a significant departure from normality for adult worm burden counts (using 27 vehicle-only control counts across experiments; $D(27) = 0.094$, $P = 0.9535$, $K = 0.4877$, skewness = 0.608), justifying the use of parametric statistics. To determine the effect of the compound on worm fecundity, female worms ($n = 41−84$, depending on the experiment and treatment group) were cultured individually, and the microfilariae secreted overnight from each worm were collected and counted. Female worms after overnight cultures ($n = 6$ per gerbil) were processed individually for embryogram analysis, and 2−8 female worms per gerbil were fixed for transmission electron microscopy (TEM). The number of gerbils infected per group were selected based on the availability of infected gerbils from the Filarial Research Reagent Resource Center (NIH funded core facility).

**4.4.3. RNA-Seq Sequencing and Analysis.** Surviving adult female and adult male worms from the *in vivo* gerbil experiment described above were collected and snap frozen in LN2. Total RNA was isolated separately from adult female (3 worms from each gerbil) and adult male (4 worms from each gerbil) *B. pahangi* using Trizol reagent (Invitrogen, Waltham, MA, USA). Worms were homogenized with 1.5 mm zirconium beads (Benchmark scientific, D1032−15) using BeadBug6 (Benchmark scientific, D1036, Sayreville, NJ, USA). 200 μL of Chloroform was added, followed by vigorous vertexing and incubation for 5 min. After phase separation, the aqueous layer containing RNA was transferred to new tube, and RNA was precipitated using 500 μL of isopropanol and incubated for 20 min. Samples were centrifuged at 12,000 x g for 10 min at 4 °C and the supernatant was discarded. The RNA pellet was washed with 1 mL of 75% ethanol, briefly vortexed, and centrifuged at 7,500 x g for 5 min at 4 °C. Pellets were air-dried for 5−10 min and resuspended in 30 μL of RNase- free water and stored −80 °C until use for library construction. cDNA libraries were prepared using PolyA selection, and processed cDNA was sequenced on the Illumina NovaSeq S4 platform (paired-end 150 bp reads), generating an average of 17.4 million read pairs per sample. The raw RNA-seq read files (fastq) are accessible on the NCBI Sequence Read Archive (SRA,[98] BioProject PRJNA1234536), and read count statistics and SRA accession information per sample are provided in Table S5A. Trimmomatic v0.36[99] was used to trim adapters, and the STAR aligner[100] (v2.7.5b; 2-pass mode, basic) was used to map RNA-seq reads to the *B. pahangi* genome assembly (PRJEB497.WBPS16[101]), which were then counted for every annotated protein-coding gene in the assembly using featureCounts,[102] with Transcripts Per Million (TPM) normalized gene expression values calculated using MS Excel. DESeq2 (v1.44.0)[103] was used to perform differential expression comparisons, comparing **C8**-treated worms to their vehicle control samples, and parsing at FDR-adjusted $P \leq 0.05$ and |Log2 Fold Changel $\geq 0.5$ for significant upregulation or downregulation. For all *B. pahangi* genes, putative functional annotations were assigned using InterProScan v72−103[104] to identify gene ontology[105] classifications and InterPro functional domains,[70] BlastKOALA v3.1[106] to assign KEGG[107] annotations, and the top-hit *C. elegans* (PRJNA13758, WS290[108]) and human (GRCh38.106[109]) ortholog for each *B. pahangi* protein (E value $\leq 10^{-5}$), determined using BLAST[110] (NCBI blastp, v2.7.1+). A total of 165 *B. pahangi* GPCRs were identified based on Compara family GPCR identifications from the previously published International Helminth Genomes Consortium study[69] (114 genes), and based on the identification "G protein-coupled receptor" or "GPCR" among the annotated InterPro domains for each protein (additional 51 genes). Functional enrichment analysis was performed using sets of differentially expressed genes of interest relative to all genes as a background using GOSTATS v2.70.0.[111] InterPro and KEGG pathway enrichment analysis were performed on the WebGestalt[71] website (version 2024) using annotation data collected as described above. For all enrichment analyses, FDR-adjusted $P$ values $\leq 0.05$ were required for significance. Z scores of log FPKM values were


https://doi.org/10.1021/acs.jmedchem.6c01435
J. Med. Chem. XXXX, XXX, XXX−XXX

calculated and visualized as heatmaps using MS Excel (version 16.94). All functional annotation data, read counts per sample, normalized expression values (TPM), and differential expression statistics are provided for every *B. pahangi* gene in Table S5B.

**4.4.4. Rodent Pharmacokinetic (PK) Studies.** Gerbils: Naïve male gerbils (Charles River Laboratory, Wilmington, MA.; 70 g each) were treated PO once with 50 mg/kg of **CLE** dissolved in 0.5% carboxymethylcellulose sodium salt (C4888, Sigma, St. Louis, MO), and other compounds dissolved in 5% DMSO, 40% PEG300 (HY-Y0873, MCE, Monmouth Junction, NJ), and 5% Tween- 80 (P1754, Sigma, St. Louis, MO) in 45% saline. The gerbils were bled 1, 4, 8, and 24 h after the PO treatment and the plasma samples were frozen until tested. Bioanalysis and quantification of compounds in plasma samples were performed after compound tuning using a standard curve of each compound diluted in gerbil plasma and routine LC-MS/MS techniques. Plasma samples and standards were extracted in acetonitrile containing 0.5 ng/mL of verapamil as an internal standard and the supernatants analyzed using a Shimadzu LC-20AD HPLC and a SCIEX Triple Quad 3500 tandem mass spectrometer. Using Analyst software (SCIEX, Framingham, MA) scan data were analyzed and the ratios of analyte peak area to internal standard peak area were used to generate a standard curve and calculate the plasma concentrations of unknowns. PK statistics were calculated using standard calculations, performed in MS Excel. Mice: Compounds were tested for their pharmacokinetic properties in mice following a single IP dose (10 mg/kg). Three animals per group (male, CD-1 strain, sourced from Beijing Weitong Lihua Experimental Animal Technology Co., Ltd., Beijing, China) were dosed and then blood was drawn at eight different sampling time points (0.08, 0.25, 0.5, 1, 2, 4, 8, 24 h) post dosing. Bioanalysis and quantification of plasma and feces samples were performed using standard and routine LC-MS/MS techniques. PK statistics were calculated using standard calculations, performed in MS Excel. $CL_{int}$ ($\mu$L/min/mg) values were converted to predicted *in vivo* $CL_{app}$ (L/h/kg) values by multiplying by the microsomal protein per gram of liver for mice (MPPGL; 35 mg/g[112]) and then by the liver weight to body weight for mice (LW BW, 54.9 g/kg[113]), and multiplying by $60/10^6$ as a unit conversion factor.

### 4.5. Bioinformatic Analyses

**4.5.1. Random Forest Analysis.** A total of 61 compound properties were calculated for all GPCR inhibitors and analogs, using Schrödinger (Release 2024-4: Maestro, Schrödinger, LLC, New York, NY, 2024). Several "Energy" values were calculated for each compound, and for downstream analysis, the properties associated with the lowest energy value were used. A supervised Random Forest machine-learning tool (RF; randomForest library in R[114]) was ran using compound property inputs on subsets of compounds, using "out of bag" (leave one out) validation, and default settings except ntree = 10000 to improve accuracy. Property importance was calculated by RF as Mean decrease accuracy (MDA) values. Model performance was evaluated using Receiver Operating Characteristic (ROC) curve analysis. Statistical significance of the RF classifier's performance was assessed using a Wilcoxon rank sum test implemented through the verification package's roc.area function, and through classification accuracy and a binomial distribution test of the accuracy. RF input data is provided in Table S3A, and property MDA values are provided in Table S3B.

**4.5.2. Statistical Analysis.** Statistical analyses are described for each section, and detailed statistical results for motility, $IC_{50}$, $CC_{50}$, mf counts, embryogram data, worm burden, gonad contents and bioaccumulation data are provided for all comparisons and compounds in Table S1. Detailed RNA-seq differential expression statistics are provided for all genes and all comparisons in Table S5B. All replicates in all tests represent distinct biological sample replicates and not technical replicates.

## ■ ASSOCIATED CONTENT

### Data Availability Statement

Table S1 provides, for all compounds tested, detailed motility inhibition and $IC_{50}$ data and statistics for all species tested, detailed HepG2 cell cytotoxicity $CC_{50}$ data and statistics, and detailed *B. pahangi* embryogram data and statistics. Supporting Information additionally provide graphs of all analyzed *in vitro* $IC_{50}$ and HepG2 $CC_{50}$ curves for all compounds. All SMILES strings, IUPAC codes, and chemical formulas for all compounds are provided in Table S1, compound structures are provided in the main figures, and synthesis details are provided in Schemes 1−4, and detailed synthesis methods and characterization of compounds, as well as 1H NMR, and LCMS Spectra for all compounds are provided in Supporting Information. All Random Forest input data is provided in Table S3, and. All RNA-seq raw sequence data files are uploaded to the NCBI Sequence Read Archive (SRA), BioProject PRJNA1234536, with accessions for all samples provided in Table S5A. All functional annotations, BLAST results to other species, raw RNA-seq read counts, normalized gene expression values and detailed DESeq2 differential expression statistics are provided for all genes and all comparisons in Table S5B. Code availability statement: DESeq2 code used for differential expression analysis was based on our previously published protocol available with no restrictions on protocols.io (dx.doi.org/10.21203/rs.3.pex-2532/v1). Random Forest analysis was based on our previously published protocol available with no restrictions on protocols.io (dx.doi.org/10.21203/rs.3.pex-2283/v3). All other statistical analyses are described in sufficient detail to be repeated. Availability of materials: All SMILES strings, IUPAC codes, and chemical formulas for all compounds are provided in Table S1, compound structures are provided in the main figures, synthesis details are provided in Schemes 1−4, and detailed synthesis methods and characterization of compounds, as well as 1H NMR, and LCMS spectra for all compounds are provided in Supporting Information. No additional unique biological materials or cell lines were generated for the study.

### Supporting Information

The Supporting Information is available free of charge at https://pubs.acs.org/doi/10.1021/acs.jmedchem.6c01435.

Supporting Figures **S1−S5**; $^1$H NMR spectra; LCMS chromatograms for all compounds; *in vitro B. pahangi* $IC_{50}$ and HepG2 cell $CC_{50}$ statistics and plots for all compounds (PDF)

SMILES Strings; biological data associated with compounds (CSV)

Supporting Tables S1−S5 (XLSX)

## ■ AUTHOR INFORMATION

### Corresponding Authors

**Makedonka Mitreva** − *Department of Medicine, Washington University School of Medicine, St. Louis, Missouri 63110, United States; McDonnell Genome Institute, Washington University School of Medicine, St. Louis, Missouri 63108, United States*; Email: Mmitreva@wustl.edu

**James W. Janetka** − *Department of Biochemistry and Molecular Biophysics, and Molecular Microbiology, Washington University School of Medicine, St. Louis, Missouri 63110, United States*; orcid.org/0000-0002-9888-5411; Email: Janetkaj@wustl.edu



https://doi.org/10.1021/acs.jmedchem.6c01435
J. Med. Chem. XXXX, XXX, XXX−XXX

**Sara Lustigman** − *Molecular Parasitology, Lindsley F. Kimball Research Institute, New York Blood Center, New York, New York 10065, United States*; Email: SLustigman@nybc.org

## Authors

**Bruce A. Rosa** − *Department of Medicine, Washington University School of Medicine, St. Louis, Missouri 63110, United States*; orcid.org/0000-0002-6820-446X

**Zhenfu Han** − *Department of Biochemistry and Molecular Biophysics, and Molecular Microbiology, Washington University School of Medicine, St. Louis, Missouri 63110, United States*

**Ashutosh Arun** − *Department of Medicine, Washington University School of Medicine, St. Louis, Missouri 63110, United States*

**Nancy Tricoche** − *Molecular Parasitology, Lindsley F. Kimball Research Institute, New York Blood Center, New York, New York 10065, United States*

**Ricardo Peguero** − *Molecular Parasitology, Lindsley F. Kimball Research Institute, New York Blood Center, New York, New York 10065, United States*

**Victoria Banas** − *Department of Biochemistry and Molecular Biophysics, and Molecular Microbiology, Washington University School of Medicine, St. Louis, Missouri 63110, United States*

**Melanie Shadrick** − *Department of Biochemistry and Molecular Biophysics, and Molecular Microbiology, Washington University School of Medicine, St. Louis, Missouri 63110, United States*

**Michelle Fath** − *Department of Biochemistry and Molecular Biophysics, and Molecular Microbiology, Washington University School of Medicine, St. Louis, Missouri 63110, United States*

**Phawiya Suksomboon** − *Department of Medicine, Washington University School of Medicine, St. Louis, Missouri 63110, United States*

**Suman Bharti** − *Department of Medicine, Washington University School of Medicine, St. Louis, Missouri 63110, United States*

**Mitchell Bancks** − *Department of Medicine, Washington University School of Medicine, St. Louis, Missouri 63110, United States*

**Elena G. Rehborg** − *Department of Pathobiological Sciences, University of Wisconsin-Madison, Madison, Wisconsin 53706, United States*

**Mostafa Zamanian** − *Department of Pathobiological Sciences, University of Wisconsin-Madison, Madison, Wisconsin 53706, United States*; orcid.org/0000-0001-9233-1760

**Fidelis Cho-Ngwa** − *ANDI Centre of Excellence for Onchocerciasis Drug Research, Biotechnology Unit, Faculty of Science, University of Buea, Buea, Cameroon*

Complete contact information is available at: https://pubs.acs.org/10.1021/acs.jmedchem.6c01435

## Author Contributions

B.A.R., Z.H., and A.A. contributed equally to the manuscript. B.A.R. performed statistical analyses, random forest, and RNA-seq analyses. Z.H., V.B., M.S., and M.F. designed and synthesized analogs. A.A., P.S., S.B., and M.B. performed biological assays on *B. pahangi* and HepG2 cells. N.T. and R.P. performed TEM analysis and *Onchocerca* biological assays. E.G.R. and M.Z. oversaw and performed the *C. elegans* reverse genetic screen. F.C.-N. supervised all work in Cameroon. S.L., J.W.J., M.M., B.A.R. wrote the manuscript. S.L., J.W.J., and M.M. jointly supervised the research. All authors reviewed and edited the manuscript.

## Notes

The authors declare the following competing financial interest(s): ZH, JWJ and MM are inventors on a patent application covering some of these compounds. All other authors declare no competing financial interests.

## ■ ACKNOWLEDGMENTS

This work was supported by the National Institutes of Health (NIH), National Institute of Allergy and Infectious Diseases (NIAID) R01EY033195 and R01AI174587 to M.M., J.W.J., and S.L. E.G.R., and M.Z. were supported by the National Institutes of Health (NIH), National Institute of Allergy and Infectious Diseases (NIAID) R01AI151171 awarded to M.Z. *Brugia pahangi* life cycle stages were obtained through the NIH/NIAID Filarial Research Reagent Resource Center (FR3) Morphological voucher specimens are stored at the Harold W. Manter Museum at the University of Nebraska, accession numbers P2021-2032. Primary receptor binding profiles and $K_i$ determinations for parent drugs and selected analogs with human GPCRs was generously provided by the National Institute of Mental Health's Psychoactive Drug Screening Program, Contract #75N95023C00021 (NIMH PDSP). The NIMH PDSP is directed by Bryan L. Roth at the University of North Carolina at Chapel Hill, with Project Officer Jamie Driscoll at NIMH, Bethesda, MD, USA. For experimental details, please refer to the PDSP website: https://pdsp.unc.edu/ims/investigator/web/. We acknowledge the Genome Technology Access Center at the McDonnell Genome Institute at Washington University School of Medicine for their assistance with genomic sequencing. The Center is partially supported by the NCI Cancer Center Support Grant #P30 CA91842 to the Siteman Cancer Center from the National Center for Research Resources (NCRR), a component of the National Institutes of Health (NIH), and the NIH Roadmap for Medical Research. Some *C. elegans* strains were provided by the CGC, which is funded by the NIH Office of Research Infrastructure Programs (P40 OD010440).

## ■ ABBREVIATIONS

$CC_{50}$, cytotoxicity concentration corresponding to 50% death of HepG2 cells; **CLE**, clemizole; GPCR, G-protein Couple Receptor; F-$IC_{50}$, inhibitory concentration corresponding to 50% inhibition of worm motility in female worms; F−SI, female worm "selectivity index" representing the ratio of $CC_{50}$ to $IC_{50}$; IVM, ivermectin; M-$IC_{50}$, inhibitory concentration corresponding to 50% inhibition of worm motility in male worms; M-SI, male worm "selectivity index" representing the ratio of $CC_{50}$ to $IC_{50}$; MDA, mass drug administration; Mf, microfilariae; **PMZ**, pimozide; **PRO**, proroxan; **SUL**, suloctidil; TEM, transmission electron microscopy; WHO, World Health Organization

## ■ REFERENCES

(1) Hoerauf, A.; Pfarr, K.; Mand, S.; Debrah, A. Y.; Specht, S. Filariasis in Africa-treatment challenges and prospects. *Clin. Microbiol. Infect.* **2011**, *17*, 977−985.

(2) Lustigman, S.; Prichard, R. K.; Gazzinelli, A.; Grant, W. N.; Boatin, B. A.; McCarthy, J. S.; Basanez, M.-G. A research agenda for helminth diseases of humans: the problem of helminthiases. *PLoS Negl. Trop. Dis.* **2012**, *6*, No. e1582.
(3) Prichard, R. K.; Basanez, M.-G.; Boatin, B. A.; McCarthy, J. S.; Garcia, H. H.; Yang, G.-J.; Sripa, B.; Lustigman, S. A research agenda for helminth diseases of humans: intervention for control and elimination. *PLoS Negl. Trop. Dis.* **2012**, *6*, No. e1549.
(4) Plaisier, A. P.; van Oortmarssen, G. J.; Remme, J.; Habbema, J. D. F. The reproductive lifespan of Onchocerca volvulus in West African savanna. *Acta Trop.* **1991**, *48*, 271−284.
(5) World Health Organization. *Global programme to eliminate lymphatic filariasis*; World Health Organization, 2010.
(6) Traore, M. O.; Sarr, M. D.; Badji, A.; Bissan, Y.; Diawara, L.; Doumbia, K.; Goita, S. F.; Konate, L.; Mounkoro, K.; Seck, A. F.; Toe, L.; Toure, S.; Remme, J. H. Proof-of-principle of onchocerciasis elimination with ivermectin treatment in endemic foci in Africa: final results of a study in Mali and Senegal. *PLoS Negl. Trop. Dis.* **2012**, *6*, No. e1825.
(7) Ottesen, E. A.; Hooper, P. J.; Bradley, M.; Biswas, G. The global programme to eliminate lymphatic filariasis: health impact after 8 years. *PLoS Negl. Trop. Dis.* **2008**, *2*, No. e317.
(8) Walker, M.; Pion, S. D. S.; Fang, H.; Gardon, J.; Kamgno, J.; Basanez, M. G.; Boussinesq, M. Macrofilaricidal Efficacy of Repeated Doses of Ivermectin for the Treatment of River Blindness. *Clin. Infect. Dis.* **2017**, *65*, 2026−2034.
(9) Turner, H. C.; Churcher, T. S.; Walker, M.; Osei-Atweneboana, M. Y.; Prichard, R. K.; Basanez, M. G. Uncertainty surrounding projections of the long-term impact of ivermectin treatment on human onchocerciasis. *PLoS Negl. Trop. Dis.* **2013**, *7*, No. e2169.
(10) Turner, H. C.; Walker, M.; Churcher, T. S.; Osei-Atweneboana, M. Y.; Biritwum, N.-K.; Hopkins, A.; Prichard, R. K.; Basanez, M.-G. Reaching the London Declaration on Neglected Tropical Diseases Goals for Onchocerciasis: An Economic Evaluation of Increasing the Frequency of Ivermectin Treatment in Africa. *Clin. Infect. Dis.* **2014**, *59*, 923−932.
(11) Molyneux, D. H.; Hopkins, A.; Bradley, M. H.; Kelly-Hope, L. A. Multidimensional complexities of filariasis control in an era of large-scale mass drug administration programmes: a can of worms. *Parasites Vectors* **2014**, *7*, 363.
(12) Vos, T.; Allen, C.; Arora, M.; Barber, R. M.; Bhutta, Z. A.; Brown, A.; Carter, A.; Casey, D. C.; Charlson, F. J.; Chen, A. Z.; et al. Global, regional, and national incidence, prevalence, and years lived with disability for 310 diseases and injuries, 1990−2015: a systematic analysis for the Global Burden of Disease Study 2015. *Lancet* **2016**, *388*, 1545−1602.
(13) Taylor, M. J.; Hoerauf, A.; Bockarie, M. Lymphatic filariasis and onchocerciasis. *Lancet* **2010**, *376*, 1175−1185.
(14) World Health Organization. *WHO launches global consultations for a new Roadmap on neglected tropical diseases*; World Health Organization, 2019.
(15) Group NTDMCO. The World Health Organization 2030 goals for onchocerciasis: Insights and perspectives from mathematical modelling: NTD Modelling Consortium Onchocerciasis Group. *Gates Open Res.* **2019**, *3*, 1545. .
(16) Kim, Y. E.; Remme, J. H.; Steinmann, P.; Stolk, W. A.; Roungou, J. B.; Tediosi, F. Control, elimination, and eradication of river blindness: scenarios, timelines, and ivermectin treatment needs in Africa. *PLoS Negl. Trop. Dis.* **2015**, *9*, No. e0003664.
(17) Hopkins, A. D. Neglected tropical diseases in Africa: a new paradigm. *Int. Health* **2016**, *8* (1), i28−33.
(18) World Health Organization*African Programme for Onchocerciasis Control: progress report, 2013-2014*World Health Organization2014
(19) Risch, F.; Kazakov, A.; Specht, S.; Pfarr, K.; Fischer, P. U.; Hoerauf, A.; Hubner, M. P. The long and winding road towards new treatments against lymphatic filariasis and onchocerciasis. *Trends Parasitol.* **2024**, *40*, 829−845.
(20) Boatin, B. A.; Basanez, M.-G.; Prichard, R. K.; Awadzi, K.; Barakat, R. M.; Garcia, H. H.; Gazzinelli, A.; Grant, W. N.; McCarthy, J. S.; N'Goran, E. K.; et al. A research agenda for helminth diseases of humans: towards control and elimination. *PLoS Negl. Trop. Dis.* **2012**, *6*, No. e1547.
(21) Osei-Atweneboana, M. Y.; Awadzi, K.; Attah, S. K.; Boakye, D. A.; Gyapong, J. O.; Prichard, R. K. Phenotypic evidence of emerging ivermectin resistance in Onchocerca volvulus. *PLoS Negl. Trop. Dis.* **2011**, *5*, No. e998.
(22) Doyle, S. R.; Bourguinat, C.; Nana-Djeunga, H. C.; Kengne-Ouafo, J. A.; Pion, S. D. S.; Bopda, J.; Kamgno, J.; Wanji, S.; Che, H.; Kuesel, A. C.; Walker, M.; Basanez, M. G.; Boakye, D. A.; Osei-Atweneboana, M. Y.; Boussinesq, M.; Prichard, R. K.; Grant, W. N. Genome-wide analysis of ivermectin response by Onchocerca volvulus reveals that genetic drift and soft selective sweeps contribute to loss of drug sensitivity. *PLoS Negl. Trop. Dis.* **2017**, *11*, No. e0005816.
(23) Lustigman, S.; McCarter, J. P. Ivermectin Resistance in Onchocerca volvulus: Toward a Genetic Basis. *PLoS Negl. Trop. Dis.* **2007**, *1*, No. e76.
(24) Boussinesq, M.; Gardon, J.; Gardon-Wendel, N.; Chippaux, J.-P. Clinical picture, epidemiology and outcome of Loa-associated serious adverse events related to mass ivermectin treatment of onchocerciasis in Cameroon. *Filaria J.* **2003**, *2*, S4.
(25) Debrah, A. Y.; Specht, S.; Klarmann-Schulz, U.; Batsa, L.; Mand, S.; Marfo-Debrekyei, Y.; Fimmers, R.; Dubben, B.; Kwarteng, A.; Osei-Atweneboana, M.; Boakye, D.; Ricchiuto, A.; Buttner, M.; Adjei, O.; Mackenzie, C. D.; Hoerauf, A. Doxycycline Leads to Sterility and Enhanced Killing of Female Onchocerca volvulus Worms in an Area With Persistent Microfilaridermia After Repeated Ivermectin Treatment: A Randomized, Placebo-Controlled, Double-Blind Trial. *Clin. Infect. Dis.* **2015**, *61*, 517−526.
(26) Wanji, S.; Nji, T. M.; Hamill, L.; Dean, L.; Ozano, K.; Njouendou, A. J.; Abong, R. A.; Obie, E. D.; Amuam, A.; Ekanya, R.; et al. Implementation of test-and-treat with doxycycline and temephos ground larviciding as alternative strategies for accelerating onchocerciasis elimination in an area of loiasis co-endemicity: the COUNTDOWN consortium multi-disciplinary study protocol. *Parasites Vectors* **2019**, *12*, 574.
(27) Milton, P.; Hamley, J. I. D.; Walker, M.; Basanez, M. G. Moxidectin: an oral treatment for human onchocerciasis. *Expert Rev. Anti-Infect. Ther.* **2020**, *18*, 1067−1081.
(28) Kura, K.; Milton, P.; Hamley, J. I. D.; Walker, M.; Bakajika, D. K.; Kanza, E. M.; Opoku, N. O.; Howard, H.; Nigo, M. M.; Asare, S.; et al. Can mass drug administration of moxidectin accelerate onchocerciasis elimination in Africa? *Philos. Trans. R. Soc., B* **2023**, *378*, 20220277.
(29) World Health Organization. *Report of the 25th WHO Expert Committee on Selection and Use of Essential Medicines*; World Health Organization, 2025.https://www.who.int/publications/i/item/B09544.
(30) Assmus, F.; Hoglund, R. M.; Monnot, F.; Specht, S.; Scandale, I.; Tarning, J. Drug development for the treatment of onchocerciasis: Population pharmacokinetic and adverse events modeling of emodepside. *PLoS Negl. Trop. Dis.* **2022**, *16*, No. e0010219.
(31) Jongo, S.; Ackermann, E.; Nyaulingo, G.; Mbaraka, H.; Reus, E.; Cicconi, S.; Saxena, M.; Kassim, K.; Tumbo, A.; Rashid, M. A.; et al. Pharmacokinetics, safety, and tolerability of an oxfendazole tablet formulation: a phase 1, randomized, placebo-controlled trial in healthy African volunteers. *Antimicrob. Agents Chemother.* **2026**, *70*, No. e01315−25.
(32) Drugs for Neglected Diseases Initiative. *Fusidic Acid Macrofilaricide Evaluation (FAME): Repurposing fusidic acid as a potential short-course treatment for onchocerciasis*; 2025. https://dndi.org/global-networks/fusidic-acid-macrofilaricide-evaluation-fame/.
(33) Tyagi, R.; Bulman, C. A.; Cho-Ngwa, F.; Fischer, C.; Marcellino, C.; Arkin, M. R.; McKerrow, J. H.; McNamara, C. W.; Mahoney, M.; Tricoche, N.; et al. An Integrated Approach to Identify New Anti-Filarial Leads to Treat River Blindness, a Neglected Tropical Disease. *Pathogens* **2021**, *10*, 71.


https://doi.org/10.1021/acs.jmedchem.6c01435
J. Med. Chem. XXXX, XXX, XXX−XXX

(34) Hauser, A. S.; Chavali, S.; Masuho, I.; Jahn, L. J.; Martemyanov, K. A.; Gloriam, D. E.; Babu, M. M. Pharmacogenomics of GPCR Drug Targets. *Cell* **2018**, *172*, 41−54.E19.
(35) Hauser, A. S.; Attwood, M. M.; Rask-Andersen, M.; Schioth, H. B.; Gloriam, D. E. Trends in GPCR drug discovery: new agents, targets and indications. *Nat. Rev. Drug Discovery* **2017**, *16*, 829−842.
(36) Berman, H.; Henrick, K.; Nakamura, H. Announcing the worldwide Protein Data Bank. *Nat. Struct. Biol.* **2003**, *10*, 980.
(37) Chan, J. D.; Acharya, S.; Day, T. A.; Marchant, J. S. Pharmacological profiling an abundantly expressed schistosome serotonergic GPCR identifies nuciferine as a potent antagonist. *Int. J. Parasitol. Drugs Drug Resist.* **2016**, *6*, 364−370.
(38) WeIz, C.; Harder, A.; Schnieder, T.; Hoglund, J.; von Samson-Himmelstjerna, G. Putative G protein-coupled receptors in parasitic nematodes−potential targets for the new anthelmintic class cyclo-octadepsipeptides? *Parasitol. Res.* **2005**, *97* (1), S22−S32.
(39) Chan, J. D.; Cupit, P. M.; Gunaratne, G. S.; McCorvy, J. D.; Yang, Y.; Stoltz, K.; Webb, T. R.; Dosa, P. I.; Roth, B. L.; Abagyan, R.; et al. The anthelmintic praziquantel is a human serotoninergic G-protein-coupled receptor ligand. *Nat. Commun.* **2017**, *8*, 1910.
(40) Le Clec'h, W.; Chevalier, F. D.; Mattos, A. C. A.; Strickland, A.; Diaz, R.; McDew-White, M.; Rohr, C. M.; Kinung'hi, S.; Allan, F.; Webster, B. L.; et al. Genetic analysis of praziquantel response in schistosome parasites implicates a transient receptor potential channel. *Sci. Transl. Med.* **2021**, *13*, No. eabj9114.
(41) Chulkov, E. G.; Palygin, O.; Yahya, N. A.; Park, S. K.; Marchant, J. S. Electrophysiological characterization of a schistosome transient receptor potential channel activated by praziquantel. *Int. J. Parasitol.* **2023**, *53*, 415−425.
(42) Park, S.-K.; Friedrich, L.; Yahya, N. A.; Rohr, C. M.; Chulkov, E. G.; Maillard, D.; Rippmann, F.; Spangenberg, T.; Marchant, J. S. Mechanism of praziquantel action at a parasitic flatworm ion channel. *Sci. Transl. Med.* **2021**, *13*, No. eabj5832.
(43) White, W. H.; Gutierrez, J. A.; Naylor, S. A.; Cook, C. A.; Gonzalez, I. C.; Wisehart, M. A.; Smith, C. K., II; Thompson, W. A. In vitro and in vivo characterization of p-amino-phenethyl-m-trifluoromethylphenyl piperazine (PAPP), a novel serotonergic agonist with anthelmintic activity against Haemonchus contortus, Teladorsagia circumcincta and Trichostrongylus colubriformis. *Vet. Parasitol.* **2007**, *146*, 58−65.
(44) Cotton, J. A.; Bennuru, S.; Grote, A.; Harsha, B.; Tracey, A.; Beech, R.; Doyle, S. R.; Dunn, M.; Hotopp, J. C. D.; Holroyd, N.; et al. The genome of Onchocerca volvulus, agent of river blindness. *Nat. Microbiol.* **2016**, *2*, 16216.
(45) Richter, J. M.; Schaefer, M.; Hill, K. Clemizole hydrochloride is a novel and potent inhibitor of transient receptor potential channel TRPC5. *Mol. Pharmacol.* **2014**, *86*, 514−521.
(46) Chadehumbe, M. A.; Greydanus, D. E.; Feucht, C.; Patel, D. R. Psychopharmacology of tic disorders in children and adolescents. *Pediatr. Clin.* **2011**, *58*, 259−272.
(47) Gurkalo, V. K.; Zabezhinskii, M. A.; Pliss, G. B.; Krylov, S. S. Adrenergic component in the hepatotropic carcinogenic effect of diethylnitrosamine. *Bull. Exp. Biol. Med.* **1977**, *83*, 536−539.
(48) Zhong, W.; Li, Y.; Yuan, Y.; Zhong, H.; Huang, C.; Huang, J.; Lin, Y.; Huang, J. Characterization of Molecular Heterogeneity Associated With Tumor Microenvironment in Clear Cell Renal Cell Carcinoma to Aid Immunotherapy. *Front. Cell Dev. Biol.* **2021**, *9*, 736540.
(49) Chan, W. K.; Zhang, H.; Yang, J.; Brender, J. R.; Hur, J.; Ozgur, A.; Zhang, Y. GLASS: a comprehensive database for experimentally validated GPCR-ligand associations. *Bioinformatics* **2015**, *31*, 3035−3042.
(50) Bulman, C. A.; Bidlow, C. M.; Lustigman, S.; Cho-Ngwa, F.; Williams, D.; Rascón, A. A., Jr.; Tricoche, N.; Samje, M.; Bell, A.; Suzuki, B.; et al. Repurposing auranofin as a lead candidate for treatment of lymphatic filariasis and onchocerciasis. *PLoS Negl. Trop. Dis.* **2015**, *9*, No. e0003534.
(51) Cho-Ngwa, F.; Mbah, G. E.; Ayiseh, R. B.; Ndi, E. M.; Monya, E.; Tumanjong, I. M.; Mainsah, E. N.; Sakanari, J.; Lustigman, S. Development and validation of an Onchocerca ochengi adult male worm gerbil model for macrofilaricidal drug screening. *PLoS Negl. Trop. Dis.* **2019**, *13*, No. e0007556.
(52) Ngwewondo, A.; Wang, M.; Manfo, F. P. T.; Samje, M.; Ganin's, J. N.; Ndi, E.; Andersen, R. J.; Cho-Ngwa, F. Filaricidal properties of Lantana camara and Tamarindus indica extracts, and Lantadene A from L. camara against Onchocerca ochengi and Loa loa. *PLoS Negl. Trop. Dis.* **2018**, *12*, No. e0006565.
(53) Voronin, D.; Tricoche, N.; Jawahar, S.; Shlossman, M.; Bulman, C. A.; Fischer, C.; Suderman, M. T.; Sakanari, J. A.; Lustigman, S. Development of a preliminary in vitro drug screening assay based on a newly established culturing system for pre-adult fifth-stage Onchocerca volvulus worms. *PLoS Negl. Trop. Dis.* **2019**, *13*, No. e0007108.
(54) Alvarez, L. I.; Mottier, M. L.; Lanusse, C. E. Drug transfer into target helminth parasites. *Trends Parasitol.* **2007**, *23*, 97−104.
(55) Sandhu, A.; Badal, D.; Sheokand, R.; Tyagi, S.; Singh, V. Specific collagens maintain the cuticle permeability barrier in Caenorhabditis elegans. *Genetics* **2021**, *217*, iyaa047.
(56) Tyagi, R.; Maddirala, A. R.; Elfawal, M.; Fischer, C.; Bulman, C. A.; Rosa, B. A.; Gao, X.; Chugani, R.; Zhou, M.; Helander, J.; Brindley, P. J.; Tseng, C. C.; Greig, I. R.; Sakanari, J.; Wildman, S. A.; Aroian, R.; Janetka, J. W.; Mitreva, M. Small Molecule Inhibitors of Metabolic Enzymes Repurposed as a New Class of Anthelmintics. *ACS Infect. Dis.* **2018**, *4*, 1130−1145.
(57) Williams, P. B.; Crandall, E.; Sheppard, J. D. Azelastine hydrochloride, a dual-acting anti-inflammatory ophthalmic solution, for treatment of allergic conjunctivitis. *Clin. Ophthalmol.* **2010**, *4*, 993−1001.
(58) Kashyap, S. S.; Verma, S.; Voronin, D.; Lustigman, S.; Kulke, D.; Robertson, A. P.; Martin, R. J. Emodepside has sex-dependent immobilizing effects on adult Brugia malayi due to a differentially spliced binding pocket in the RCK1 region of the SLO-1 K channel. *PLoS Pathog.* **2019**, *15*, No. e1008041.
(59) Harder, A.; Schmitt-Wrede, H. P.; Krucken, J.; Marinovski, P.; Wunderlich, F.; Willson, J.; Amliwala, K.; Holden-Dye, L.; Walker, R. Cyclooctadepsipeptides−an anthelmintically active class of compounds exhibiting a novel mode of action. *Int. J. Antimicrob. Agents* **2003**, *22*, 318−331.
(60) Hubner, M. P.; Townson, S.; Gokool, S.; Tagboto, S.; Maclean, M. J.; Verocai, G. G.; Wolstenholme, A. J.; Frohberger, S. J.; Hoerauf, A.; Specht, S.; Scandale, I.; Harder, A.; Glenschek-Sieberth, M.; Hahnel, S. R.; Kulke, D. Evaluation of the in vitro susceptibility of various filarial nematodes to emodepside. *Int. J. Parasitol. Drugs Drug Resist.* **2021**, *17*, 27−35.
(61) Lotz, C. N.; Mrimi, E. C.; Schneeberger, P. H. H.; Ali, S. M.; Hattendorf, J.; Keiser, J. Performance of real-time polymerase chain reaction and Kato-Katz for diagnosing soil-transmitted helminth infections and evaluating treatment efficacy of emodepside in randomized controlled trials. *PLoS Negl. Trop. Dis.* **2025**, *19*, No. e0012872.
(62) Mrimi, E. C.; Welsche, S.; Ali, S. M.; Hattendorf, J.; Keiser, J. Emodepside for Trichuris trichiura and Hookworm Infection. *N. Engl. J. Med.* **2023**, *388*, 1863−1875.
(63) Brooks, W. H.; Guida, W. C.; Daniel, K. G. The significance of chirality in drug design and development. *Curr. Top. Med. Chem.* **2011**, *11*, 760−770.
(64) Zeniou, M.; Feve, M.; Mameri, S.; Dong, J.; Salome, C.; Chen, W.; El-Habr, E. A.; Bousson, F.; Sy, M.; Obszynski, J.; et al. Chemical Library Screening and Structure-Function Relationship Studies Identify Bisacodyl as a Potent and Selective Cytotoxic Agent Towards Quiescent Human Glioblastoma Tumor Stem-Like Cells. *PLoS One* **2015**, *10*, No. e0134793.
(65) Richter, M. F.; Drown, B. S.; Riley, A. P.; Garcia, A.; Shirai, T.; Svec, R. L.; Hergenrother, P. J. Predictive compound accumulation rules yield a broad-spectrum antibiotic. *Nature* **2017**, *545*, 299−304.
(66) Obach, R. S. Prediction of Human Clearance of Twenty-Nine Drugs from Hepatic Microsomal Intrinsic Clearance Data: An Examination of In Vitro Half-Life Approach and Nonspecific Binding to Microsomes. *Drug Metab. Dispos.* **1999**, *27*, 1350−1359.


https://doi.org/10.1021/acs.jmedchem.6c01435
J. Med. Chem. XXXX, XXX, XXX−XXX

(67) Walker, M.; Hamley, J. I. D.; Milton, P.; Monnot, F.; Pedrique, B.; Basanez, M.-G. Designing antifilarial drug trials using clinical trial simulators. *Nat. Commun.* **2020**, *11*, 2685.
(68) Drugs for Neglected Diseases Initiative. *Target product profile for river blindness*; DNDI, 2025. https://dndi.org/diseases/parasitic-worms/river-blindness/target-product-profile/.
(69) International Helminth Genomes Consortium. Comparative genomics of the major parasitic worms. *Nat. Genet.* **2019**, *51*, 163−174. .
(70) Blum, M.; Andreeva, A.; Florentino, L. C.; Chuguransky, S. R.; Grego, T.; Hobbs, E.; Pinto, B. L.; Orr, A.; Paysan-Lafosse, T.; Ponamareva, I.; Salazar, G. A.; Bordin, N.; Bork, P.; Bridge, A.; Colwell, L.; Gough, J.; Haft, D. H.; Letunic, I.; Llinares-Lopez, F.; Marchler-Bauer, A.; Meng-Papaxanthos, L.; Mi, H.; Natale, D. A.; Orengo, C. A.; Pandurangan, A. P.; Piovesan, D.; Rivoire, C.; Sigrist, C. J. A.; Thanki, N.; Thibaud-Nissen, F.; Thomas, P. D.; Tosatto, S. C. E.; Wu, C. H.; Bateman, A. InterPro: the protein sequence classification resource in 2025. *Nucleic Acids Res.* **2025**, *53*, D444−D456.
(71) Elizarraras, J. M.; Liao, Y.; Shi, Z.; Zhu, Q.; Pico, A. R.; Zhang, B. WebGestalt 2024: faster gene set analysis and new support for metabolomics and multi-omics. *Nucleic Acids Res.* **2024**, *52*, W415−W421.
(72) Van Oekelen, D.; Luyten, W. H.; Leysen, J. E. 5-HT2A and 5-HT2C receptors and their atypical regulation properties. *Life Sci.* **2003**, *72*, 2429−2449.
(73) Rajagopal, S.; Shenoy, S. K. GPCR desensitization: Acute and prolonged phases. *Cell. Signalling* **2018**, *41*, 9−16.
(74) Pu, L.; Wang, J.; Lu, Q.; Nilsson, L.; Philbrook, A.; Pandey, A.; Zhao, L.; Schendel, R. V.; Koh, A.; Peres, T. V.; et al. Dissecting the genetic landscape of GPCR signaling through phenotypic profiling in C. elegans. *Nat. Commun.* **2023**, *14*, 8410.
(75) Fawcett, G. L.; Santi, C. M.; Butler, A.; Harris, T.; Covarrubias, M.; Salkoff, L. Mutant analysis of the Shal (Kv4) voltage-gated fast transient K+ channel in Caenorhabditis elegans. *J. Biol. Chem.* **2006**, *281*, 30725−30735.
(76) Hayashi, Y.; Ono, K.; Ono, S. Mutations in Caenorhabditis elegans actin, which are equivalent to human cardiomyopathy mutations, cause abnormal actin aggregation in nematode striated muscle. *F1000Research* **2019**, *8*, 279.
(77) Tan, K. T.; Luo, S. C.; Ho, W. Z.; Lee, Y. H. Insulin/IGF-1 receptor signaling enhances biosynthetic activity and fat mobilization in the initial phase of starvation in adult male C. elegans. *Cell Metab.* **2011**, *14*, 390−402.
(78) Spremulli, L. L.; Coursey, A.; Navratil, T.; Hunter, S. E. Initiation and elongation factors in mammalian mitochondrial protein biosynthesis. *Prog. Nucleic Acid Res. Mol. Biol.* **2004**, *77*, 211−261.
(79) Philippe, L.; Pandarakalam, G. C.; Fasimoye, R.; Harrison, N.; Connolly, B.; Pettitt, J.; Muller, B. An in vivo genetic screen for genes involved in spliced leader trans-splicing indicates a crucial role for continuous de novo spliced leader RNP assembly. *Nucleic Acids Res.* **2017**, *45*, 8474−8483.
(80) Ding, C. C.; Rose, J.; Sun, T.; Wu, J.; Chen, P. H.; Lin, C. C.; Yang, W. H.; Chen, K. Y.; Lee, H.; Xu, E.; Tian, S.; Akinwuntan, J.; Zhao, J.; Guan, Z.; Zhou, P.; Chi, J. T. MESH1 is a cytosolic NADPH phosphatase that regulates ferroptosis. *Nat. Metab.* **2020**, *2*, 270−277.
(81) Zuela, N.; Dorfman, J.; Gruenbaum, Y. Global transcriptional changes caused by an EDMD mutation correlate to tissue specific disease phenotypes in C. elegans. *Nucleus* **2017**, *8*, 60−69.
(82) Fox, E. M.; Morris, C. P.; Hubner, M. P.; Mitre, E. Histamine 1 Receptor Blockade Enhances Eosinophil-Mediated Clearance of Adult Filarial Worms. *PLoS Negl. Trop. Dis.* **2015**, *9*, No. e0003932.
(83) Griffin, A.; Hamling, K. R.; Knupp, K.; Hong, S.; Lee, L. P.; Baraban, S. C. Clemizole and modulators of serotonin signalling suppress seizures in Dravet syndrome. *Brain* **2017**, *140*, 669−683.
(84) Brenner, S. The genetics of Caenorhabditis elegans. *Genetics* **1974**, *77*, 71−94.
(85) Wheeler, N. J.; Ryan, K. T.; Gallo, K. J.; Henthorn, C. R.; Ericksen, S. S.; Chan, J. D.; Zamanian, M. Multivariate chemogenomic screening prioritizes new macrofilaricidal leads. *Commun. Biol.* **2023**, *6*, 44.
(86) Rehborg, E. G.; Wheeler, N. J.; Zamanian, M. Mapping resistance-associated anthelmintic interactions in the model nematode Caenorhabditis elegans. *PLoS Negl. Trop. Dis.* **2023**, *17*, No. e0011705.
(87) Roy, P. J. Drug screens using the nematode Caenorhabditis elegans. *Genetics* **2025**, *231*, iyaf141.
(88) Burns, A. R.; Wallace, I. M.; Wildenhain, J.; Tyers, M.; Giaever, G.; Bader, G. D.; Nislow, C.; Cutler, S. R.; Roy, P. J. A predictive model for drug bioaccumulation and bioactivity in Caenorhabditis elegans. *Nat. Chem. Biol.* **2010**, *6*, 549−557.
(89) Walker, M.; Hamley, J. I. D.; Milton, P.; Monnot, F.; Kinrade, S.; Specht, S.; Pedrique, B.; Basanez, M.-G. Supporting Drug Development for Neglected Tropical Diseases Using Mathematical Modeling. *Clin. Infect. Dis.* **2021**, *73*, No. e1391−e1396.
(90) Beld, L.; Jung, H.; Bulman, C. A.; Rosa, B. A.; Fischer, P. U.; Janetka, J. W.; Lustigman, S.; Sakanari, J. A.; Mitreva, M. Aspartyl Protease Inhibitors as Anti-Filarial Drugs. *Pathogens* **2022**, *11*, 707.
(91) Gunderson, E. L.; Bryant, C.; Bulman, C. A.; Fischer, C.; Luo, M.; Vogel, I.; Lim, K. C.; Jawahar, S.; Tricoche, N.; Voronin, D.; Corbo, C.; Ayiseh, R. B.; Manfo, F. P. T.; Mbah, G. E.; Cho-Ngwa, F.; Beerntsen, B.; Renslo, A. R.; Lustigman, S.; Sakanari, J. A. Pyrvinium Pamoate and Structural Analogs Are Early Macrofilaricide Leads. *Pharmaceuticals* **2022**, *15*, 189.
(92) Bulman, C. A.; Chappell, L.; Gunderson, E.; Vogel, I.; Beerntsen, B.; Slatko, B. E.; Sullivan, W.; Sakanari, J. A. The Eagle effect in the Wolbachia-worm symbiosis. *Parasites Vectors* **2021**, *14*, 118.
(93) Kroeze, W. K.; Sassano, M. F.; Huang, X.-P.; Lansu, K.; McCorvy, J. D.; Giguere, P. M.; Sciaky, N.; Roth, B. L. PRESTO-Tango as an open-source resource for interrogation of the druggable human GPCRome. *Nat. Struct. Mol. Biol.* **2015**, *22*, 362−369.
(94) Storey, B.; Marcellino, C.; Miller, M.; Maclean, M.; Mostafa, E.; Howell, S.; Sakanari, J.; Wolstenholme, A.; Kaplan, R. Utilization of computer processed high definition video imaging for measuring motility of microscopic nematode stages on a quantitative scale: "The Worminator". *Int. J. Parasitol. Drugs Drug Resist.* **2014**, *4*, 233−243.
(95) Statistics Kingdom. *Kolmogorov-Smirnov Test Calculator*; Statistics Kingdom, 2017. https://www.statskingdom.com/kolmogorov-smirnov-test-calculator.html.
(96) Wheeler, N. J.; Gallo, K. J.; Rehborg, E. J. G.; Ryan, K. T.; Chan, J. D.; Zamanian, M. wrmXpress: A modular package for high-throughput image analysis of parasitic and free-living worms. *PLoS Negl. Trop. Dis.* **2022**, *16*, No. e0010937.
(97) Hess, J. A.; Zhan, B.; Bonne-Annee, S.; Deckman, J. M.; Bottazzi, M. E.; Hotez, P. J.; Klei, T. R.; Lustigman, S.; Abraham, D. Vaccines to combat river blindness: expression, selection and formulation of vaccines against infection with Onchocerca volvulus in a mouse model. *Int. J. Parasitol.* **2014**, *44*, 637−646.
(98) Leinonen, R.; Sugawara, H.; Shumway, M. on behalf of the International Nucleotide Sequence Database Collaboration. The Sequence Read Archive. *Nucleic Acids Res.* **2011**, *39*, D19−D21.
(99) Bolger, A. M.; Lohse, M.; Usadel, B. Trimmomatic: a flexible trimmer for Illumina sequence data. *Bioinformatics* **2014**, *30*, 2114−2120.
(100) Dobin, A.; Davis, C. A.; Schlesinger, F.; Drenkow, J.; Zaleski, C.; Jha, S.; Batut, P.; Chaisson, M.; Gingeras, T. R. STAR: ultrafast universal RNA-seq aligner. *Bioinformatics* **2013**, *29*, 15−21.
(101) Howe, K. L.; Bolt, B. J.; Shafie, M.; Kersey, P.; Berriman, M. WormBase ParaSite - a comprehensive resource for helminth genomics. *Mol. Biochem. Parasitol.* **2017**, *215*, 2−10.
(102) Liao, Y.; Smyth, G. K.; Shi, W. featureCounts: an efficient general purpose program for assigning sequence reads to genomic features. *Bioinformatics* **2014**, *30*, 923−930.
(103) Anders, S.; Huber, W. Differential expression analysis for sequence count data. *Nat. Prec.* **2010**, 1.
(104) Jones, P.; Binns, D.; Chang, H. Y.; Fraser, M.; Li, W.; McAnulla, C.; McWilliam, H.; Maslen, J.; Mitchell, A.; Nuka, G.;


https://doi.org/10.1021/acs.jmedchem.6c01435
J. Med. Chem. XXXX, XXX, XXX−XXX

Pesseat, S.; Quinn, A. F.; Sangrador-Vegas, A.; Scheremetjew, M.; Yong, S. Y.; Lopez, R.; Hunter, S. InterProScan 5: genome-scale protein function classification. *Bioinformatics* **2014**, *30*, 1236−1240.
(105) Carbon, S.; Douglass, E.; Good, B. M.; Unni, D. R.; Harris, N. L.; Mungall, C. J.; Basu, S.; Chisholm, R. L.; Dodson, R. J.; Hartline, E.; et al. The Gene Ontology resource: enriching a GOld mine. *Nucleic Acids Res.* **2021**, *49*, D325−D334.
(106) Kanehisa, M.; Sato, Y.; Morishima, K. BlastKOALA and GhostKOALA: KEGG Tools for Functional Characterization of Genome and Metagenome Sequences. *J. Mol. Biol.* **2016**, *428*, 726−731.
(107) Kanehisa, M.; Furumichi, M.; Sato, Y.; Ishiguro-Watanabe, M.; Tanabe, M. KEGG: integrating viruses and cellular organisms. *Nucleic Acids Res.* **2021**, *49*, D545−D551.
(108) Sternberg, P. W.; Van Auken, K.; Wang, Q.; Wright, A.; Yook, K.; Zarowiecki, M.; Arnaboldi, V.; Becerra, A.; Brown, S.; Cain, S.; et al. WormBase 2024: status and transitioning to Alliance infrastructure. *Genetics* **2024**, *227*, iyae050.
(109) Dyer, S. C.; Austine-Orimoloye, O.; Azov, A. G.; Barba, M.; Barnes, I.; Barrera-Enriquez, V. P.; Becker, A.; Bennett, R.; Beracochea, M.; Berry, A.; et al. Ensembl 2025. *Nucleic Acids Res.* **2025**, *53*, D948−D957.
(110) Altschul, S. F.; Gish, W.; Miller, W.; Myers, E. W.; Lipman, D. J. Basic local alignment search tool. *J. Mol. Biol.* **1990**, *215*, 403−410.
(111) Falcon, S.; Gentleman, R. Using GOstats to test gene lists for GO term association. *Bioinformatics* **2007**, *23*, 257−258.
(112) Medinsky, M. A.; Leavens, T. L.; Csanady, G. A.; Gargas, M. L.; Bond, J. A. In vivo metabolism of butadiene by mice and rats: a comparison of physiological model predictions and experimental data. *Carcinogenesis* **1994**, *15*, 1329−1340.
(113) Brown, R. P.; Delp, M. D.; Lindstedt, S. L.; Rhomberg, L. R.; Beliles, R. P. Physiological parameter values for physiologically based pharmacokinetic models. *Toxicol. Ind. Health* **1997**, *13*, 407−484.
(114) Knights, D.; Costello, E. K.; Knight, R. Supervised classification of human microbiota. *FEMS Microbiol. Rev.* **2011**, *35*, 343−359.




https://doi.org/10.1021/acs.jmedchem.6c01435
J. Med. Chem. XXXX, XXX, XXX−XXX